Cape Peninsula
University of Technology

SMALL WIND TURBINE TECHNOLOGY APPLICATION FOR RESIDENTIAL USES

by

AHMED TAHER AHMED ZENTANI

Thesis submitted in fulfilment of the requirements for the degree

Master of Technology: Electrical Engineering

in the Faculty of Engineering and the Built Environment

at the Cape Peninsula University of Technology

Supervisor: Prof MTE Kahn
Co-supervisor: Dr AMA Almaktoof

Bellville
November 2020

DECLARATION

I, Ahmed Taher Ahmed Zentani, declare that the contents of this dissertation/thesis represent my own unaided work, and that the dissertation/thesis has not previously been submitted for academic examination towards any qualification. Furthermore, it represents my own opinions and not necessarily those of the Cape Peninsula University of Technology.

Signed **Date**

ABSTRACT

As a result of environmental concerns, the depletion of fossil fuel, and the increase in energy demand, renewable sources' penetration is expanding day after day. However, because of their dependency on weather conditions, renewable sources impose new challenges on the power system. To accommodate these sources into the conventional power system, the structure of the power system should be changed. The concept of the microgrids is regarded as the appropriate solution for the grid integration of renewable sources. Microgrids refer to small power systems with control capabilities operating in grid connection and in offgrid modes. Microgrids can be classified as DC, AC, or hybrid microgrids. DC microgrids have emerged as sustainable solutions combining both energy storage and distributed generation to provide power to DC loads such as LED lights, computer chargers, Electric Vehicles, computers, laptops, TVs, tablets, phones, printers, etc. This study considers a DC microgrid based on a small wind turbine. The aim is to design a 3 kW standalone wind turbine DC microgrid to provide power to residential appliances operating at 240 V in case of power shortage or power cuts from the primary power grid. The system consists of a small wind turbine using an AC permanent magnet synchronous generator, a three-phase diode rectifier, a DC-to-DC boost converter, and a maximum power point tracker based on the Perturb and Observe (P&O) technique. MATLAB/Simulink software package is used for the modelling and simulation.

Keywords: DC microgrids, power converters, MPPT, P&O method, small wind turbine.

ACKNOWLEDGEMENTS

First and foremost, all praise be to ALLAH for giving me the knowledge, opportunity, and ability to successfully complete this degree.

I would also like to express my deepest gratitude to my supervisor, Professor MTE Kahn, and Co. supervisor Dr. Ali Almaktoof, for their support, encouragement, guidance, and commitment throughout this research.

My genuine thanks also goes to all members of Faculty of Engineering, staffs at the centre for distributed power electronics system (CDPES) and friends for their immeasurable suggestions and support.

For all the unconditional love and support and patience, for all the encouragement and sacrifices, I thank my parents, my wife, my brothers and sisters and my in-laws; may ALLAH bless them and reward them abundantly in this life and in the hereafter.

Special thanks to Dr. Khalid Ben Hamad for his help and encouragement throughout this journey.

Also, I thank Libyan Embassy in Pretoria for their support.

To my friends and colleagues, I am also grateful for their moral support and encouragements.

Ahmed Zentani 2020

DEDICATION

This thesis is dedicated to those who are dear to me, more particularly my parents, my wife Dr. Asma Alwakwak, my angels Yummna, Yussif and Yacob.

TABLE OF CONTENTS

LIST OF FIGURES

LIST OF TABLES

APPENDICE

GLOSSARY

$\mathbf{A}$	Area swept by the rotor
AC	Alternating current
ANN	Artificial Neural Network
DC	Direct current
DFIG	Doubly fed induction generator
FLC	Fuzzy Logic Control
GW	Giga watt
HAWT	Horizontal axis wind turbine
HCS	Hill Climb Search
IGBT	Insulated-gate bipolar transistor
INC	Incremental Conductance
kW	Kilowatt
LED	Light emitting diode
MPPT	Maximum Power Point Tracking
m/s	Metre per second
MOSFET	Metal Oxide Silicon Field Effect Transistor
MW	Mega watt
ORB	Optimum Relation Based
OTC	Optimal Torque Control
PMSG	Permanent magnet synchronous generator
P&O	Perturb & Observe
PSF	Power Signal Feedback
SCIG	Squirrel cage induction generator
SEIG	Self-Excited induction generator
SFIG	Singly Fed Induction Generator
SWT	small wind turbine
TSR	Tip Speed Ratio
V	Volt
VAWT	Vertical axis wind turbine
rpm	Revolution per minute
$\mathbf{P_w}$	Kinetic power of the wind

$\boldsymbol{\rho}$	Air density
$\mathbf{V_w}$	Wind speed
$\mathbf{C_p}$	Power coefficient
$\boldsymbol{\lambda}$	Tip speed ration
$\boldsymbol{\lambda_{opt}}$	Tip speed ration
$\boldsymbol{\omega}$	Rotational speed of the turbine
$\boldsymbol{R}$	Radius of the turbine blade
$\boldsymbol{C_p}$	Power coefficient
β	Pitch angle
$\boldsymbol{V_0}$	Output voltage
$\boldsymbol{V_{in}}$	Input voltage
$\boldsymbol{D}$	Duty cycle
$\boldsymbol{T_m}$	Turbine torque
$\boldsymbol{T_g}$	Generator torque
$\boldsymbol{T_{m\_opt}}$	Optimum torque
f	Frequency
$\boldsymbol{n_s}$	Speed of the rotor
p	Number of poles
ϕf	Flux per poles.
$\boldsymbol{P_{dc}}$	DC link power
$\boldsymbol{V_{dc}}$	DC link voltage

CHAPTER ONE
INTRODUCTION

1.1 Introduction

Currently, energy shortage has become one of the most significant issues that many countries are facing. For instance, some countries adopt electricity usage regulations that restrict households from controlling the quantity of electric power used daily (Kesraoui et al., 2018). On the other hand, the cost of energy from power utilities is increasing. More and more homes and businesses have been installing small renewable generators to cut energy bills and carbon dioxide emissions and sell extra electricity back to the national grids. If there is a power cut, these small renewable generators are introduced as backup sources to maintain continuous electricity supply (Kesraoui et al., 2011). Among various types of renewable generators, the wind turbine is one of the cleanest and efficient technologies. Depending on the application, their size can range from large to small (EARNEST & RACHEL, 2019). Standalone small wind turbines have become attractive choices for powering residential areas. In the case of grid failure, load shedding, or in places with no access to the grids, they can provide power to local loads. Compared to large wind turbines, which are widely used in wind farms, medium and small-scale wind turbines can be implemented in more flexible environments. For instance, small-scale wind turbines are commonly implemented in residential and urban distributed energy systems to provide alternating current (AC) or direct current (DC). In this research, the targeted residential utilities include DC appliances such as LED lighting, computers, variable speed drives, etc. These appliances significantly increase the power demand in residences.

The advantages of DC microgrids include energy efficiency improvement, a decrease of the overall energy consumption, network operational benefits, and cost-efficient electricity infrastructure replacement (Muhssin, 2015). DC microgrids are preferred over AC microgrids due to the following benefits (Shaikh et al., 2017):

a. higher reliability,
b. improved quality of power supply,
c. reduced losses due to absence of reactive power,
d. higher efficiency,
e. simple structure,
f. better performance and efficiency of DC converters.

The quantity of power obtained at the output of a wind generator is dependent on the accuracy at which the peak power points are being tracked by the maximum power point tracking (MPPT) controller of the wind turbine control system. MPPT algorithms are generally considered in systems such as photovoltaic and wind turbines to increase the extracted power for various operating conditions. Several MPPT algorithms are

presented in the literature; the conventional techniques are performed by measuring mechanical parameters such as wind speed or storing optimal generator speed values with their corresponding maximum power (torque) at various wind speeds. These techniques include Tip Speed Ratio (TSR), Optimal Torque Control (OTC), and Power Signal Feedback (PSF) MPPT techniques. On the other hand, MPPT controllers are also realised by measuring electrical parameters such as voltage, current, or power. MPPT techniques part of this group includes Hill Climb Search (HCS), Incremental Conductance (INC), Optimum Relation Based (ORB), soft computing methods such as Fuzzy Logic Control (FLC), Artificial Neural Network (ANN), etc. Among these MPPT techniques, the P&O method, also known as the Hill Climb Search, is one of the commonly used and easy-to-implement MPPT technique providing high efficiency if the correct predictive and adaptive hill-climbing process is used (Gite & Pawar, 2017).

Generators for wind turbines include permanent magnet synchronous generators (PMSG), squirrel cage induction generators (SCIG), and doubly-fed induction generator (DFIG), etc.; however, for small wind turbines, PMSGs are preferred due to their high reliability and efficiency. Moreover, PMSGs are dominant in gearless standalone small wind turbines developed for urban residential use. Generally, besides the PMSG, such a system includes a three-phase bridge rectifier, a DC-to-DC boost converter driven from an MPPT controller. The DC microgrid adopted in this research consists of a 3 kW wind turbine supplying a DC load at 240 VDC. The 240 V is obtained via a DC-to-DC boost converter driven by an MPPT controller based on the Perturb and Observe (P&O) algorithm.

1.2 Statement of the Research Problem

Some countries have restrictions on the amount of power usage for households per day. If the allocated amount of power for the day is depleted, then the concerned household's power supply automatically cuts off. The problem is to get additional and sufficient power to supply some appliances and avoid depleting the daily power rations, therefore preventing power cuts.

1.3 Research Aims and Objectives

1.3.1 Research aims

The research aim to design a 3 kW standalone wind turbine DC microgrid to provide power to residential appliances in case of power shortage or power cuts from the main utility grid.

1.3.2 Research objectives

The specific research objectives are:

- To develop a model for a small wind turbine standalone DC microgrid for residential use
- To develop the MPPT using the Perturb and Observe method.
- To simulate the system using MATLAB/Simulink environment.

1.4 Research Methodology

The methodology adopted in this research consists of the following:

- A comprehensive literature review will be conducted on DC microgrid, wind turbines, three-phase rectifiers, DC-to-DC converters and maximum power point tracking algorithm for wind turbines.
- Design of the small wind turbine DC microgrid and the maximum power point tracking algorithm using Matlab/Simulink
- Systematically analysis, and evaluate the results
- Present a thesis based the study conducted

1.5 Research Significance

This research will add value to existing available academic literature geared towards evaluating the different options to ensure energy security and facilitate the use of small-scale renewable sources.

1.6 Organization of the Thesis

The thesis is organised as follows:

Chapter two provided an overview of islanded mode operation of DC microgrids as well as small-scale wind turbines, including their components and current market. A section dedicated to wind energy conversion principle and operation was presented. Additionally, sections on power electronic converters for wind turbines and voltage flow stability and control compared with the other methods were also considered. Lastly, a review on wind turbine power control approaches and maximum power point tracking algorithms were presented.

Chapter three deals with the design considerations of a DC microgrid based on an SWT. The topics covered in this chapter include a brief investigation on standalone small wind turbine in DC microgrids, including the site selection, the technologies, the power electronic converters topologies and their maximum power point techniques.

Chapter four is dedicated to the development of SWT standalone DC microgrid model. The system is designed to operate as an auxiliary power entity for a residential building to provide power to appliances such as LED lighting, computers, variable speed drives, etc. in order to reduce or hinder power outages. Such SWTs are usually HAWTs attached in short towers of few metres or placed on top of buildings roofs, cellular communication towers, etc. In SWTs, the aerodynamic section is directly coupled to a PMSG without a gear system. The blowing wind causes the turbine to rotate and generate electricity. Such system can be used to improve power supply of applications including residences, farms, schools, small commercial businesses or even isolated community installations, etc. as they are practical and economic in places with high wind potential.

Chapter five deals with the presentation, analysis and discussion of the results obtained from the simulation. These results were presented in three sections namely wind turbine results, SWT results and DC-to-DC boost converter results. The wind turbine results focused on the aerodynamics of the wind turbine including the wind speed and the pitch angle. The SWT results comprised the simulation results of the voltage and the current of the 3 kW PMSG model used in this study. Lastly, the DC-to-DC boost converter results consisted of the results of the voltage, current and power of the converter using the P&O MPPT controller. Additionally, to case studies were considered to assess the performance of the system. The first case considered the operation of the SWT DC microgrid without an MPPT control for the boost converter and the system was simulated for different wind speeds. And the second case considered the simulation of the SWT DC microgrid operating under a constant speed at 12 m/s and the boost converter is controlled using a P&O MPPT controller.

Chapter six gives the conclusion of the thesis and the recommendations for further research.

CHAPTER TWO
LITERATURE REVIEW

2.1 Introduction

The DC microgrids have emerged as sustainable solutions combining both energy storage and distributed generation to provide power to DC loads such as LED lights, computer chargers, Electric Vehicles (EV), computers, laptops, TVs, tablets, phones, printers, etc. Most past research has focused on AC microgrid, because of the AC power experience, however, consistent progress in power electronics and enhancements in the computational power of real-time systems have made DC power capable of achieving larger roles than just the basic control. Moreover, DC technologies are becoming attractive solutions for industrial applications such as data centres, telecom stations, fast Electrical Vehicles (EV) charging, zero net electricity energy buildings, railways, electric ships, etc. Figure 2.1 depicts a layout of a DC microgrid comprising several nanogrids.

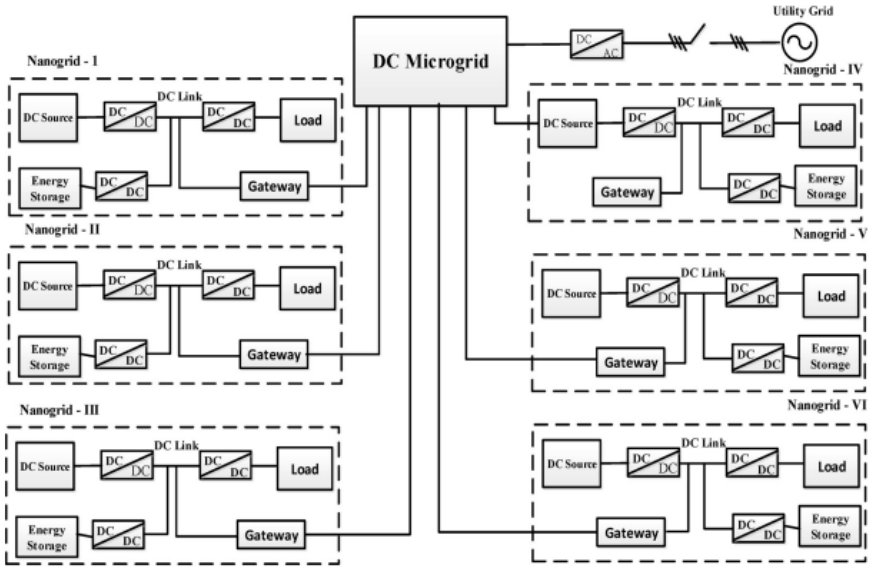

Figure 2.1: Nanogrids forming a DC microgrid. (Kumar et al., 2019)

In DC systems, concerns such as reactive power management and frequency synchronisation that characterise AC systems are irrelevant. Moreover, the lack of frequency makes DC systems liberated from proximity effect, skin effect, and inrush current issues and harmonics. DC systems are also viewed as safer than AC systems due to the decrease of the electromagnetic field.

Renewable generators such as photovoltaic and fuel cell can easily be integrated with DC systems as their output is in DC, while power sources such as wind turbines, wave power, and gas turbines can be more efficient by utilising only one converter instead of two back-to-back converters (AC to DC and DC to AC). Hence, the system complexity

can be improved, and conversion losses reduced by avoiding unnecessary conversion stages. Apart from their advantages, DC systems also have some issues such as the maturity of the technology, the lack of standards or norms, the instability because of the mismatch of impedance between lightly damped filters on the source side and tightly regulated power converter, the investigation of proper grounding, etc.

Figure 2.2 shows the layout of the microgrid adopted in this research. The system includes components such as the wind turbine, power conditioning device which consists of power electronic converters, and the MPPT controller to regulate energy from the wind turbine to the load.

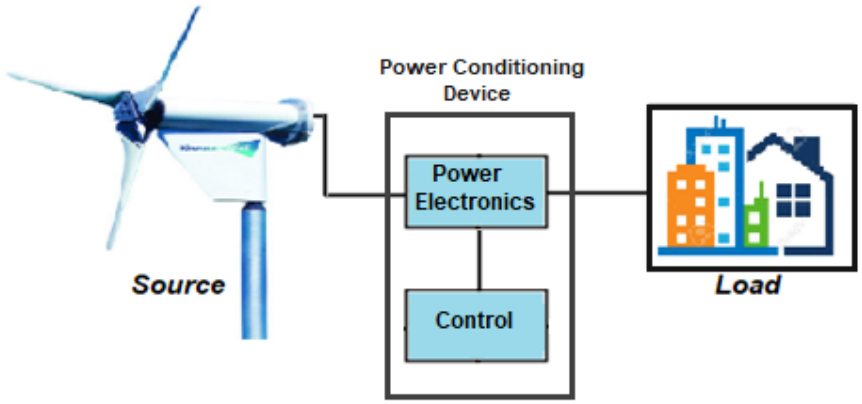

Figure 2. 2: Small wind turbine forming a DC microgrid

The kinetic energy from the wind is converted into mechanical energy by the rotor blades of the wind turbine. The mechanical energy is then transformed into electrical energy through an electric generator coupled to the rotor. Depending on the structure and shape of the blades, the wind energy extraction takes place at various rotational speeds. Generally, the wind turbine can extract maximum power out of the wind when facing fluctuating wind conditions.

This chapter gives an overview on the islanded mode operation of DC microgrids as well as small-scale wind turbines including their components and current market. A section dedicated to wind energy conversion principle and operation is also considered. Additionally, sections on power electronic converters for wind turbines and voltage flow stability and control compared with the other methods are also presented. Lastly, a review of wind turbine power control approaches and maximum power point tracking algorithms are considered.

2.2 Islanded Mode operation of DC Microgrids

Microgrids consist of low voltage distribution systems including distributed generation units and energy storage devices. Such an entity can operate tied to the grid, or in islanded mode (offgrid) if disconnected from the grid. In islanded mode, the microgrid must generate enough power to supply sensitive loads. Insensitive loads may not be supported as these loads are generally dependent on the main grid. Once the connection to the utility grid is restored, these loads will be reconnected and the microgrid will operate again tied to the grid (Katiraei et al., 2005; Pogaku et al., 2007). The number of distributed generation units in a microgrid is determined by the amount of energy that needs to be stored and the loads. In case there is an excess of energy when the microgrid is operating in the islanded mode, some of the distributed generation units might be stopped so that the remaining operating units can only meet the load (Kakigano et al., 2010; Kakigano et al., 2013).

Most home appliances operate using DC voltage which is usually provided by either a battery or a conversion from AC-to-DC using a rectifier. Figure 2.3 shows a DC microgrid consisting of both AC and DC distributed generation units as well as AC and DC loads. Such topology is often adopted to avoid power loss from several power conversion stages. In this case, the wind turbine generates AC power that requires an AC-to-DC conversion for the connection to the DC current bus, while the energy storage system and the photovoltaic panels provide DC power and are connected to the DC bus through DC-to-DC conversions.

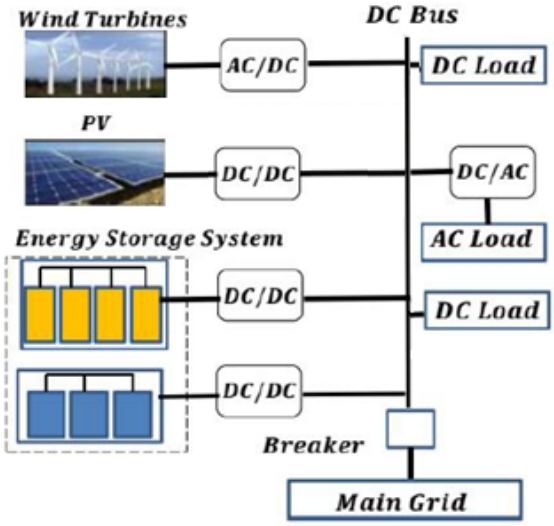

Figure 2. 3: DC microgrid. (Wang, 2018)

2.3 Small-Scale Wind Turbines (SWTs)

SWTs are the types of wind turbines that generate only a few kilowatts of energy (1 kW to 100 kW) and are often installed as single units. They are usually connected directly to the loads, or generally, to a power charging unit such as a battery bank. In the past years, there has been a significant increase in the use of SWTs; big companies are finding it economical to generate their own electricity. Additionally, in remote locations, SWTs are often integrated into local AC or DC microgrids consisting of renewable and other conventional energy sources to power households, farms, schools, or small businesses, etc. (Anila & Divya, 2016). These microgrids are seen as reliable and effective means to increase small scale renewable energy penetration while minimising the cost. The basic design approach applied for these types of wind turbines is similar to that of large-scale wind turbines. The most important factor when planning the installation of a wind turbine is to assess if a location has enough wind to generate electricity as the output power of a wind turbine is directly proportional to the wind speed (Abraham & Plourde, 2014).

Two topologies of SWTs can be found in the market namely the horizontal axis wind turbine (HAWT) and the vertical axis wind turbine (VAWT) (Figure 2.4) (Bin Wu, Yongqiang Lang, Navid Zargari, 2011). The HAWTs dominate the majority of wind turbine applications. They consist of a tower, a nacelle and rotor blades. The nacelle holds the gearbox and the generator. The power electronic interface of a small HAWT is often placed at the base of the tower. On the other hand, VAWTs usually comprise a tower, rotary blades,, and a rotor base that includes a generator and a gearbox. They can be further classified into Darrieus rotor and H-Darrieus rotor (Figure 2.5) (Abraham & Plourde, 2014). Table 2.1 gives a comparison between the types of wind turbines. In general, HAWTs have better wind energy conversion efficiency compared to VAWTs, other benefits include self-starting capability, and quick access to higher wind speed because of the tower height (Bin Wu, Yongqiang Lang, Navid Zargari, 2011; Bratcu & Ceangx, 2014).

SWTs can be fixed speed or variable speed wind turbines. The major differences between the two types are the way the aerodynamic efficiency of the rotor would be limited for different wind speeds. The process of wind energy conversion system is comparatively simple. However, without appropriate planning, a large portion of wind energy might be wasted.

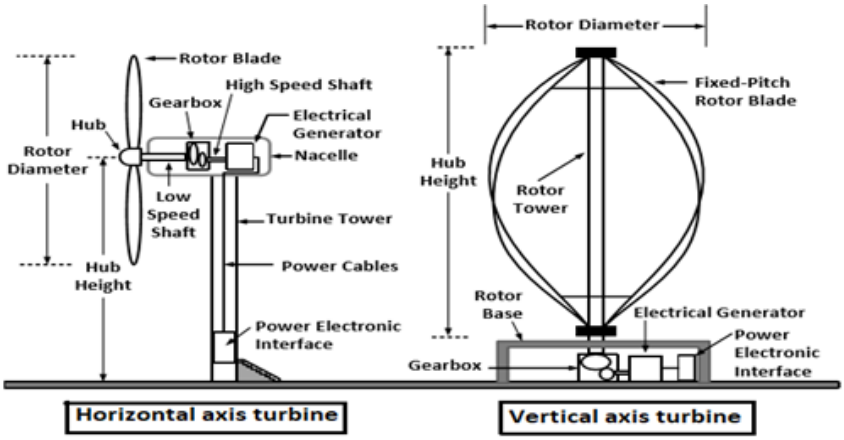

Figure 2. 4: HAWT and VAWT Characteristics. (Bin Wu, Yongqiang Lang, Navid Zargari, 2011)

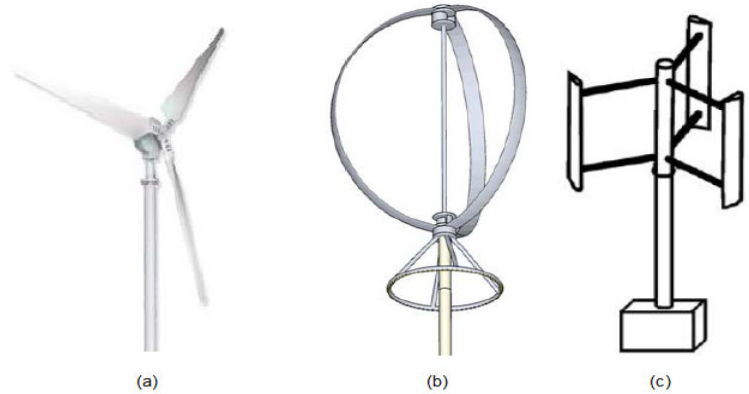

Figure 2. 5: (a) HAWT, (b) Darrieus and (c) H-rotor VAWT. (El Chaar et al., 2011)

Table 2. 1: Advantages and disadvantages of various wind turbines. (El Chaar et al., 2011)

Type of wind turbines	Advantages	Disadvantages
HAWT	• Majority use three blades less than those in VAWT. • HAWT blades are self-supporting on the ground, they are simply attached at the base, and the top is lighter thus, decreasing the cost of the structure • Pitch control can be used to control pitch energy supplied by wind speed and stopping the turbine system when required. • Contemporary mass production in this system has lower value of cost rather than the other.	• HAWT tower interference makes noise problem • The structure is complex because it has a yaw mechanism and a dynamic stall • More uncovered periodical loads that can reduce lifespan of the system • Reducing maximum power output due to system restrictions • Maintenance required is difficult
VAWT Darrieus and H-rotor	• Since the angle of contact with the wind blade is not vital in this system, it may be sited in turbulent and divergent places of wind. • No need to control rotor direction • The generator and control unit are placed at the bottom of the tower, which exposes it to demand a high possibility of operation, installation and maintenance. • VAWT can be installed in the residential areas with few noises • Darrieus is not heavy because of the structure • Easy components manufacturing • There is no Yaw system for this application, which decreases cost • VAWT technology such as Darrieus application needs simple foundations • Available with low power but more suitable used in offshore technology system	• Under discontinued challenges such as the starting of the poor torque at high levels of angles from the wind attack • actual torque ripple that affects the life of fatigue from drive as well as quality power output • H rotor blade capacity is large, thus require more materials used • H-rotor blades undergo bending moments decreased wind turbine size since gravitational acceleration decrease with increasing turbine radius of constant speed • In the application of Darrieus which is the control of the pitch angle considered as not possible • Darrieus wind turbine blades specifications are complex to industry

2.4 Market of Small Wind Turbines

Small Wind Turbines market is still in its early stage, however, according to recent reports from the international trade, the market is growing faster, and statistics show that as of the end of 2014, more than 830 MW, which indicates an increasing of 10,9% over 2013 was registered. Most of this growth has occurred in countries like China, the USA, and the UK (Pitteloud, 2016). Globally, the average installed size in 2010 was around 0,66 kW while in 2014 it reached 0,87 kW. For example, in China, the average installed size in 2012 was around 0,5 kW, while the USA and UK were at 1,4 kW and 4,7 kW respectively. The UK started with no existing Small Wind Turbines market before 2012, however, the country improved rapidly during 2013 and 2014 (Pitteloud, 2016).

The Chinese market represents the largest market with around 72 % share of installed units, followed by the USA with 18 % of installed units, then the UK with 3 % of installed units and the rest of the world with the remaining 7 % (Figure 2.6 a). However, comparing the total installed capacities, the situation appears different; China leads with only 41 %, followed by the USA 30 %, then the UK with 15 %, and lastly the rest of the world with 14% (Figure 2.6b) (Pitteloud, 2016).

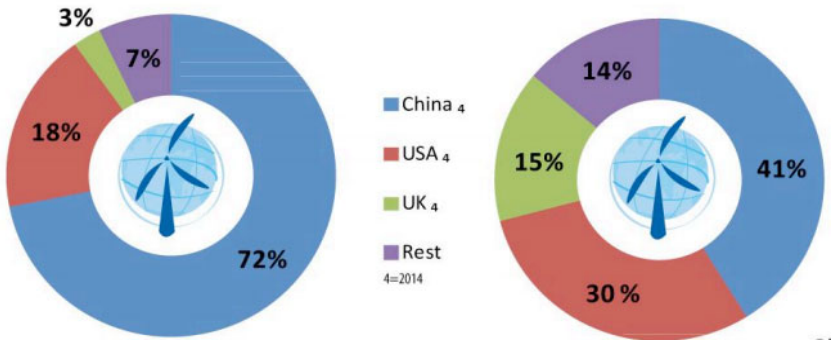

(a) **(b)**

Figure 2. 6: SWTs Comparison of (a) installed units and (b) installed capacity. (Pitteloud, 2016)

The latest development of the small wind turbines market showed a yearly increase of 11 % in new installations capacity. As shown in Figure 2.7, in 2016, the growth rate increased to 115 MW of installed capacity with regulated standards and policies. The market is expected to reach around 240 MW of recently installed capacity. Additionally, the market is expected to see a steady growth rate of 20 % and installed capacity accumulated around 175 GW by 2020 (Pitteloud, 2016).

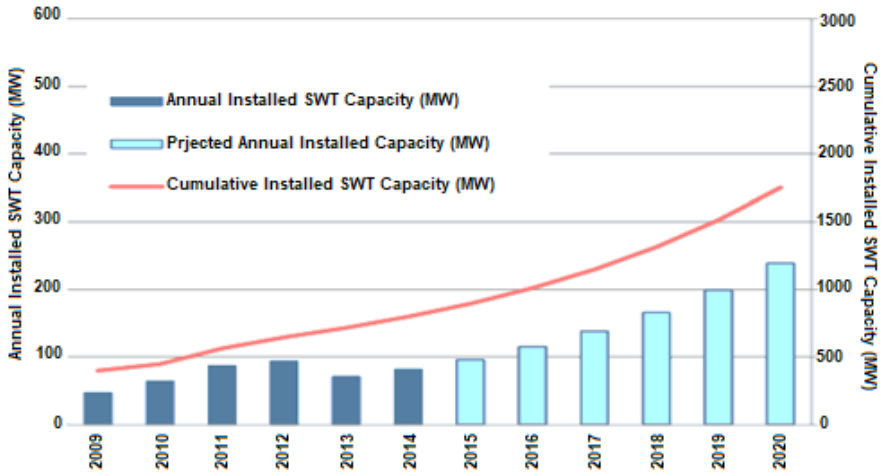

Figure 2. 7: SWT Installed Capacity World Market Forecast 2009-2020. (Pitteloud, 2016)

2.5 Components of Small Wind Turbines

As shown in Figure 2.8, small wind turbines components include the rotor, the blades, the tail, and the tower. However, wind turbines consist of blades, rotor hub, turbine shaft, gearbox, generator shaft, etc. The system is designed to transfer the mechanical energy generated from blowing wind into electric power.

2.5.1 Rotor

The components of a wind turbine that accumulates energy from the wind are known as the blades. The rotor coil usually consists of two or three evenly distributed wooden, fibreglass or steel blades which rotate an axis (horizontal or vertical) at a rate defined by the wind velocity and the design of the blade. The blades are connected to the centre, and the centre is attached to the main base.

2.5.2 Drag and lift design

Blade designs run by utilising either drag or lift. With the drag concept, the wind moves the blades out of the way. Drag based wind generators are viewed as slower rotational speeds systems with high torque capabilities. They may be used in applications such as pumping, cutting, or grinding work. On the other hand, lift edge design uses a similar rule that makes aeroplanes, kites, and birds fly. When air travel flows past the blade, a type of wind speed and force differential occur between the top and lower blade segments. The demand at the lower segment is greater and thus proceeds to “lift” the blade. While blades join the main axis, similar to a wind turbine rotor, the lift is converted into rotational movements. Lift-based wind generators have higher rotational speeds and are designed for electricity generation.

2.5.3 Tip speed ratio

The tip speed would be proportional to the rotational movement of the blade towards the wind speed. With a greater percentage of tip speed ratio, the rotation of a real wind turbine rotor at the given wind speed will be high. Lift-based wind generators have maximal tip-swiftness proportions of around 10, while drag-based proportions are generally approximated. Considering the high rotational speed demands of electrical generators, it is obvious that this lift-based wind turbine is almost practical.

2.5.4 Number of blades

The blades' volume consists of the total number of blades and the total area covered to facilitate wind generator performance. For a lift-based wind turbine to operate

effectively, the wind must easily flow over these blades. Spacing between blades must be greater to prevent a particular blade from encountering the potentially disturbing blade to avoid turbulence. Because of that, most wind turbines have either two or three blades.

2.5.5 Generator

The wind generator transforms the rotation of the blades directly into electricity. These generators can produce alternating current (AC) or direct current (DC) depending on the design and can be found in the market with various standardised electrical power ratings. The length of the blades can influence the wind generator size. Generators that produce AC power are often equipped with features to generate the accurate voltage at a constant frequency, even if they vary. DC generators are generally useful for battery charging applications in addition to being used for other devices.

2.5.6 Transmission

The rotation of the wind turbine rotor ranges between 45 and 400 rpm (revolution per minute), depending on the type of rotor and the wind velocity. Generators generally require revolution per minute of 200 to around 800. Hence, most wind turbines require gear systems to increase the generator's rotation to adequate speeds to allow efficient electricity generation. Few DC wind turbines do not require transmission systems. Instead, they use a direct connection between the rotor and generator, generally referred to as direct thrust systems. Since the transmission is not performed, wind turbine complexity and maintenance are decreased. However, to deliver the same power as AC wind turbines, large turbines are required.

2.5.7 Towers

Towers are not just supporting frames on which wind generators are installed. They also raise the wind turbine to some height so that the blades can be safely and securely clear from the ground, in addition to allowing stronger winds. The maximum tower height selection is optional in many cases, except in areas subjected to restrictions. The major factor to consider when deciding about the height that the tower should have is the cost.

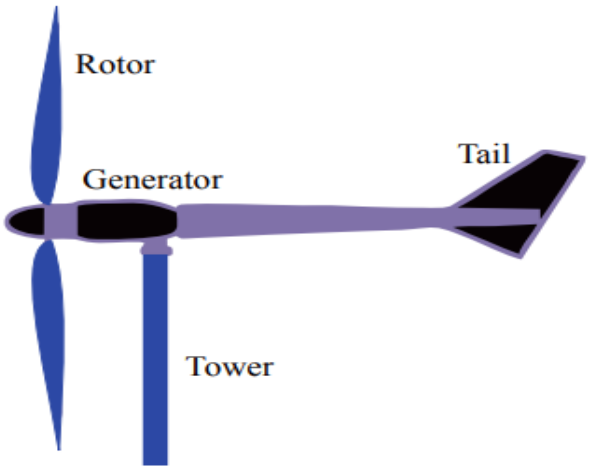

Figure 2. 8: Components of a SWTs. (Mahesa et al., 2020)

2.6 Principle and Operation of Wind Energy Conversion

2.6.1 Wind aerodynamics

In the 1980s, most wind turbines could not generate efficient and reliable electricity (Yaramasu et al., 2015). Since then, significant development and technological advancement have occurred. Still, based on aerodynamics laws, it is not physically possible to convert all kinetic energy surrounding a wind turbine into usable energy. The kinetic power of the wind (disc) that flows across the turbine rotor swept area, as shown in Figure 2.9 can be expressed using the following equation (Echchhibat, 2017):

$$P_w = 0.5\rho A V_w^3 \tag{2.1}$$

where $\boldsymbol{P_w}$ is the kinetic power of the wind, $\boldsymbol{\rho}$ is the air density, $\boldsymbol{A}$ is the area swept by the rotor and $\boldsymbol{V_w}$ is the wind speed.

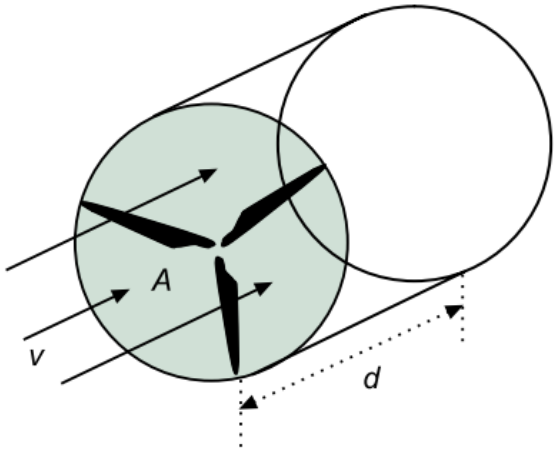

Figure 2. 9: Power in the Wind. (EARNEST & RACHEL, 2019)

2.6.2 Power of wind turbine

The disc concept provides the wind turbine's aerodynamics and gives the maximum efficiency that an ideal turbine can never exceed. This efficiency is referred to as the Betz limit, equal to 59.3% (Bratcu & Ceangχ, 2014). In practice, wind turbines have less extraction efficiency than the Betz limit, and the power coefficient C_p quantifies the efficiency. The power coefficient represents a fraction of the power in the wind extracted by the rotor. Moreover, it evaluates wind turbine performance. The two variables of the power coefficient are defined by the tip speed ratio and the pitch angle.

The tip speed ratio λ expresses the ratio of the turbine blade tip speed onto the wind speed, and it is expressed by equation 2.2 as follows (Zammit et al., 2018):

$$\lambda = \frac{\omega R}{V_w} \tag{2.2}$$

Where ω is the rotational speed of the turbine and R is the radius of the turbine blade.

The pitch angle is the angle at which the blades are perpendicular to the axis blades. The pitch angle can control the quantity of power extracted by aligning blades out depending on the operating conditions. In large-scale wind turbines, mechanical control is employed to regulate the pitch angle. However, in SWTs, the pitch angle controllers are not used because of their technical complexity and cost. In most cases, the pitch angle is considered to be zero.

The power coefficient is used to measure the power captured by the wind turbine, and it is given by equation 2.3 as follows (Zammit et al., 2018):

$$C_p(\lambda, \beta) = \frac{P}{P_w} \tag{2.3}$$

Where P is the power from wind

The power captured by a wind turbine can be expressed using the power coefficient as follows (Bratcu & Ceangχ, 2014):

$$P = 0.5 \rho A C_p(\lambda, \beta) V_w^3 \tag{2.4}$$

2.6.3 Fixed and variable HAWTs

The HAWTs can have either fixed pitch or variable pitch angles. In fixed pitch angle wind turbines (β = 0), the maximum power occurs when the tip speed ration is optimal ($\boldsymbol{\lambda_{opt}}$). The efficiency of the extracted power depends on the power coefficient and the tip speed ratio. The typical power curves of fixed pitch angle wind turbines are shown in Figure 2.10.

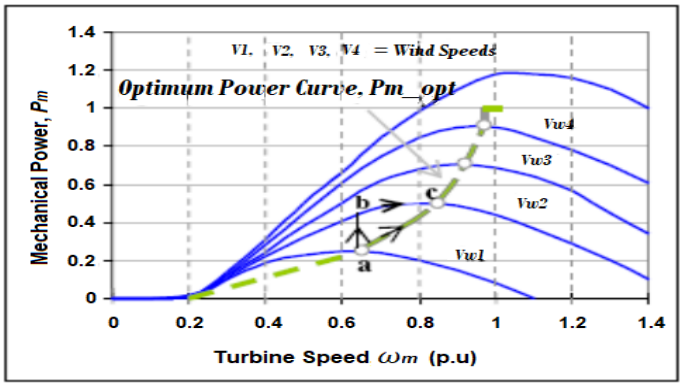

Figure 2. 10: Power curve of fixed pitch HAWTs. (Haque et al., 2009)

In variable pitch wind turbines, the rotor blades can twist to align with its longitudinal axis. The power coefficient curves of such wind turbine under various pitch angle is depicted in Figure 2.11.

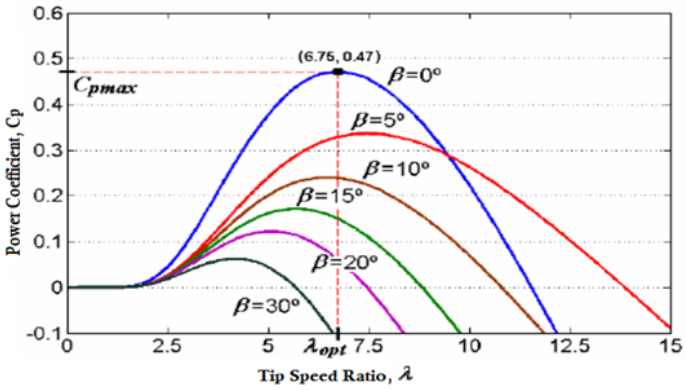

Figure 2. 11: Power Coefficient (C_p) under different pitch angles β. (Echchhibat, 2017)

2.6.4 Turbine power versus rotational speeds

Figure 2.12 shows the wind turbine power curve as a rotor rotational speed function at various wind speeds. The curve shows the cubic power dependence of the wind turbine over the wind speed. Additionally, it shows the wind turbine's ability to achieve maximum power generation depending on the rotation speed.

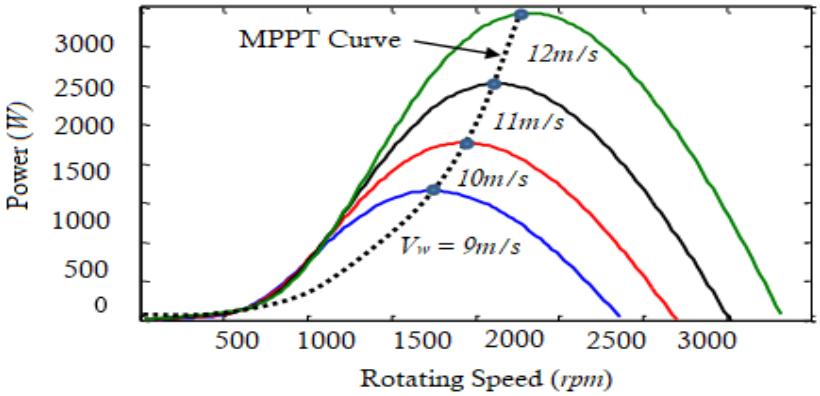

Figure 2. 12: Power versus rotor rotational speed at various rotational wind speeds. (Dalala et al., 2013)

2.6.5 Turbine torque versus rotational speeds

The wind turbine torque as a function of the rotor rotational speed at different wind speeds is depicted in Figure 2.13. As the power, the torque is also dependent on both the rotational speed and the wind speed. The maximum power occurs at optimum torque. The torque curve's right side is referred to as the stable operation zone of the wind turbine.

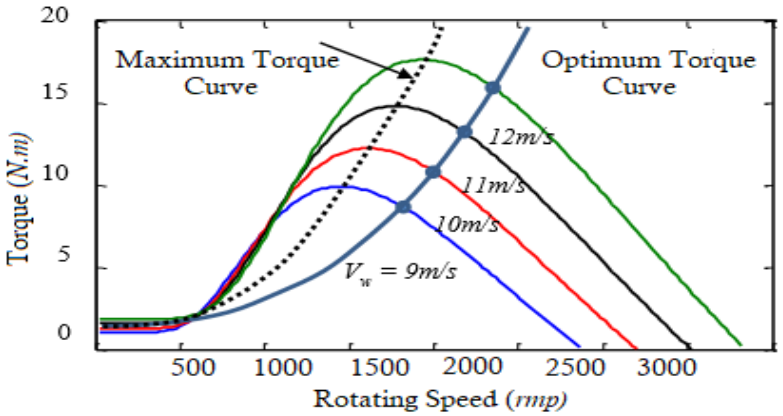

Figure 2. 13: Torque versus rotational speed at various wind speeds. (Dalala et al., 2013)

2.6.6 Wind turbine power curve

A wind turbine power curve shown in Figure 2.14 refers to a standard characteristic obtained from the wind turbine manufacturer to predict the output power. The cut-in speed is the minimum wind speed at which the wind turbine generates functional power. The rated speed represents the optimum wind speed at which the wind turbine generates its rated power, and the cut-out speed is the wind speed at which the wind turbine is shut down for protection reasons.

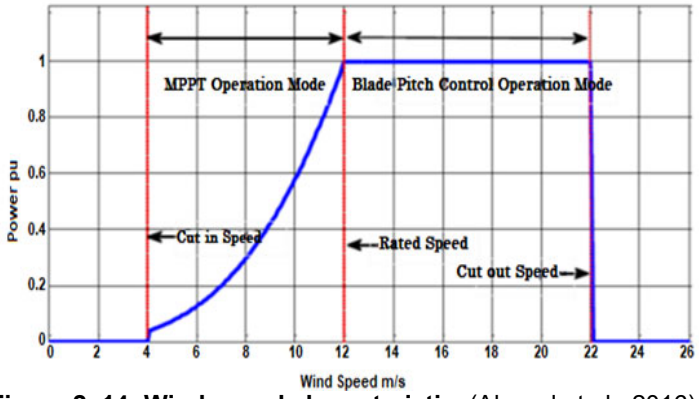

Figure 2. 14: Wind speed characteristic. (Ahmed et al., 2016)

2.7 Wind Generators

The shaft of a turbine is coupled to the generator rotor's shaft to transmit the mechanical power of the turbine to the generator rotor. According to Faraday's electromagnetic induction law, if an electric conductor is moved inside a rotating magnetic field, an electromotive force will be induced in the conductor. An electric current will start flowing through the conductor. Most generators used in wind turbines generate AC power, and generators for wind turbines can be synchronous or induction generators. Synchronous generators can be grouped as constant speed or variable speed synchronous generators. Furthermore, synchronous generators can be permanent magnet or electromagnet field generators depending on the magnetic field. On the other hand, induction generators used in wind turbines are classified into three types, namely Singly Fed Induction Generator (SFIG), Doubly Fed Induction Generator (DFIG), and Self-Excited induction generator (SEIG). Wind generators are grouped into permanent magnet synchronous generators, direct-coupled generators, and doubly-fed induction generators in this section.

2.7.1 Permanent magnet synchronous generators (PMSG)

PMSGs are more flexible and more efficient compared to other types of generators. They can achieve full speed control and do not provide slip rings and brushes. PMSGs can also enable variable speed operation, allowing maximum power tracking between the cut-in and the rated wind speeds. They also connect the wind turbine without a gearbox and do not require an excitation current. Additionally, this type of generator's control systems are modest and easily implemented, thus achieving active and reactive power control (Subbiah & Neelaveni, 2017). However, PMSGs present some disadvantages, such as they can run the risk of demagnetisation at a high temperature, and power electronics devices have a full scale-power rating, which may result in lots

of losses (Subbiah & Neelaveni, 2017). Figure 2.15 shows a layout of a PMSG wind generator feeding a three-phase rectifier.

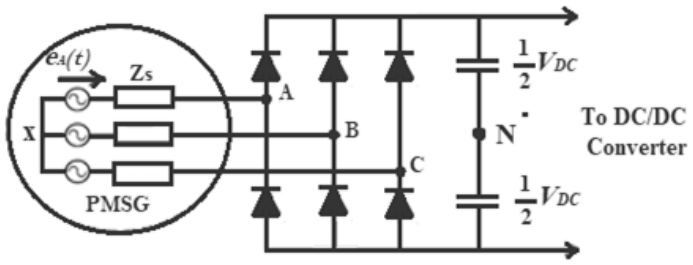

Figure 2. 15: PMSG connected to a three-phase rectifier. (Zammit et al., 2018)

2.7.2 Direct-coupled generator

Fixed-speed squirrel-cage enlistment generators were broadly utilised in large-scale wind turbines during the 1980s, during which a large portion of wind turbines was straightforwardly coupled to the power grid. Because of the wind speed variation, the generator rotor speed needs to change marginally to adjust the variation of the driving torque.

The rotational speed of the generator is, in this manner, not constant. To produce a magnetic field for wound rotor induction generators, it is important to have additional power to the rotor through a slip ring. However, the rotational speed variation is commonly under 1% because of the nature of small slip of induction generators (Bin Wu, Yongqiang Lang, Navid Zargari, 2011), which is defined as the rate of the differential of the revolution speed of magnetic fields between the synchronous speed and rotational speed, divided by the simultaneous speed (Lee et al., 2005). Figure 2.16 shows a fixed-speed wind turbine design, which comprises a squirrel-confine induction generator, bridge soft starter, a bunch of capacitor bank, and a transformer.

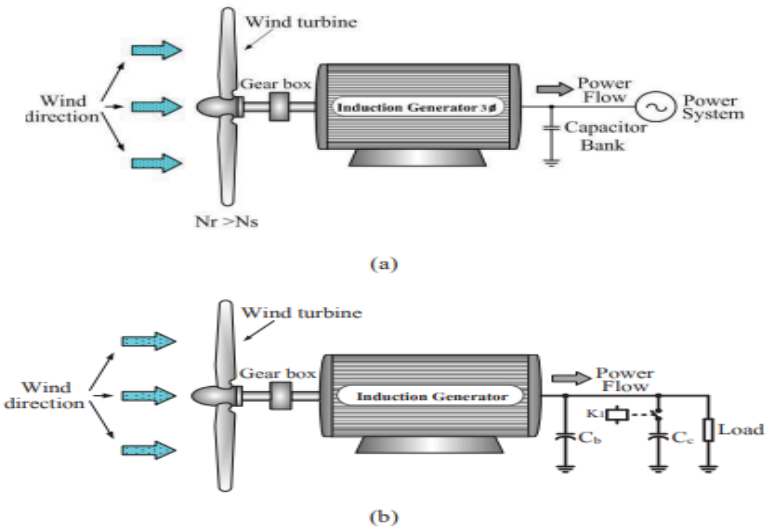

Figure 2. 16: (a) Grid-tied induction generator, (b) Self-excited induction generator.
(Kinnares & Sawetsakulanond, 2013)

Generally, squirrel-cage induction generators require reactive power compensation, and the compensation is achieved by connecting the generator to a capacitor bank (Jahromi et al., 2012). The advantages of squirrel-cage induction generators are as follows: (Jahromi et al., 2012)

- Straightforward structure
- Low cost
- Easy maintenance
- Simple solution for grid connection
- High performance-to-price ratio

However, they do not operate under optimal tip speed ratio with the wind speed variation, and their efficiency and power factor are low (Hau, 2006).

2.7.3 Doubly fed induction generator (DFIG)

DFIGs are gaining interest because of the disadvantages of fixed-speed induction generators. The difference between both types is that the stator windings of DFIG can directly be tied to the grid. Power output from the stator of a DFIG can be supplied directly to the grid, and the generator rotor consumes excitation current from the grid. As shown in Figure 2.17, the rotor of the DFIG is connected to the grid employing a power converter. The power converter can transmit power in both ways by delivering power to the grid and is also absorbing power from the grid, based on the generator's rotational speed (Kumar Tiwari et al., 2018).

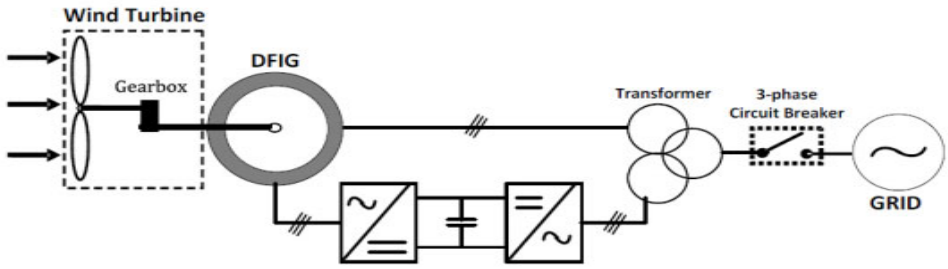

Figure 2. 17: DFIG Indirect Drives Variable Speed Wind Turbine with Gearbox. (Ontiveros et al., 2011)

Advantages of the DFIG include the following (Ontiveros et al., 2011):

- The ability to decouple the active and reactive power control by controlling the rotor voltage. Thus, the power factor control can be implemented.
- simplicity in construction

On the other hand, the disadvantages of DFIG are

- frequent maintenance.
- Gearbox adds extra weight,
- produce noise,
- increases losses.

2.8 Power Electronic Converters for DC Wind Turbines

The most widely utilised power electronic converters for wind turbines are AC-to-DC converters, DC-to-AC converters, and DC-to-DC converters. The voltage generated is first rectified to DC to either feed DC loads or converted back to AC to feed the grid or any AC load. Generally, in DC wind turbines, the continuous variation of wind speed affects the DC link voltage, which may vary in an uncontrolled way. To obtain a stable DC voltage, a DC-to-DC boost converter is usually used in the DC link.

2.8.1 AC-to-DC converters

AC-to-DC converters are also known as rectifiers. A three-phase bridge rectifier shown in Figure 2.18 is usually employed in wind turbines to convert the AC voltage into DC. The topology is a full-wave rectifier providing six pulse ripples at the output voltage. Each diode conduct for 120º, and diodes' pair connected between that pair of supply phases with the highest instantaneous line voltage will conduct (Rashid, 2014).

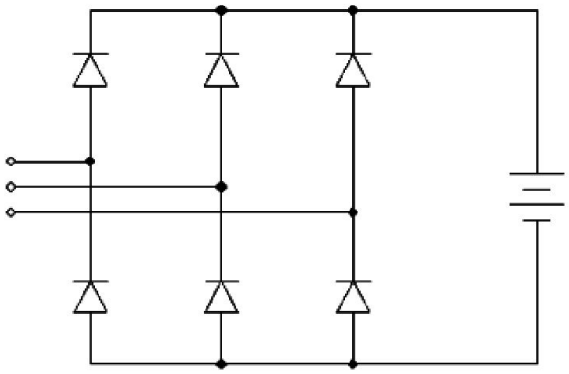

Figure 2. 18: Three-phase bridge rectifier.

2.8.2 DC-to-DC converters

DC-to-DC converters are devices that take DC inputs voltage and produce desired DC outputs voltage with the output voltage being different from the input. DC-to-DC converters are also employed to isolate noise and for power bus control. In general, there are three types of DC-to-DC converters, namely buck converter, boost converter, and buck-boost converter. DC-to-DC converters consist of an inductor, a capacitor, a diode, and an IGBT or a MOSFET.

2.8.2.1 Buck converter

Figure 2.19 depicts the schematic diagram of a buck converter. This type of converter takes a high input voltage and produces a lower output voltage.

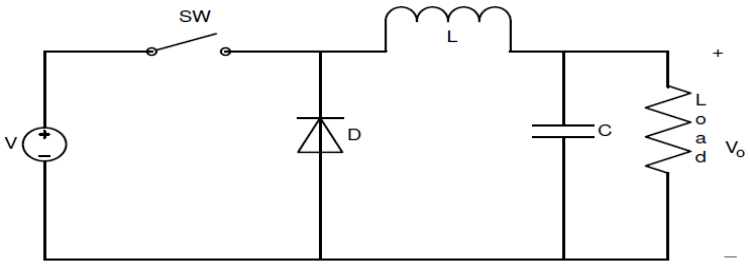

Figure 2. 19: Schematic of a buck converter.

If the switch SW is in on-state mode, the voltage across the inductor is equal to the voltage difference between the input and output, and the current through the inductor increases linearly. The diode will be in reverse biased, and no current will flow through it. On the other hand, if the switch SW is in off-state mode, the diode will be forward biased and across the inductor will be negative and equal to the output voltage. Hence, the inductor current, which will decrease.

The following equation gives the output voltage of a buck converter:

$$V_0 = DV_{in} \quad (2.5)$$

where, V_0 is the output voltage, V_{in} is the input voltage and D the duty cycle of the converter.

2.8.2.2 Boost converter

The boost converter shown in Figure 2.20 takes a DC input voltage and provides an output voltage bigger than the input. It generally consists of an inductor, a diode, a switch, and at least one energy storage element. Capacitors are often connected at the output terminal of the converter to remove output voltage ripples. When the switch (IGBT) is in on-state mode, the current flowing in the inductor increases, and when the switch is in off-state mode, the only path for inductor current to flow is through the diode and the capacitor and the load, thus, enabling the capacitor to transfer ,the energy stored during the on-state mode. The output voltage V_o of a boost converter is given equation 2.6 as follows (Aubrée et al., 2012):

$$V_o = \frac{1}{1-D} V_S \quad (2.6)$$

where V_S and D are the input voltage and duty ratio respectively.

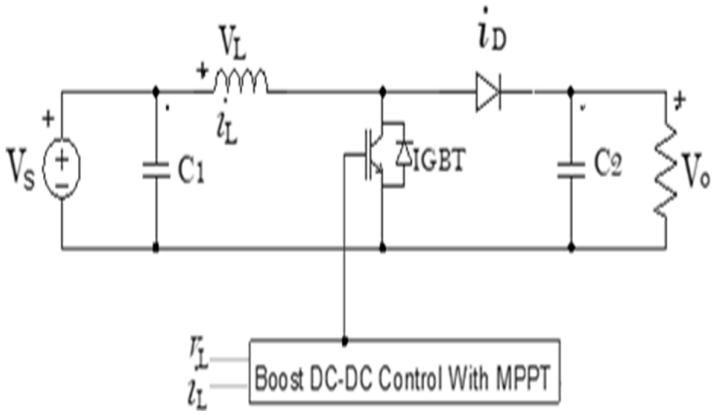

Figure 2. 20: Schematic of a boost converter.

Some of the advantages of a boost converter include:

- Low component count, complexity, and cost
- Simple design and implementation,
- High efficiency and low input ripple current.

On the other hand, the disadvantages are:

- Non-Isolated power supply,
- Prone to failure due to the absence of DC isolation,
- High output currents will stress the switching element, the diode, and therefore limit the output power capability of this supply.
- Hazardous transients can easily reach the load.
- The supply has a high output ripple.

2.8.2.3 Buck-Boost converter

The buck-boost depicted in Figure 2.21 provides an output voltage that can be less than or bigger than the input voltage based on the duty ratio value. This converter operates such that if the duty ratio is greater than 0.5, the converter is in a boost mode, while if the duty ratio is less than 0.5, the converter operates in a buck mode.

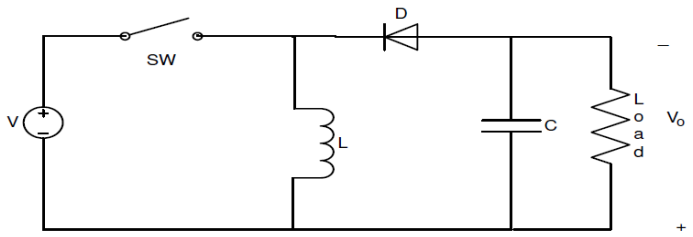

Figure 2. 21: Schematic of a buck-boost converter.

The output voltage $\boldsymbol{V_0}$ of a buck-boost converter can be determined using equation 2.7 given as (Khadiri & Qjidaa, 2014):

$$\boldsymbol{V_0} = \left(\frac{\boldsymbol{D}}{\boldsymbol{1-D}}\right) \boldsymbol{V_{in}} \tag{2.7}$$

where $\boldsymbol{V_{in}}$ and $\boldsymbol{D}$ are the input voltage and duty ratio respectively.

2.9 Voltage flow stability and control in DC grids

Voltage and frequency are the parameters that require control in AC systems. The frequency can be regulated by controlling the apparent power. In contrast, the voltage can be regulated by keeping the reactive power stable. No reactive power characterises DC grids since both the voltage and the current are in phase, and their frequency is equal to zero. Hence, the voltage is the only parameter that requires to be controlled. In DC grids, the voltage is controlled by supplying the required power to the loads (Sun et al., 2016). By controlling the voltage of the DC link, the nominal voltage flow can be realised. In case the grid is overloaded, the voltage drops will occur in the

system. Therefore, to stabilise a DC grid's voltage, it is important to maintain the balance between the supply and the demand. Stabilising the voltage level also depends on the number of converters employed to regulate the DC voltage. Various techniques can be used to stabilise the voltage of a DC microgrid. The common method is the Master/slave drop control. Typically, the DC link is where the voltage can be regulated because it is directly linked to the grid, and an adequate voltage level should be realised (Bounechba et al., 2016). Converters should operate accurately, and dependency should not be kept only on the DC link. Communication between the different converters is also gainful to control a DC grid's power flow and to monitor the voltage drops and faults that may occur in the system. The Master/slave drops control technique is recommended where a DC link master controller controls many other converters and devices. Using a battery bank is another way of maintaining DC grid power during the lower power generation. The bank can be utilised to support the grid in maintaining an adequate voltage level. However, batteries cannot perform a voltage regulation for a long period because of their capacity.

2.10 Wind turbine power control

Depending on the wind turbine topology, various techniques can be employed to control the power. These techniques include the pitch angle control, the stall mode control, the yaw control, and the power electronics control (Labidi, et al., 2017).

2.10.1 Pitch angle control

Figure 2.22 shows the schematic of pitch angle control. The technique is commonly used to control the aerodynamic power generated by a turbine. It consists of turning the blades faster either into or out of the wind to decrease or increase the power output. The pitch angle is modified by a portion of a degree to change the wind speed, thus, keeping a fixed power output. This control method's disadvantage is the rotor geometry change, which makes the system more expensive.

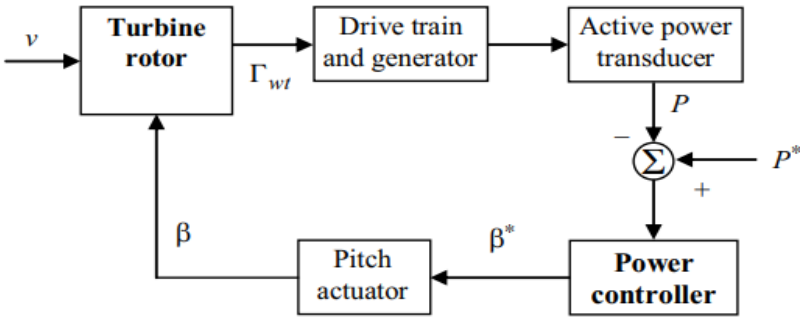

Figure 2. 22: Pitch angle control structure. (Bratcu & Ceangx, 2014)

2.10.2 Stall control

During high wind speed, the turbine blade turns a couple of degrees the other way to control the pitch angle. By doing that, constant wind energy are obtained even when the wind speed is high. Additionally, constant power soft stalling has been proposed to restrict the power generated and the rotor speed to send the wind turbine into the low-speed stall zone. The stall control concept is illustrated in Figure 2.23; as the wind speed rises from the cut-in speed, the rotor speed rises to keep the maximum power. For wind speeds beyond that range, the power will be maintained constant at its rated value (Ahmed et al., 2010).

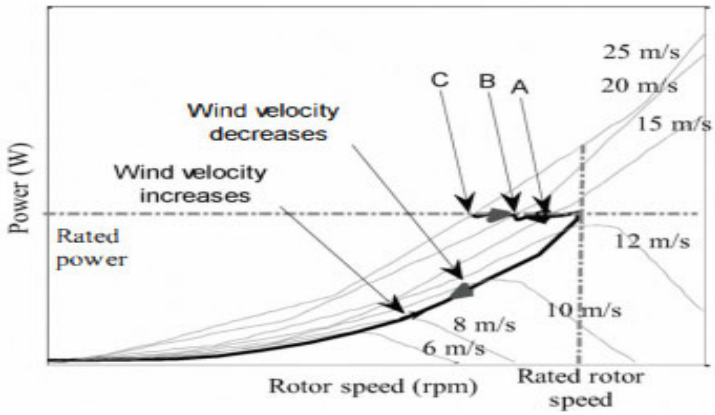

Figure 2. 23: Power versus rotor speed in stalling control. (Ahmed et al., 2010)

2.10.3 Yaw control

A layout of a yaw mechanism is shown in Figure 2.4; generally, the turbine tends to acquire optimum force by changing the wind turbine direction. For small-scale wind turbines, the tail vane is used to achieve that, and for large-scale wind turbines, the yaw system is used. Whenever the turbine is operating in certain zones, the yaw system turns the nacelle from the wind direction, and the yaw regulator creates a fake yaw error to restrict power and the rotor speed. Since the yaw system is mechanical, it is not as quick as an electrical regulator (Mohammadi et al., 2018).

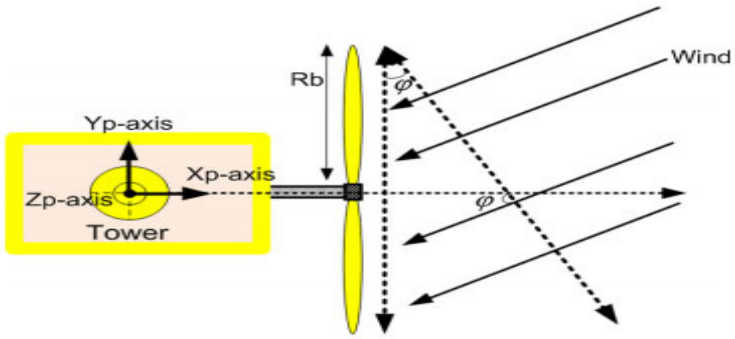

Figure 2. 24: Yaw Control Mechanism. (Mohammadi et al., 2018)

2.10.4 Power electronic control

The power electronics-based control of wind turbines does not involve any changes in the turbine blades' positions or a mechanical control scheme. Instead, the electrical load changes with power electronic controllers, and the generator rotor speed is automatically modified to track the maximum power using a maximum power tracking system. A vector control method is employed where control is done on the rotor flux reference frame. Figure 2.25 shows the machine side converter control system's schematic. The MPPT controller produces the reference speed ω*, set as the command speed for the speed control loop of the machine side converter control system to track the maximum power (Thongam et al., 2009).

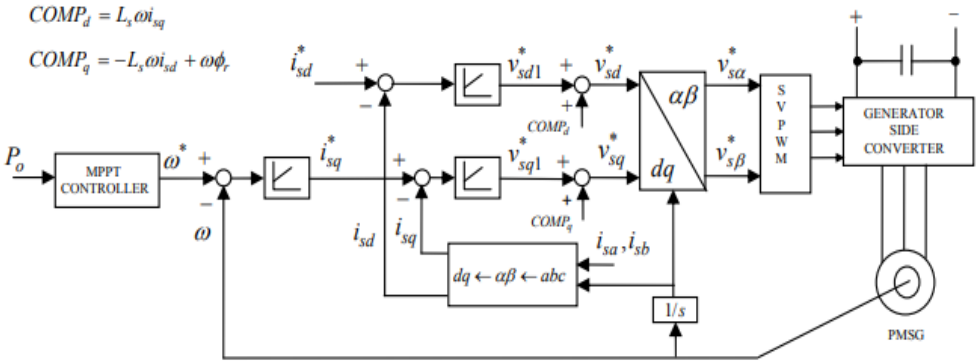

Figure 2. 25: Schematic of machine side converter controller. (Thongam et al., 2009)

2.11 Maximum Power Point Tracking (MPPT) Algorithms

The concept of Maximum Power Point Tracking (MPPT) is employed to augment the turbine output power and modifies the generator speed. Based on the wind speed, the MPPT changes the power transferred so that the turbine can operate at the maximum power (Barote & Marinescu, 2010). Figure. 2.26 shows the block diagram of the control system with the MPPT system. It includes a PI controller to regulate the inductor current, whose current reference value is provided by the MPPT system.

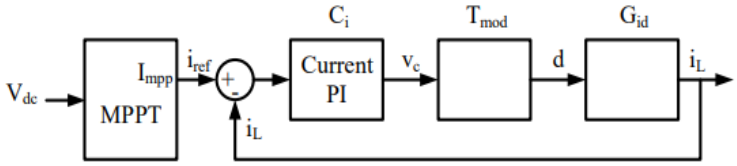

Figure 2. 26: PI with MPPT Control of Boost Converter System. (Zammit et al., 2018)

Generally, an MPPT algorithm inputs the DC link current and voltage to deliver the necessary MPPT current at the output side. This current serves as the reference current to the current controller. In SWTs, maximum power point tracking controllers are used for better energy extraction and faster convergence. In DC SWTs, the peak

power is often obtained by inserting a DC-to-DC boost converter between the SWT and the load, as shown in Figure 2.27. Various methods are used for MPPT. The most commonly employed wind turbines are optimal torque control, power signal feedback control, tip speed ratio control, perturbation and observation control, and incremental conductance.

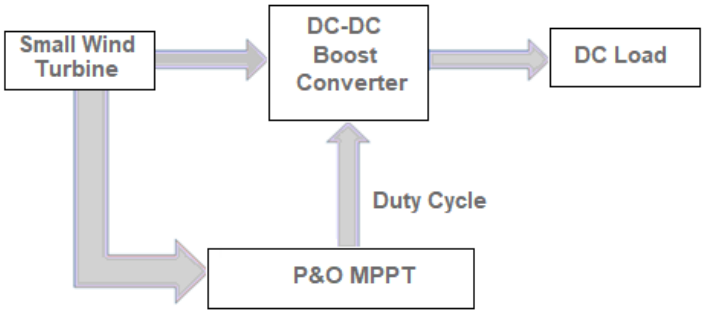

Figure 2. 27: SWT supplying a load via a boost converter controlled from a P&O MPPT.

2.11.1 Optimal torque control (OT)

The optimal torque control is a classic and simple MPPT technique generally implemented in commercial wind turbines. The technique relies on imposing the torque based on the rotor speed and requires only a sensor to measure the shaft speed. Optimal torque control is commonly used as a baseline for comparison with other MPPT controllers. The schematic of optimal torque control is shown in Figure 2.28.

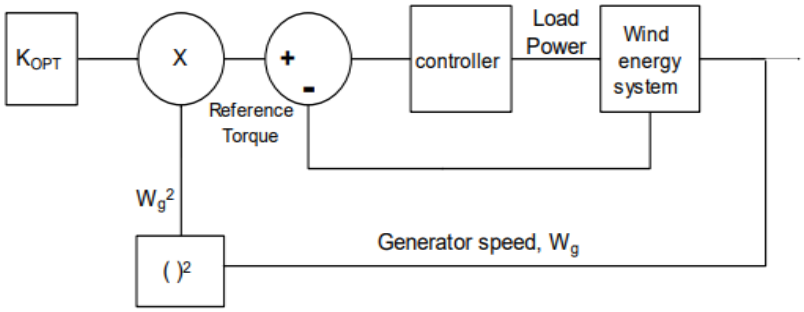

Figure 2. 28: Optimal torque control diagram. (Ali M. Eltamaly, 2012)

2.11.2 Power signal feedback control (PSF)

The schematic of power signal feedback control is depicted in Figure 2.29. This control technique requires the reference optimum power curve of the wind turbine from the experimental results. The maximum power operating points and their corresponding wind turbine speeds are kept in a lookup table.

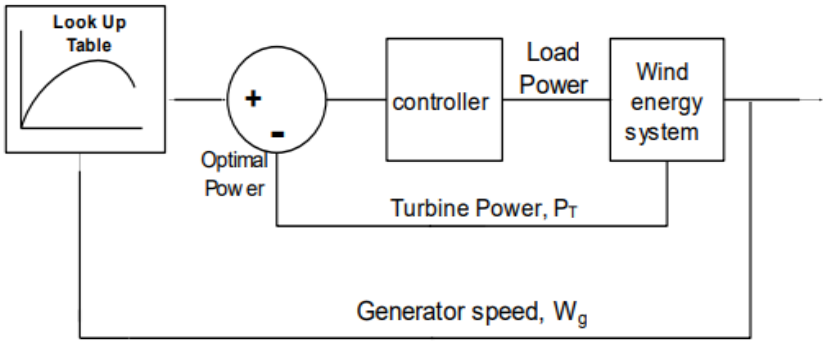

Figure 2. 29: PSF MPPT Control Diagram. (Ali M. Eltamaly, 2012)

2.11.3 Tip speed ratio (TSR) control

The optimal TSR is always a fixed value, even when the wind speed varies (Figure 2.30). Its schematic is shown in Figure 2.31. Whenever a wind turbine operates at its optimal TSR, the power extracted from the conversion is the maximum. MPPT technique forces the system to operate at its optimal TSR by comparing this TSR with the real value and inputting the error into the MPPT controller. The system reacts by modifying the generator speed to minimise this error. Although the technique is basic as wind speed is estimated directly, an exact measurement for wind speed is impossible, and the system's price increases.

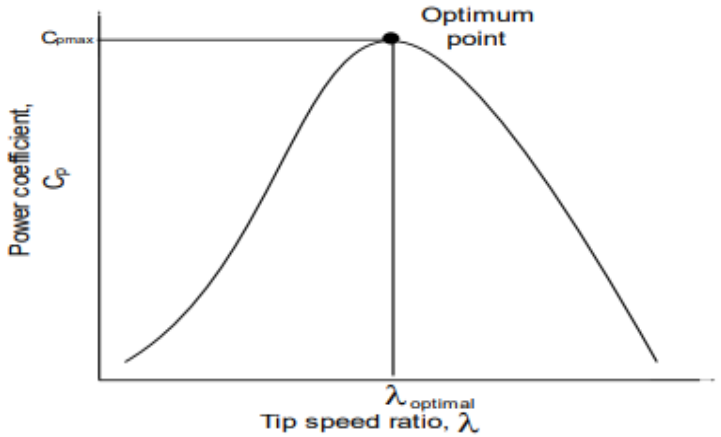

Figure 2. 30: Power Coefficient versus Tip Speed Ratio.

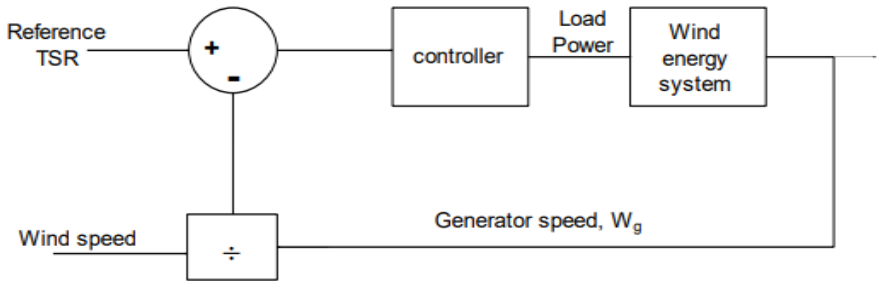

Figure 2. 31: Tip Speed Ratio MPPT Control Diagram. (Ali M. Eltamaly, 2012)

2.11.4 Perturbation and Observation (P&O) control

The P&O technique is based on the search-remember-reuse principle for finding the optimal power point. The technique starts functioning by perturbing a small step-size control parameter and observing the subsequent modifications in the target function except if the slope gets to zero. However, this technique can lose its tracking capability in case of changes in wind conditions. Additionally, the perturbation step size decision can complicate and deteriorate the operation. In summary, the P&O concept depicted in Figure 2.32 is based on the following consideration:

Given dp and dv the variation in power and the variation in voltage respectively, for dp > 0 and dv > 0, the power is located in the left side of the maximum power point. Hence, the voltage must be increased. Furthermore, for dp < 0 and dv > 0, the power is located in the right side of the maximum power point, and the voltage must be decreased. The flowchart of the P&O algorithm is shown in Figure 2.33.

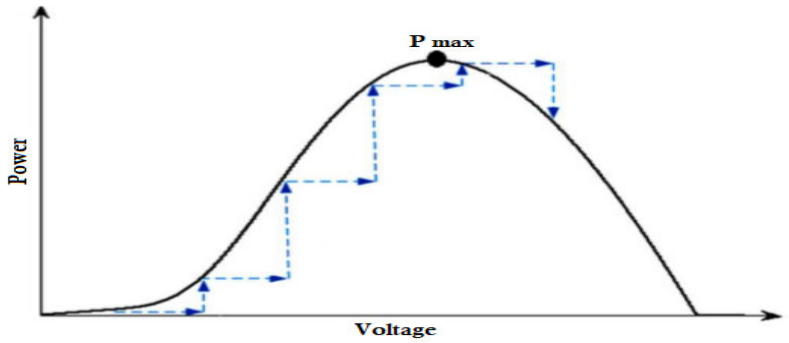

Figure 2. 32: P&O Control Process. (Badreddine et al., 2014)

2.11.5 Incremental conductance (IC)

The incremental conductance technique is a common MPPT algorithm which consists of ascertaining the optimum point by making a correlation between current conductance $\frac{I}{V}$ with the incremental conductance $\left(\frac{dI}{dV}\right)$ and continues knowing that the slope of power versus voltage characteristic is zero at maximum power point and that the power is given as the product of the current and the voltage. The incremental conductance method is defined by the following equations (Yu & Liao, 2015):

$$\left(\frac{dP}{dV}\right)mpp = \frac{d(VI)}{dV} \tag{2.8}$$

$$I + V\left(\frac{dI}{dV}\right)mpp = 0 \tag{2.9}$$

$$\left(\frac{dI}{dV}\right)mpp = -\frac{I}{V} \tag{2.10}$$

Equation 10 represents the principal condition to realise the maximum power point, when the variance of the output conductance is equal to the negative of the output conductance. The flowchart of the incremental conductance method is depicted in Figure 2.33.

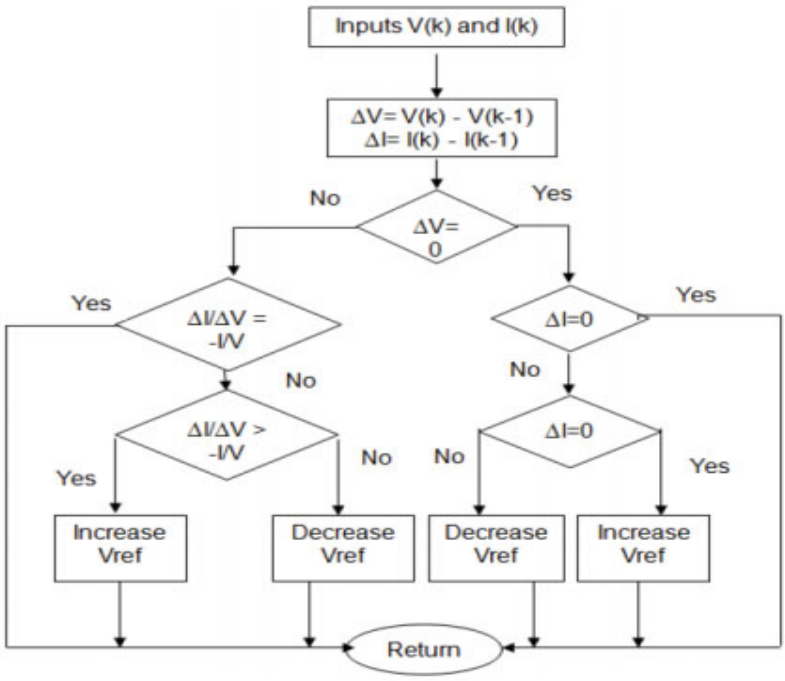

Figure 2. 33: Flowchart of incremental conductance method. (Masood et al., 2015)

2.11.6 Comparison of two MPPT techniques

Among the MPPT techniques considered in this section, P&O and IC are the most used ones. The P&O algorithm is simple and requires a lot of hardware compared to other techniques. However, in this technique, the power losses are slightly higher than other techniques because of the oscillating wind turbine's output around the maximum power point. Similarly, the IC technique has better control with low fluctuation. However, it requires more hardware. The technique can achieve a steady-state before the P&O method. However, the results obtained from both algorithms are similar.

2.12 Summary

This chapter provided an overview of the islanded mode operation of DC microgrids and small-scale wind turbines including their components and current market. A section dedicated to wind energy conversion principle and operation was presented. Additionally, sections on power electronic converters for wind turbines and voltage flow stability and control compared with the other methods were also considered. Lastly, a review of wind turbine power control approaches and maximum power point tracking algorithms were presented.

CHAPTER THREE
SMALL WIND TURBINE DESIGN TECHNOLOGY IN A DC MICROGRID

3.1 Introduction

Generally, SWTs comprise components such as a rotor with a variable number of blades to convert the power from wind to mechanical power, an electric generator, control and protection systems, and power electronic interface for feeding electricity into a battery bank, a utility grid, or into an immediate application such as a water pump (Hau, 2006) (Chowdhury, 2014). The generator is the major component of a small wind turbine and converts the mechanical power into electricity. There is extensive interest in using of the multiple-pole permanent magnet synchronous generators operated from a wind turbine shaft with no gear system (Yin Win, 2014).

A permanent magnet generator does not necessitate an excitation regulation, and its output voltage is proportional to the rotor speed. Hence, in the control of a wind turbine, the rotor speed is obtained by measuring of the output voltage. The continuous variation of wind speed will lead to a DC link voltage variation in an uncontrolled way. To obtain variable speed operation and stable DC bus voltage, a DC-to-DC boost converter could be placed in the DC link (Blaabjerg et al., 2007). Since there is a unidirectional active power flows from the PMSG to the DC link via a power converter, only a simple diode rectifier can be used to the generator side converter to acquire a cost-efficient arrangement (Nayar & Dehbonei, 2008; Pathmanathan et al., 2008).

The concept of microgrids has gained lots of interest because of the progress of renewable energy technologies. A microgrid can be designed to incorporate different types of renewable sources and energy storage units controlled by an observing method to provide quality power to the loads (Barra et al., 2020). This chapter deals with the design considerations of a DC microgrid based on an SWT. The topics covered in this chapter include a brief investigation on a standalone small wind turbine in DC microgrids, including the site selection, the technologies, the power electronic converters topologies, and their maximum power point techniques.

3.2 Standalone SWT in DC microgrids

As stated previously, DC microgrids have gained interest recently as they do not present several technical challenges compared to AC microgrids. Furthermore, DC microgrids facilitate smooth communication between DC sources, and as a result, there is a decrease in power wastage and losses. The standalone DC microgrid adopted in this research comprises an SWT with a PMSG, an AC-to-DC converter, a DC-to-DC converter, a battery bank, and a DC load can represent an LED lighting and other appliances at a residential. No standard value of voltage is currently available. However, most DC microgrids usually use 24 V or 48 V due to safety reasons, battery

bank requirements, power converter selection, and improved reliability (Dragicevic et al., 2014). DC microgrids appear to be the solution to obtain high-power quality.

Power converters have significant roles to play in microgrids since they link various renewable generators and transfer energy between different microgrid components. Semiconductors including diodes, switches, and passive components such as inductors, resistors, and capacitors are the major elements of power converters.

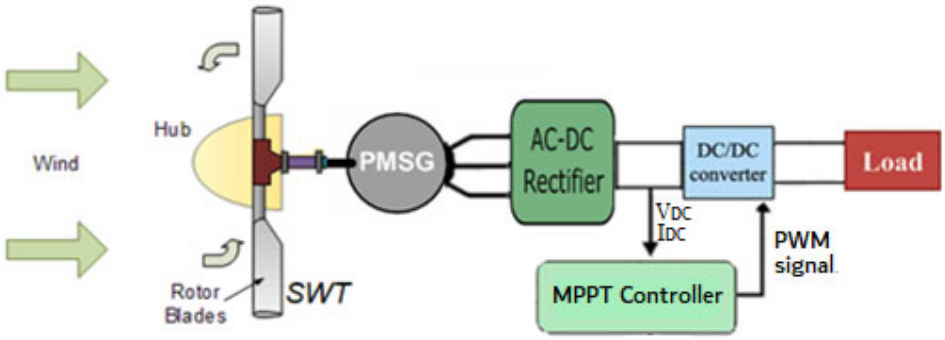

Figure 3. 1: SWT in a DC Microgrid. (Belakehal et al., 2009)

Figure 3.1 illustrates a DC microgrid supplying a load. The topology is often adopted in SWTs powering lighting systems as well as electric vehicle charging stations. The MPPT controller is used to control the power converter to provide maximum output power. Depending on the SWT's voltage, the power converter can be either a boost or a buck converter. Usually, the system also includes an energy storage unit linking the DC bus to feed the load whenever the SWT output power fluctuates due to the variation of speed wind.

One of the biggest issues for voltage standardisation in DC microgrids is the use of various voltage levels in distributed generation with residential, commercial, and industrial loads. For instance, with no voltage standards, it is difficult to standardise appliances and devices supplied with power directly from DC microgrids. Table 3.1 provides the preferred voltage levels in the main applications (D. Kumar et al., 2017).

Table 3. 1. DC power application with their preferred voltage level. (D. Kumar et al., 2017)

No	Application	DC Voltage (V)
1	USB and other small electronic equipment's	≤ 5
2	Cars, desktop computer	12
3	LED, trucks, fans	24
4	Future PV units	48
5	Telecom	48
6	Power over Ethernet	50
7	Batteries	110/220
8	Data centre	380
9	Electric vehicle charging stations	400
10	Future distribution systems for residential and commercial buildings	350-450
11	Industries and transportation	600-900
12	Traction, marine and aircraft systems	1000-1500

3.3 Site selection for SWTs

For instance, the presence of obstacles, such as large trees or tall structures, can prevent proper airflow, making vortexes that can decrease any wind turbine's performance. It is imperative to give a lot of consideration while picking the site to erect the structure for wind turbines, keep the turbine at a minimum point from the surrounding obstacles, and the goal that the rotor's lowest bottom is put higher than the most elevated obstacle. In general, the wind turbine needs to be 30 ft (9 metres) above any object, as shown in Figure 3.2. Besides that, the length of wires connected from the wind turbine to load must be taken into consideration to avoid power losses because of the resistance and heat of the wires (Rosato, 2019).

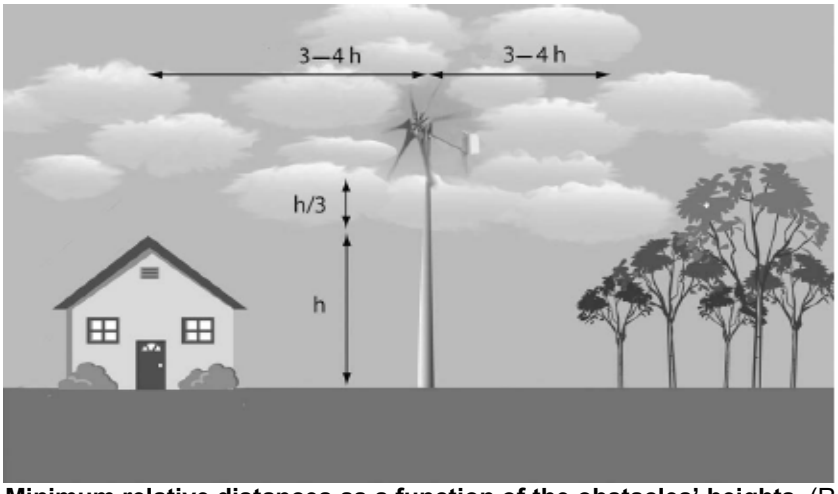

Figure 3. 2: Minimum relative distances as a function of the obstacles' heights. (Rosato, 2019)

3.4 SWT technologies

SWTs consist of a wind turbine converting wind energy into mechanical energy. The shaft of the turbine is linked to the shaft of a PMSG via a gear system. The gear system transmits the rated torque to the generator, and the generator develops the rated power to supply loads. A typical layout of an SWT is shown in Figure 3.3.

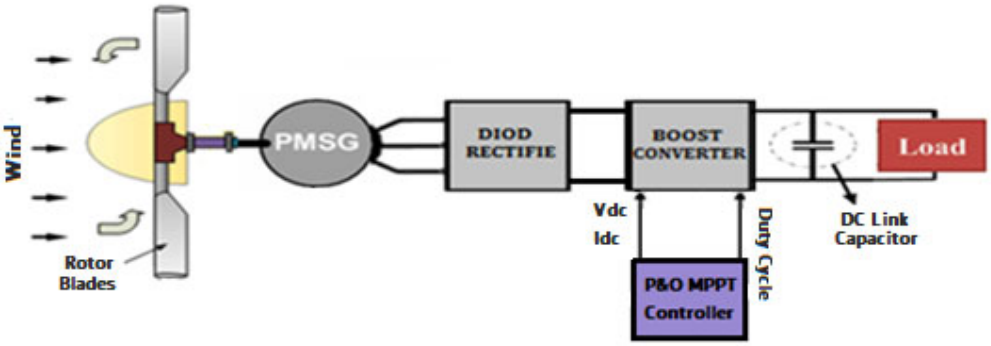

Figure 3. 3: Model of SWT DC microgrids.

3.4.1 Horizontal-axis SWTs

The rotors of the horizontal axis of SWTs are mounted perpendicular to the tower axis. Hence, the rotor axis is parallel to the ground axis, as shown in Figure 3.4, which includes two SWT configurations, namely upwind and downwind configurations.

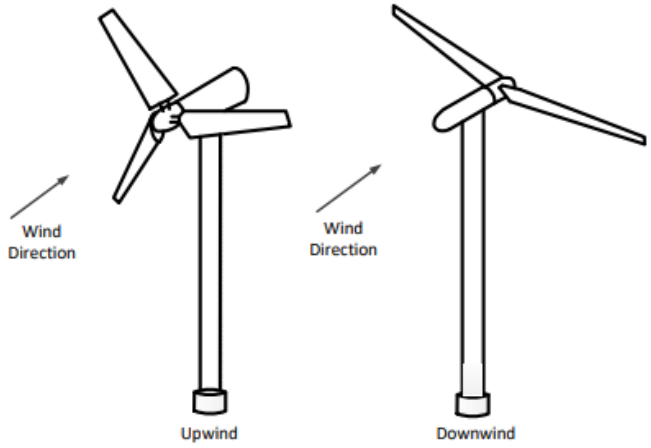

Figure 3. 4: Upwind and Downwind HAWTs. (J.F. Manwell, 2002)

In upwind SWTs, the rotor faces the incoming wind directly, hence, avoiding the wind shade behind the tower. Upwind SWTs have some loss of power from the interference because of the air bending around the tower before passing through it. In downwind SWTs, on the other hand, the rotor is on the backside of the turbine. The nacelle seeks

the wind. Hence there is no need for a separate yaw system. Their rotor blades are flexible as there is no danger of a tower strike. (Reddy et al., 2015)

3.4.2 SWTs characteristics

In SWTs, the amount of kinetic energy stored can be expressed mathematically as (Nayak & Vinod, 2017):

$$\boldsymbol{E = \frac{1}{2}\,\rho A C_p V_w^3} \tag{3.1}$$

where $\boldsymbol{\rho}$ is the density of air, $\boldsymbol{V_w}$ is the wind speed, $\boldsymbol{A}$ is the volume of air at the cross section of wind turbine.

The cross-section of the air in interaction with the rotor per second, is equal to the rotor's cross-section. Likewise, the thickness of the air stream is equivalent to that of the wind velocity. The conversion efficiency is close to 60 %. It can be examined as a portion of kinetic energy supplied to the rotating part, while the remainder of the energy is wasted. The overall energy so converted is mathematically correlated to the power coefficient, which a function of several components, such as blades configuration, rotor, setting, etc. Therefore, optimised power coefficient is obtained through the precise and accurate arrangement of these components.

In SWTs, the pitch angle is assumed to be zero. Therefore, the power coefficient characteristic depends on the thrust force, tip speed ratio, and the rotor torque from the rotor blades. The ratio of the torque generated, and theoretical torque refers to the torque coefficient. The power generated by the rotor is dependent on the tip speed ratio. The dynamic between the wind stream and the rotor affects the rotor efficiency in the power extraction. The power coefficient versus the tip speed ratio characteristic gives the rotor performance irrespective of the rotor and site features' size. From Figure 3.5, it can be seen that the power coefficient raises with the increase of the tip speed ratio. However, when the tip speed ratio raises above its optimised value, the power coefficient declines at the same slope.

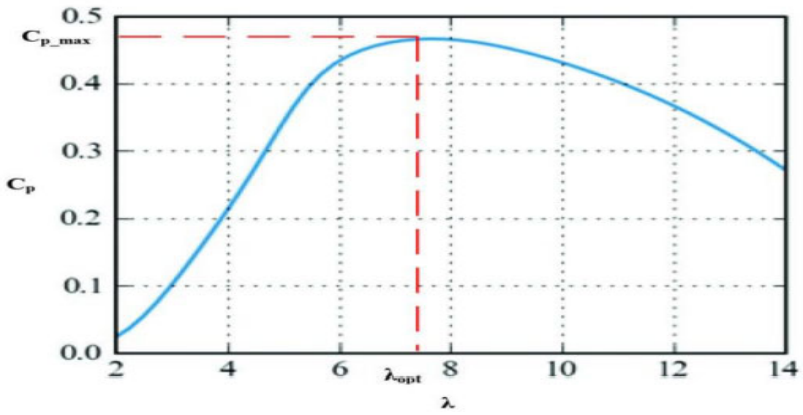

Figure 3. 5: Power coefficient versus tip speed ratio. (Swapnil S. Sonekar, 2020)

3.4.3 Variable-speed SWTs

In variable-speed SWTs, the generators are indirectly connected to the utility grid or individual loads through power electronic units that provide decoupling and control of the system (Blaabjerg et al., 2007). The generator used in SWTs is the PMSG. This type of generator is compact, reliable, has high efficiency, and does not require external excitation (Díaz et al., 2009). Unlike induction generators, PMSGs do not require external windings to produce rotor flux; the machine's flux is supplied by its permanent magnets (Bin Wu, Yongqiang Lang, Navid Zargari, 2011). Since PMSGs do not require bulky rotor windings (like those used in Wounded Rotor Synchronous Generators) to produce the necessary magnetic flux, they can be significantly more compact. Also, the permanent magnet structure of PMSGs enables designers to incorporate a larger number of magnetic poles into the machine (Bin Wu, Yongqiang Lang, Navid Zargari, 2011). As a direct result of the larger number of poles, these multi-pole PMSGs can operate at low-speeds (Chen et al., 2009). These low-speed multi-pole PMSGs enable eliminating the gearbox since the turbine's low-speed shaft can directly drive them. The elimination of the gearbox reduces the overall wind turbine system size and cost while increasing reliability (Chen et al., 2009). With the permanent magnet material cost steadily decreasing, PMSGs have also become attractive for large MW wind turbines (Yang et al., 2012). Therefore, to evaluate the proposed MPPT algorithm and the power management control scheme for a standalone wind turbine system, the PMSG based wind energy system has been selected for this study.

Another benefit of variable-speed operation is the decrease of stress on the turbine shafts and gears since the blades absorb the wind torque peaks during the changes of the SWT speed of rotation (Padmanabhan & Kaliyappan, 2014). The drawback of variable speed operation is that a power conditioner must be employed to play the wind turbine's role apparent load. However, the evolution of power electronics helps reduce

the power converter cost and increases its reliability, while the energy production gain balances the higher cost. The torque curves of the SWT, consisting of the interconnected wind-turbine/generator system, for various generator output voltage levels under different wind speeds, are shown in Figure 2.11. The generator is designed to operate in a linear zone corresponding to the straight portion of the generator torque curves under any wind-speed condition.

The generator torque is regulated in the optimum torque curve in Figure 3.6 based on the generator speed. The generator acceleration or deceleration is defined by the difference between the turbine torque T_m and generator torque T_g. For the generator speeds less than the optimal speed, the turbine torque will be larger than the generator torque, and the generator will accelerate. The generator will decelerate for the generator speeds higher than the optimal speed. Therefore, the turbine torque and generator torque will settle down to the optimum torque point T_{m_opt} at any wind speed, and the wind turbine will operate at the maximum power point (Haque et al., 2009).

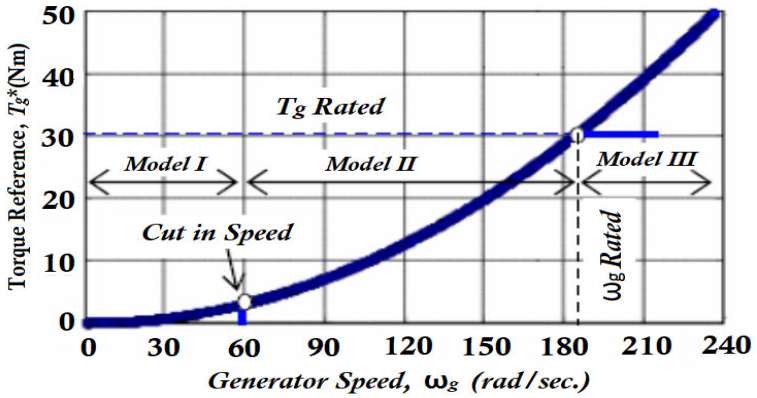

Figure 3. 6: Wind turbine torque vs. rotor speed.(Haque et al., 2009)

3.4.4 Permanent magnet synchronous generator (PMSG)

As stated above, in this type of generator, the excitation field is provided by a permanent magnet, unlike a coil in a synchronous generator. The speed of the rotor and speed of the magnetic field is equal to synchronous speed. Two types of PMSGs based on the rotor configuration can be distinguished: the salient pole and cylindrical rotor type. In the salient pole rotor, air gap flux changes based on the rotor's shape, whereas in the cylindrical rotor, the magnitude of air gap flux remains steady. Hence, magnetic strength and structural strength are better in the case of cylindrical rotors. The windings are inserted in the rotor slots. The cylindrical rotor provides better dynamic balancing than a salient pole rotor. Hence, it is appropriate for fast turbo generators. The rotor poles project outside from the rotor's centre, whereas the cylindrical rotor is employed in salient pole machines with two or four-poles.

Consequently, the salient pole rotor is utilised in low-speed hydropower generators. Due to the constant air gap flux, the magnetomotive force's permeance is not dependent on the rotor poles and the magnetomotive force axis angle. In the salient pole rotor type, the permeance varies with the magnetomotive force axis and the rotor poles angle because of variation in air gap flux. Therefore, due to its several benefits, the cylindrical rotor is the most employed. Because of constant nature, it is trivial to model the machine and analyse its operation. The expression linking the frequency of the generator and rotor speed is given as (Acharya et al., 2016):

$$\boldsymbol{f} = \frac{\boldsymbol{pn_s}}{\boldsymbol{120}} \tag{3.2}$$

where f is the frequency, $\boldsymbol{n_s}$ is the speed of the rotor and p the number of poles

When linked to an isolated load, a synchronous generator acts as a voltage source whose frequency is determined based on its prime mover speed. Generally, synchronous generators are connected in parallel via transmission lines. The system is expected to keep synchronism despite mechanical and electrical stress. The benefits of such an interconnected platform are the security of power supply and low capital cost. Industrial applications of synchronous motors are in constant speed operations. Another benefit of employing synchronous motors is the easy control of power factor by varying the field current. Therefore, most industries use the synchronous motors as loads leading the power factor to produce a high-power factor.

The magnetisation curve is linear if the permeability of iron is considered infinite. The relationship between the magnetomotive force and the flux per poles is given as (Ayodele et al., 2017):

$$\emptyset_{\boldsymbol{f}} = \boldsymbol{pF_f} \tag{3.3}$$

Where ϕf is flux per poles.

The torque can be determined as:

$$\boldsymbol{T_t} = \frac{\boldsymbol{\pi}}{\boldsymbol{2}}\left(\frac{\boldsymbol{p}}{\boldsymbol{2}}\right)^{\boldsymbol{2}}\emptyset_{\boldsymbol{f}}\boldsymbol{F_f}\,\boldsymbol{\sin\delta} \tag{3.4}$$

Where δ is the angle by which $\boldsymbol{F_f}$ leads $\boldsymbol{F_r}$

The electromagnetic torque acts on the field poles towards rotation to deliver the mechanical power, hence, functioning as a motor. On the other hand, if the output

voltage is similar to the air gap of the electromotive force and its frequency is kept constant by an external three-phase supply, the machine operates as a generator or motor based on the shaft mechanical conditions. The equivalent circuit of the electrical machine operating as a generator is shown in Figure 3.6.

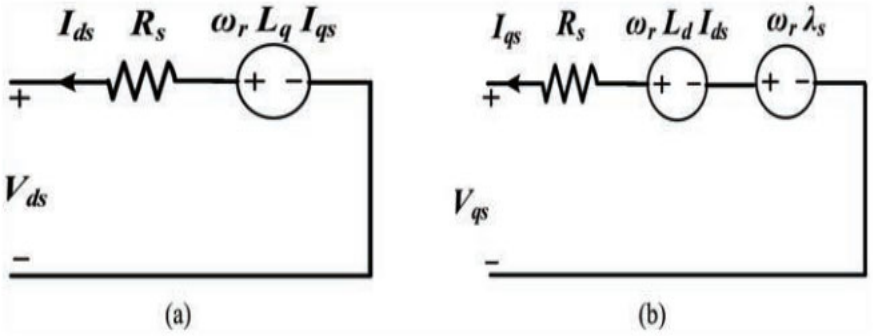

Figure 3. 7: Circuit diagram of PMSG. (Jain et al., 2018)

3.5 Power converters for SWTs

Various power converter topologies for SWTs have been proposed. However, all of them have advantages and disadvantages. The most widely used topology in SWTs for converting AC power to DC is the unidirectional phase-phase diode rectifier. The three-phase diode rectifier combined with a DC-to-DC converter is often selected over the active rectifier topology due to lower circuit cost, lower controller complexity, and higher reliability (Baroudi et al., 2007)(De Freitas et al., 2016). The DC-to-DC converter is employed to achieve maximum power extraction. A variable speed SWT with power electronics conversion linked to a DC load is shown in Figure 3.7.

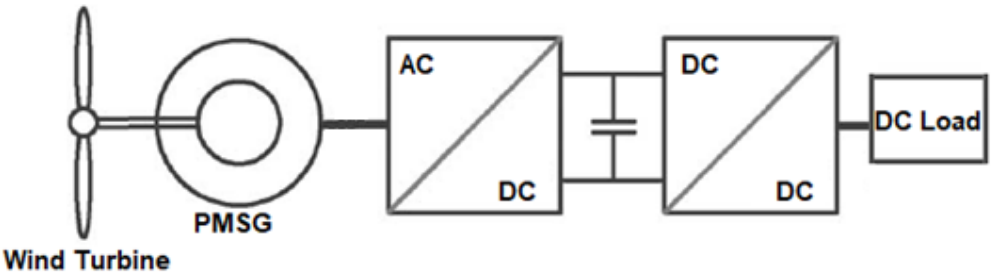

Figure 3. 8: Power converter interfacing a wind generator.

3.5.1 Three-phase diode rectifier

The three-phase diode rectifiers are commonly employed to convert the AC power produced by the generator into its corresponding DC power. A capacitor serves as a voltage filter. In general, rectifiers are designed from elements such as diodes, IGBTs, MOSFET and thyristors. Rectifiers designed from diodes are referred to as uncontrolled rectifiers.

Rectifiers are classified as half-wave and full-wave rectifiers. An half-wave rectifier rectifies either a positive or a negative half cycle of an AC signal. In contrast, the full-wave rectifier rectifies both the positive and the negative cycles of an AC input wave. Figure 3.8 depicts a full-wave three diode rectifier receiving AC power from an SWT using a PMSG.

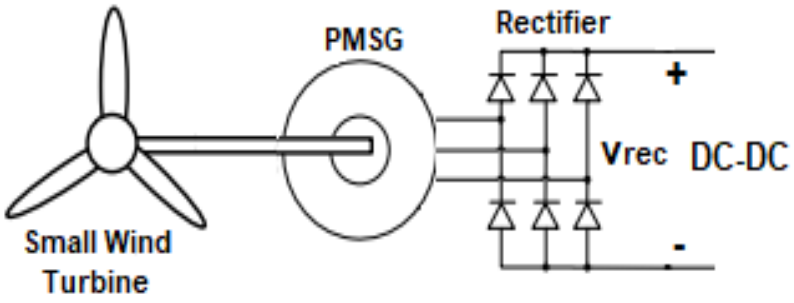

Figure 3. 9: PMGS connected to three-phase diode rectifier.

Generally, a three-phase diode rectifier comprises two sets of diodes. One set is connected to the positive DC output, and the other one is connected to the negative terminal of the DC output. The previous set of diodes are in on-state during the positive half cycle, while the latter set of diodes are switched on during the second half cycle.

The design of uncontrolled bridge rectifiers involves a proper selection of diodes to obtain the correct blocking voltage, which refers to the maximum reverse voltage that the diodes comprising the rectifier can handle. Moreover, diodes must be sized to handle the maximum conduction current even in the event of a surge. The conduction current refers to the current that passes through a diode as it is forward biased. Besides diodes, such a rectifier should include a smoothening filter to obtain a smooth DC output and a heat sink for thermal management.

3.5.2 DC-to-DC boost converter

The DC-to-DC converter considered in this research is a boost converter, which is used to step up the voltage of an SWT DC microgrid to supply residential appliances in case of a power cut. The boost converter is expected to provide 240 VDC to a 3 kW load. By boosting the voltage to 240 VDC, the output current will be reduced, reducing thermal losses due to the current.

The general layout of a boost converter is depicted in Figure 2.20 and consists of a diode, a switch, and an energy storage device. Generally, an IGBT is used as the switching element, while the inductor serves as an energy storage unit.

When a boost converter is controlled from an MPPT controller, it boosts the voltage and controls it to reach the MPP. The MPPT produces the precise duty ratio used to drive the boost converter to an appropriate direction to reach the MPP as fast and as accurately as possible.

3.6 Analysis of adopted MPPT Control Technique

The adopted MPPT is based on directly modifying the duty ratio of the DC-to-DC boost converter. In a fixed step size-based P&O technique, to decrease oscillation around the operating point, the duty ratio of the converter can be changed by inserting a step size ΔD at every sample depending on the operating conditions. The MPPT can be obtained when the following equation is satisfied:

$$\frac{dP_{dc}}{dV_{dc}} = \mathbf{0} \tag{3.5}$$

where $\boldsymbol{P_{dc}}$ and $\boldsymbol{V_{dc}}$ are the DC link power and voltage respectively.

The curve $\boldsymbol{P_{dc}}$ versus $\boldsymbol{V_{dc}}$ has only a single operating point where the maximum power can be achieved. Therefore, the maximum power point tracking can be performed through a step by step search rather than considering parameters such as the wind speed.

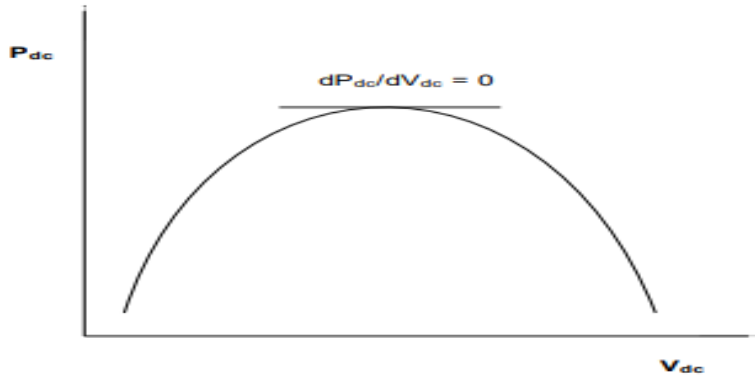

Figure 3. 10: DC Link Power vs DC Link Voltage. (Badreddine et al., 2014)

The duty ratio modification follows by the slope's direction $\frac{dP_{dc}}{dV_{dc}}$; it raises in the high-speed zone of the generator characteristic (Figure 3.9). Thus, the generator rotor-speed reduces, and the power raises until the controller reaches the MPP. Similarly, when the initial point is in the low-speed zone, following the slope direction $\frac{dP_{dc}}{dV_{dc}}$, which results in a decrease of the duty ratio. Thus, the generator rotor speed is increased slowly, and the controlling variable tends toward the MPP.

3.6.1 SWT-based DC microgrid with P&O MPPT control

A schematic of an SWT-based DC microgrid with P&O MPPT control is shown in Figure 3.10

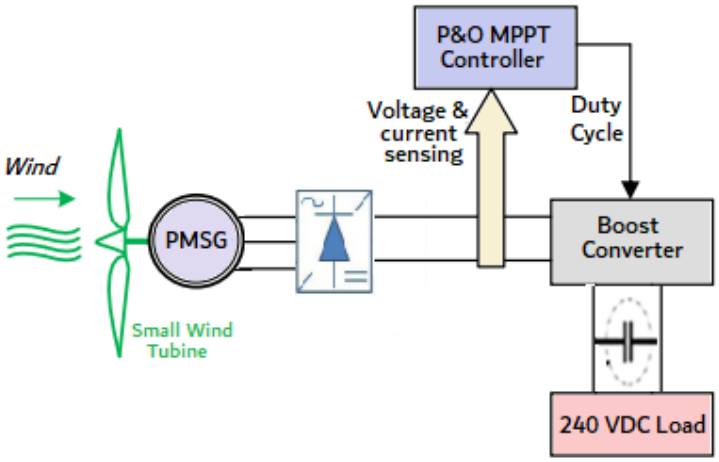

Figure 3. 11: SWT-based DC microgrid with Used P&O control.

The P&O technique is a proficient optimisation method based on searching for a given function's local optimum point. It is utilised for the searching of the ideal operating point. Thus, it assists in maximising energy extraction. This method is based on inserting a small step size change in a control variable and observing the objective function adjustments until the slope of the function gets to zero. As illustrated in Figure 3.11, the controller directs the working point by finding the position and the distance between the working point and the peak point. The working point moves towards the right if it is in the extreme left zone and vice versa. In this technique, the boost converter's duty ratio is perturbed, and the DC link power is observed. The method does not require a wind speed measurement; hence, mechanical sensors are not needed.

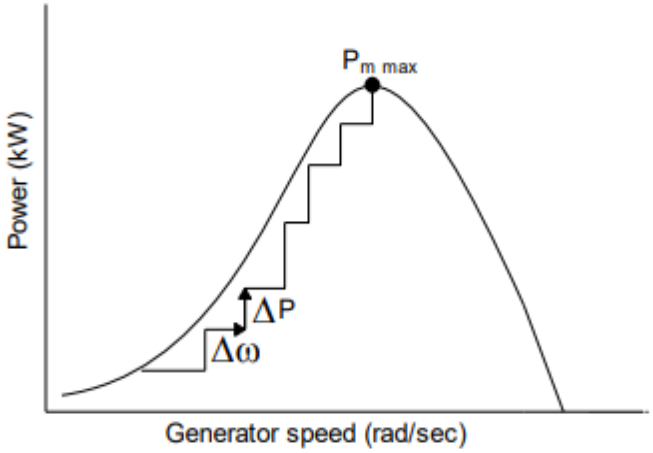

Figure 3. 12: Power versus speed. (Muhammad et al., 2011)

An adjusted P&O MPPT algorithm has been suggested to realise quick MPP tracking under a rapid wind speed change. The recommended MPPT technique requires no information on wind turbine parameters or mechanical sensors. The algorithm is utilized in two operating modes to manage the previously mentioned limitations of the conventional P&O technique. Shifts from one operating mode to the next are done based on the variation of the wind speed. The ordinary P&O technique with a small step size cannot track the MPP under the slow wind speed variation. At the same time, a predictive mode is switched if a fast wind speed is observed to shift the operating point fast around the MPP. DC link voltage change is utilised to identify rapid wind speed variation.

The P&O algorithm operation is as follows:

In the first step, the power is determined using the voltage and current and then compared to the power's past value. In case the difference is equal to zero, the same voltage will be maintained, and the algorithm will try to oscillate around the same MPP. In case of a change of power, the algorithm will continue and verify the difference between both voltage levels. If the power difference is positive, the algorithm will lead the voltage into a similar direction by either increasing or decreasing it as in the previous case. Thus, if the voltage difference is positive, the algorithm will keep increasing the voltage and vice versa. However, if the power difference is, the algorithm will lead the voltage in the opposite direction. Hence, the voltage change will be negative, and the algorithm will increase the voltage. Lastly, in case the change in voltage is positive, the algorithm will reduce the voltage. The algorithm can control the operating voltage freely by changing the duty ratio. Any variation of the duty ratio will lead to an inverse effect on the DC-to-DC converter's input resistance and modify the operating voltage to fulfil the four cases.

3.6.2 Implementation of MPPT for a DC-to-DC boost converter

The output voltage of a DC-to-DC boost converter is dependent on the duty ratio. Figure 3.12 shows a layout of a boost converter controlled from an MPPT controller. The controller's input is connected to the voltage and current measurements from the SWT after the rectification stage. The power is then evaluated from these two parameters and compares with the previous value. The sign of the power determines the duty ratio output of the MPP controller. The duty ratio of the boost converter represents the control variable. Perturbing the duty ratio will result in the perturbation of the SWT current, and consequently, the SWT voltage will be perturbed. The range of the duty

ratio is limited between zero and ensures that the converter will step up the input voltage within the limit.

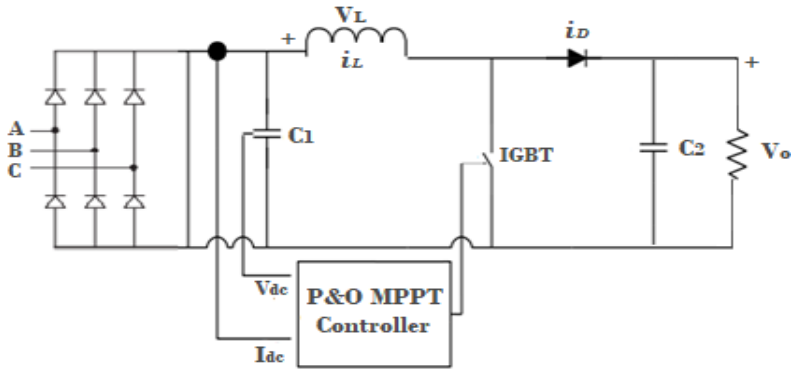

Figure 3. 13: Boost converter with P&O MPPT controller. (Chen et al., 2013)

The duty ratio must be chosen appropriately. Since the P&O technique oscillates around the MPP, reducing the duty ratio step can minimise the oscillation and the steady-state losses. However, the controller is less efficient when the atmospheric conditions change fast. The following equation expresses the duty ratio (Femia et al., 2004):

$$\alpha = \frac{T_{on}}{T_{on}+T_{off}} = \frac{T_{on}}{T} \tag{3.6}$$

Equation 3.6 provides the control law produced by the MPPT controller to operate the SWT at its MPP depending on the wind speeds. In case the operating voltage of the generator voltage is perturbed in a specific direction, and the perturbation shifts the operating point toward the MPP. The P&O algorithm would then carry on perturbing the generator voltage in a similar direction. In the event that the change in operating point shifts away from the MPP and the P&O algorithm reverses the direction of the perturbation. Therefore, the system operates by increasing or decreasing the operating voltage and observing its impact on the output power. The operating voltage is perturbed with every MPPT cycle. Once the MPP is reached, it will oscillate around the ideal operating voltage. For instance, if the controller senses that the input power increases and the voltage, it will decrease the voltage reference close to the MPP.

3.7 Summary

A microgrid can be designed to include various types of renewable sources and energy storage systems to operate either grid-connected or in standalone mode to provide power to loads. This chapter dealt with the design considerations of a DC microgrid based on an SWT. The topics covered in this chapter included a brief investigation on

a standalone small wind turbine in DC microgrids, including the site selection, the technologies, the power electronic converters topologies, and their maximum power point techniques.

CHAPTER FOUR
MODEL DESIGN DEVELOPMENTS

4.1 Introduction

This chapter is dedicated to the development of the SWT standalone DC microgrid model. The system is designed to operate as an auxiliary power entity for a residential building to provide power to appliances such as LED lighting, computers, variable speed drives, etc. to reduce or hinder power outages. Such SWTs are usually HAWTs attached in short towers of few metres or placed on top of buildings roofs, cellular communication towers, etc. In SWTs, the aerodynamic section is directly coupled to a PMSG without a gear system. The blowing wind causes the turbine to rotate and generate electricity. Such a system can improve applications' power supply, including residences, farms, schools, small commercial businesses, or even isolated community installations. They are practical and economical in places with high wind potential.

The SWT standalone DC microgrid generates 3 kW at 120 V, and it is expected that it delivers the 3 kW at 240 VDC. The system's structural representation is shown in Figure 4.1, which includes an SWT based on PMSG, a three-phase diode bridge rectifier, a DC link capacitor, and a DC-to-DC boost converter connected to a DC load. The role of the DC link capacitor is to maintain the voltage of the DC bus constant. To extract the maximum power and control the converter's output voltage, an adjusted P&O MPPT algorithm is used to drive the switching element to accomplish fast MPP tracking and maintain the voltage constant irrespective of wind speed variation.

To verify the designed system's effectiveness, a MATLAB Simulink model of an SWT DC microgrid was developed, and the results will be presented in the next chapter.

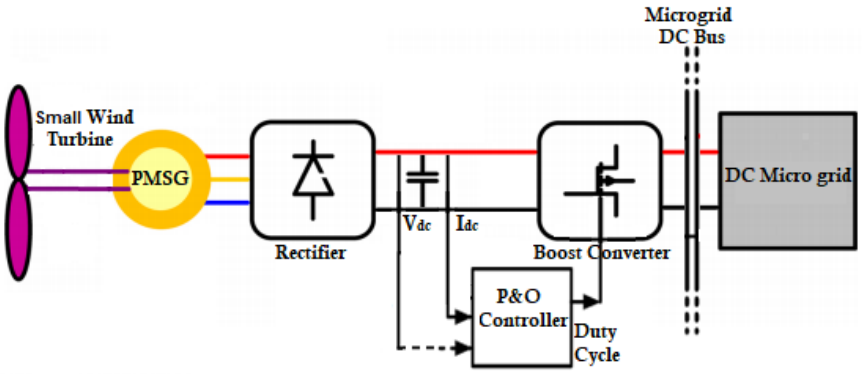

Figure 4. 1:Structure of Small Wind Turbine connected to DC microgrid.

This chapter focuses on the development of an SWT DC microgrid model. The first section is dedicated to the considered load profile presentation, while the next section focuses on wind aerodynamics modelling. Thereafter, the microgrid components such

as the permanent magnet synchronous generator, the full-bridge diode rectifier, and the DC-to-DC boost converter are modelled. The last section of this chapter covers the P&O MPPT controller's modelling to track the maximum power while also regulating the boost converter's output voltage.

4.2 Load Profile

The SWT DC microgrid considered in this study generates 3 kW at 240 VDC. It is expected to supply electric power to a household, including loads such as LED light, computer, mobile phone charger, television, printer, coffee maker, fan, radio, refrigerator, and hairdryer in the event of power cut from the main utility grid. The power requirement of each appliance, the number of each appliance, and their hours of operation are given in Table 4.1.

Table 4. 1: DC appliances used in one house.

Type of DC Equipment	Power (W)	Units	Time Per day per unit (hours)
led light	30	6	8
Laptop computer	65	2	5
Mobile phone charger	19	2	6
Television	133	1	6
Printer Laser	15	1	2
Coffee Maker	22	1	1
Fan	72	1	4
Radio	70	1	5
DC refrigerator	2040	1	24
Hair dryer	300	1	1

4.3 Model development

4.3.1 Wind turbine aerodynamic modelling

The relationship between speed and output power of wind turbine is given by the following equation (Daili et al., 2015):

$$P_m = \tfrac{1}{2}\rho A V^3 \, C_p \, (\lambda, \beta) \tag{4.1}$$

Where $\boldsymbol{\rho}$ air density at 1 atm equal to 1.225 $\boldsymbol{kg/m^3}$, $\boldsymbol{A}$ is the swept area in $\boldsymbol{m^2}$, $\boldsymbol{V}$ is the wind speed (m/s), $\boldsymbol{C_p}$ is the power coefficient dependent on $\boldsymbol{\lambda}$ given in equation and $\boldsymbol{\beta}$.

The power coefficient can be modelled as (John & Divya, 2016):

$$\boldsymbol{C_p(\lambda, \beta) = c_1 \left(\frac{c_2}{\lambda_i} - c_3\beta - c_4\right) e^{\frac{-c_5}{\lambda_i}} + c_6\lambda} \tag{4.1}$$

Where C_1 = 0.5176, C_2 = 116, C_3 = 0.4, C_4 = 5, C_5 = 21 and C_6 = 0.0068.

The relationship between the tip speed ratio and the pitch angle is given as follows (John & Divya, 2016):

$$\frac{1}{\lambda_i} = \frac{1}{\lambda + 0.089\beta} - \frac{0.035}{\beta^3 + 1} \tag{4.2}$$

The wind turbine mechanical torque τ_w can be modelled using the following equation (Ayodele et al., 2017):

$$\tau_w = \frac{P_m}{\omega} \tag{4.3}$$

Where ω is the rotor speed of the wind turbine.

Figure 4.2 shows the Simulink model of the wind turbine aerodynamics developed based on equations (2.2), (2.4), (4.1), (4.2) and (4.3).

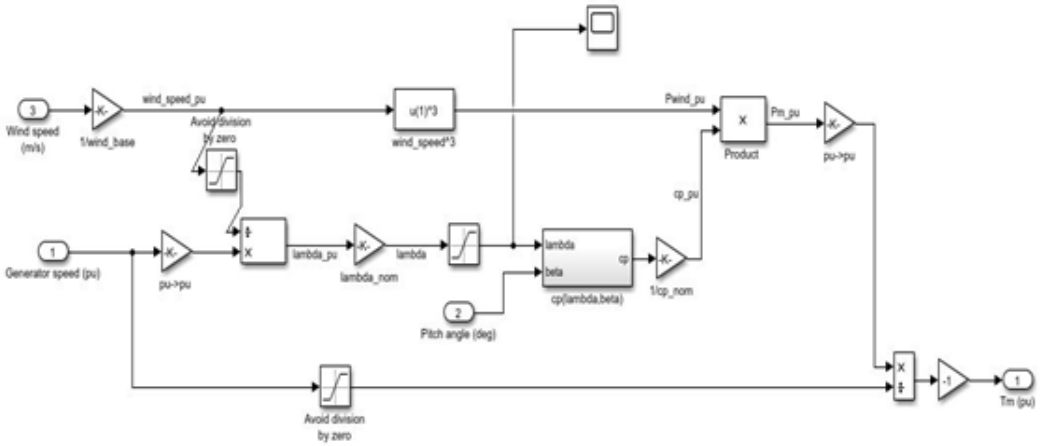

Figure 4. 2: Simulink model of wind turbine aerodynamics.

Generally, for wind turbines with a pitch angle equal to zero, the maximum power coefficient value is 0.48. Figure 4.3 shows the power characteristics curve of the SWT considered expressed per unit for various wind speeds when the pitch angle is equal to zero. The power coefficient is maximised for an optimum tip-speed ratio when the blades pitch angle is equal to zero. It is observed from Figure 4.3 that, for each wind speed, there exists a specific point in the SWT power characteristic where the power is maximum.

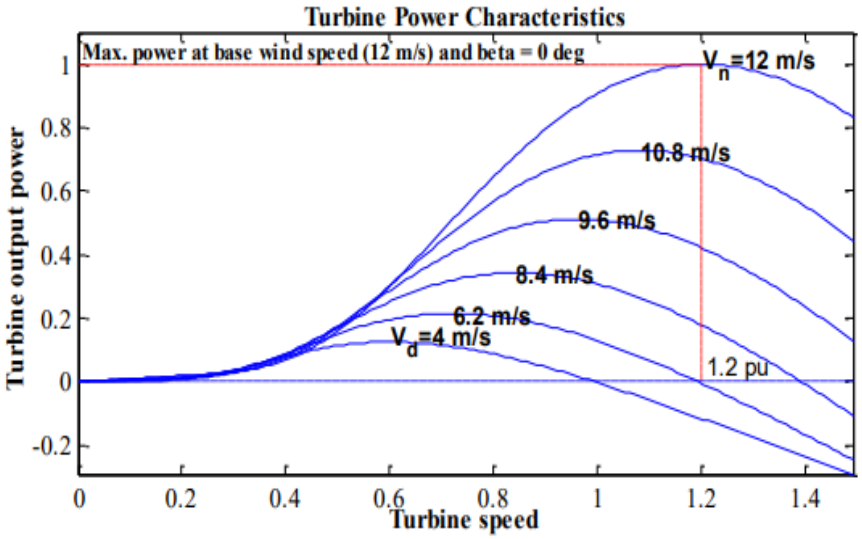

Figure 4. 3: Turbine power characteristic with MPPT.

The value of the tip speed ratio is constant for all maximum power points. The relationship between the optimum tip speed ratio and the rotational speed of the turbine $\boldsymbol{\Omega_n}$ is given as (Matayoshi et al., 2018):

$$\boldsymbol{\Omega_n = \lambda_{opt}\ \frac{V_n}{R}} \tag{4.5}$$

Where $\boldsymbol{V_n}$ is the wind velocity.

4.3.2 PMSG modelling

The dynamic of a PMSG can be represented using mathematical models of voltages, currents, and rotor speed of the generator. These models are parametric and can be employed irrespective of generator size. A circuit that describes the generator behaviour needs to be defined to develop these models, considering variables such as internal voltage, resistances, and reactance. Thereafter, the models can be transformed into equivalent circuits in two axis frames. In this section, the PMSG stator and rotor are modelled in the dq0 axis.

4.3.2.1 Dynamic model of the PMSG

Figure 4.4 shows the phasor diagram of the transformation abc to dq0 in which the d-axis is aligned with the north pole of the rotor, and the q-axis is 900 ahead of the d-axis to the direction of rotation.

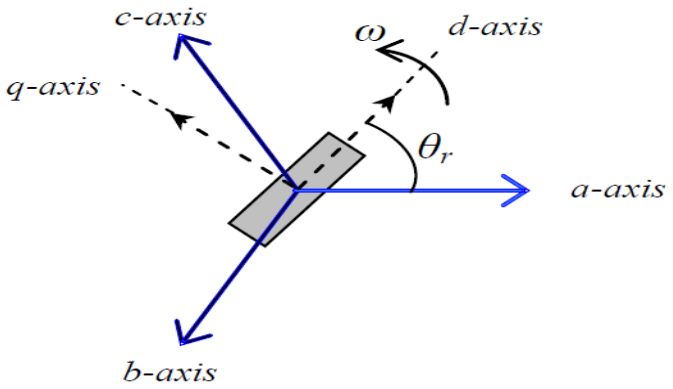

Figure 4. 4: : abc-dq axis.(Chowdhury, 2014)

The PMSG voltage in dq0 reference frame is given by equations In these equations below (4.6) and (4.7) as (Matayoshi et al., 2018):

$$\boldsymbol{v_d = R_d i_d + L_d \frac{di_d}{dt} - Lq\omega_e iq} \quad (4.6)$$

$$\boldsymbol{v_q = R_q i_q + L_q \frac{di_q}{dt} + L_d \omega_e i_d + \psi \omega_e} \quad (4.7)$$

Whereas the flux is expressed as:

$$\boldsymbol{\psi_q = L_q i_q} \quad (4.8)$$

$$\boldsymbol{\psi_d = L_d i_d + \psi_{PM}} \quad (4.9)$$

where $\boldsymbol{L_d}$ and $\boldsymbol{L_q}$ are the inductances of the rotor in d and q axis, $\boldsymbol{R_d}$ and $\boldsymbol{R_q}$ are the resistance of the rotor in d axis and q axis, $\boldsymbol{i_d}$ and $\boldsymbol{i_q}$ are the generator currents in d axis and q axis, $\boldsymbol{\psi_{PM}}$ is the permanent magnet flux and $\boldsymbol{\omega_e}$ is the electrical angular speed of the PMSG which is defined as:

$$\boldsymbol{\omega_e = p_n \omega_m} \quad (4.10)$$

Where $\boldsymbol{p_n}$ is the number of pole pairs of the generator

The electromagnetic torque of the PMSG can be expressed as (Shehata, 2017):

$$\boldsymbol{T_e = \frac{3}{2} p_n [\left(L_{sd} - L_{sq} \right) i_{sd} i_{sq} + \psi_{PM} i_{sq}]} \quad (4.11)$$

In case the PMSG surface mounted is considered and the q-axis of the stator current is assumed to be a round-rotor ($\boldsymbol{L_d = L_q}$), Equation 4.11 can then be written as:

$$T_e = \frac{3}{2} p_n \psi_{PM} i_{sq} \quad (4.12)$$

The PMSG equation of motion can be expressed as (Estima, 2012):

$$\frac{d\omega_m}{dt} = \frac{1}{J} [\, T_e - T_m - F\omega_m \,] \quad (4.13)$$

The active and reactive powers of the PMSG can be expressed as in equations (4.14) and (4.15) respectively (Urasaki et al., 2004):

$$P_{gen} = \frac{3}{2} [\, v_{sd} i_{sd} + v_{sq} i_{sq}]$$

(4.14)

$$Q_{gen} = \frac{3}{2} [\, v_{sq} i_{sd} - v_{sd} i_{sq}]$$

(4.15)

4.4 Power electronics modelling

In general, electronic power devices' role is to efficiently manage and control the flow of electric power by providing voltages and currents using semiconductor devices to fit the load requirements best. A control system for power electronics usually consists of linear combined circuits and/or digital signal processors. The power conversion output usually compares the feedback controller unit to the required or reference value, and the controller reduces the error between the two. The flow of power in a power electronic unit can involve a reversible state change when sufficient semiconductor devices are used, thus exchanging roles between inputs and outputs. This section covers the modelling of the rectifier as well as the modelling of the boost converter.

4.4.1 AC-to-DC converter modelling

Uncontrolled three-phase rectifiers are three-phase converters that use diodes to supply power to a DC circuit from an AC source. They consist of two diodes in each arm, with a total number of three arms. Figure 4.7 shows the circuit of a three-phase, full-wave diode bridge rectifier.

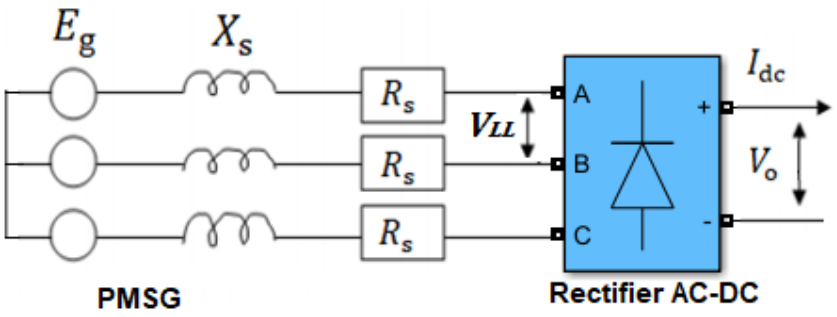

Figure 4. 5: Three-phase, full-bridge diode rectifier with PMSG. (Rahimi, 2017)

The average output voltage of the rectifier is given by the following equations (Fan et al., 2011):

$$\boldsymbol{V_o = \frac{1}{\frac{\pi}{3}} \int_{-\frac{\pi}{6}}^{\frac{\pi}{6}} \sqrt{6}\ V_{LL} cos(\omega t) d(\omega t)}$$

(4.16)

$$\boldsymbol{V_o = \frac{3\sqrt{2}}{\pi}\ V_{LL}} \qquad (4.17)$$

where $\boldsymbol{V_{LL}}$ is the phase to phase nominal voltage.

4.4.2 DC-to-DC boost converter

The purpose of designing a DC-to-DC boost converter (Figure 4.6) is to provide a regulated DC output voltage to the constant load of the SWT standalone DC microgrid from a fluctuating DC input voltage. The DC-to-DC boost converter can increase the voltage while decreasing the current and keeping the same power at the output side.

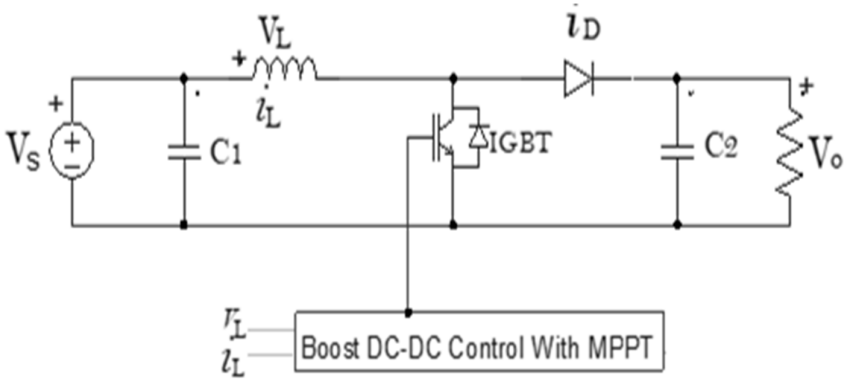

Figure 4. 6: DC-to-DC Boost Converter. (Subbiah & Neelaveni, 2017)

4.4.2.1 Design considerations

Most boost converters are designed for continuous-current operation. The inductance to give continuous current is given by equation (4.26), and equations express the output voltage ripple. (4.28) and (4.31).

High switching frequencies are desirable to reduce the size of both the inductor and the capacitor as the inductor's minimum size to produce continuous current and the minimum size of the capacitor to limit output ripple both decreases with the increase of the switching frequency. However, high switching frequencies can increase power loss in the switches, decreasing the converter's efficiency. Typical switching frequencies are greater than 20 kHz to avoid audio noise and go up to MHz ranges. Some designers consider switching frequencies around 500 kHz to be the best trade-off between small component size and efficiency. In contrast, others prefer to use switching frequencies of around 50 kHz to keep switching losses lower, while some still use frequencies above 1 MHz.

4.4.2.2 Voltage and current relationships

Assumption made in this section include the following:

1. Steady-state conditions exist.
2. The switching period is $\boldsymbol{T}$, and the switch is closed for time $\boldsymbol{DT}$ and open for $(\boldsymbol{1-D})\boldsymbol{T}$.
3. The inductor current is continuous (always positive).
4. The capacitor is very large, and the output voltage is kept constant at voltage $\boldsymbol{V_0}$.
5. The components are ideal.

The relationship between the boost convert voltage and current in Figure 4.7 is investigated by examining the inductor voltage and current when the switch is closed and when it is the switch open.

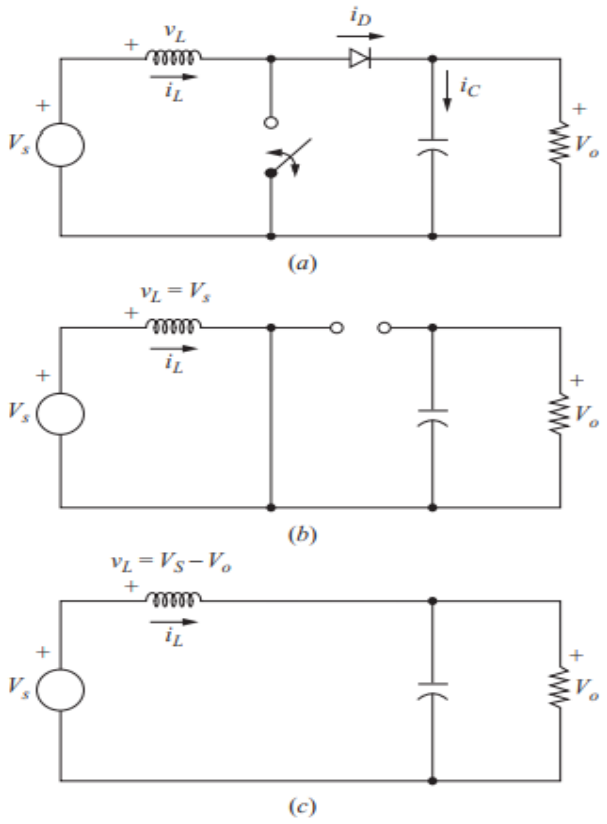

Figure 4. 7: The boost converter. (a) Circuit; (b) Equivalent circuit when the switch is closed; (c) Equivalent circuit when the switch is open. (W. Hart Danial, 2011)

When the switch is closed (Figure 4.7c), the diode is reverse-biased, and the Kirchhoff's voltage law can be written as:

$$\boldsymbol{V_S = L\frac{di_L}{dt}} \tag{4.18}$$

The current variation rate is constant; hence, the current will increase linearly, as depicted in Figure 4.8b. The variation in inductor current is expressed by equations (4.19) and (4.20) as:

$$\boldsymbol{\frac{\Delta i_L}{\Delta t} = \frac{\Delta i_L}{DT} = \frac{V_S}{L}} \tag{4.19}$$

$$\boldsymbol{(\Delta i_L)_{closed} = \frac{V_S DT}{L}} \tag{4.20}$$

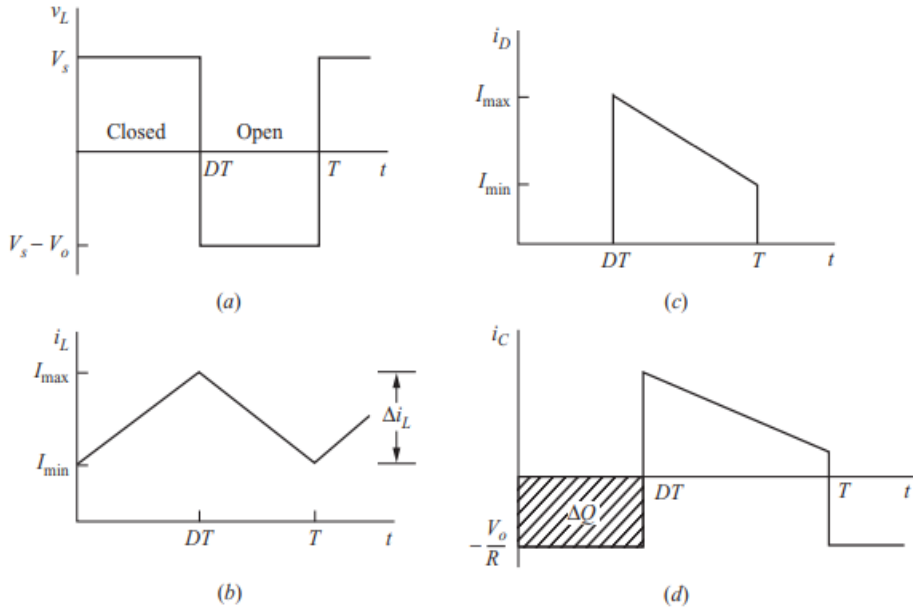

Figure 4. 8: (a) Inductor voltage and (b) current; (c) Diode and (d) Capacitor currents. (W. Hart Danial, 2011)

When the switch is opened, the inductor current cannot vary instantaneously. Hence, the diode is forward-biased, and the voltage across the inductor and the variation of the inductor current are given as:

$$\boldsymbol{v_L = V_S - V_O = L\frac{di_L}{dt}} \tag{4.21}$$

$$\boldsymbol{\frac{di_L}{dt} = \frac{V_S - V_O}{L}} \tag{4.22}$$

The rate of variation of inductor current is a constant, hence, the current varies linearly while the switch is open. The variation in inductor current is expressed in equations (4.23) and (4.24) as follows (W. Hart Danial, 2011):

$$\boldsymbol{\frac{\Delta i_L}{\Delta t} = \frac{\Delta i_L}{(1-D)T} = \frac{V_S - V_O}{L}} \tag{4.23}$$

$$\boldsymbol{(\Delta i_L)_{open} = \frac{(V_S - V_O)(1-D)T}{L}} \tag{4.24}$$

For steady-state operation, the net variation in inductor current is equal to zero, and the output voltage of the converter is given as:

$$\boldsymbol{V_O = \frac{V_S}{1-D}} \tag{4.25}$$

As the switch's duty ratio gets to 1, the converter's output voltage tends to infinity. However, real components always have losses that prevent such an occurrence. Figure 4.8 shows the inductor voltage and current and the diode and Capacitor currents voltage and current for the boost converter. The average current in the inductor is evaluated by recognising that the source's average power is equal to the average power absorbed by the load. Therefore, the output power can be determined as:

$$\boldsymbol{P_O = \frac{V_O^2}{R} = V_O I_O} \tag{4.26}$$

The average inductor current can be expressed as:

$$\boldsymbol{I_L = \frac{V_S}{(1-D)^2 R} = \frac{V_O^2}{V_s R} = \frac{V_O I_O}{V_s}} \tag{4.27}$$

The maximum inductor current $\boldsymbol{I_{max}}$ and the minimum inductor current $\boldsymbol{I_{min}}$ are expressed as follows:

$$\boldsymbol{I_{max} = I_L + \frac{\Delta i_L}{2} = \frac{V_S}{(1-D)^2 R} + \frac{V_S DT}{2L}} \tag{4.28}$$

$$\boldsymbol{I_{min} = I_L - \frac{\Delta i_L}{2} = \frac{V_S}{(1-D)^2 R} - \frac{V_S DT}{2L}} \tag{4.29}$$

A boost converter designed for continuous-current operation must have an inductor value greater than $\boldsymbol{L_{min}}$. The minimum inductance for continuous current in the boost converter is given as:

$$\boldsymbol{L_{min} = \frac{D(1-D)^2 R}{2f}} \tag{4.30}$$

The inductance $\boldsymbol{L}$ can be expressed in terms of a desired variation in the inductor current $\boldsymbol{\Delta i_L}$ as (W. Hart Danial, 2011):

$$\boldsymbol{L = \frac{V_S DT}{\Delta i_L} = \frac{V_S D}{\Delta i_L f}} \tag{4.31}$$

4.4.2.3 Voltage ripples

The preceding equations assumed that the output voltage is constant, which implies an infinite capacitance. Practically, a finite capacitance will cause fluctuation in output voltage or ripples. The peak-to-peak voltage ripple can be evaluated from the capacitor current in Figure 4.8d.

The variation in capacitor voltage can be determined as:

$$\frac{\Delta V_O}{V_O} = \frac{D}{RCf} \tag{4.32}$$

where f is the switching frequency.

Therefore, the capacitance can be expressed in terms of voltage ripples as (W. Hart Danial, 2011):

$$C = \frac{D}{R(\Delta V_O/V_O)f} \tag{4.33}$$

The equivalent series resistance (ESR) of the capacitor can significantly impact the voltage ripple. The peak-to-peak variation in capacitor current in Figure 4.10d is similar to the inductor's maximum current.

The voltage ripple because of the ESR is given as (W. Hart Danial, 2011):

$$\Delta V_{o,ESR} = \Delta i_C r_C = I_{L,max} r_C \tag{4.34}$$

4.5 Boost converter control for maximum power extraction

To extract optimum power under fluctuating wind speeds, the generator speed must be regulated through the converter switch's control. The control of the converter, in this case, is achieved using the MPPT algorithm based on the P&O method because of its simplicity and ease of implementation structure. The duty ratio is automatically varied to generate the voltage required to extract maximum power.

The SWT output power P_w can be written as as:

$$P_w = V_w \ I_w \tag{4.35}$$

Where V_w and I_w are the voltage and the current of the SWT respectively.

The relationship between the SWT voltage V_w and DC link voltage V_{dc} is given by the following equation (K. Kumar et al., 2017):

$$V_w = \left(\frac{1}{1-D}\right) V_{dc} \tag{4.36}$$

4.5.1 Perturb and observe method control strategy

The SWT's voltage and current are measured, as shown in Figure 4.9, and used as inputs to the MPPT controller. These values are then processed based on the P&O

algorithm to track the maximum power. The signal from the P&O MPPT controller is used as input to the boost converter to keep the operating voltage at the MPP by modifying the converter's duty ratio. A small perturbation is introduced in the system to cause a variation of power of the SWT. If the power increases because of the perturbation, the perturbation will carry on in the same direction. Once the maximum power is reached, the power at the next instant reduces, and the perturbation reverses. At the steady-state, the algorithm will oscillate around the MPP. To keep the power variation small, the perturbation size is kept small.

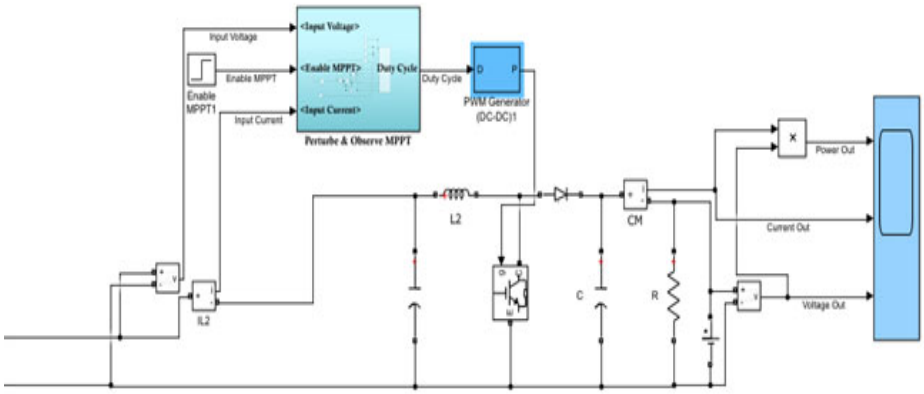

Figure 4. 9: Perturb and observe method to regulate the voltage on the DC microgrid.

Figure 4.10 shows the flowchart of the developed algorithm; the SWT's operating voltage is perturbed by a small increase of dV, resulting in a change dP. If dP is positive, the operating voltage's perturbation is kept in a similar direction as the small increase. In contrast, if dP is negative, the operating point shifts away from the MPP, and the operating voltage must shift in the opposite direction of the small increase.

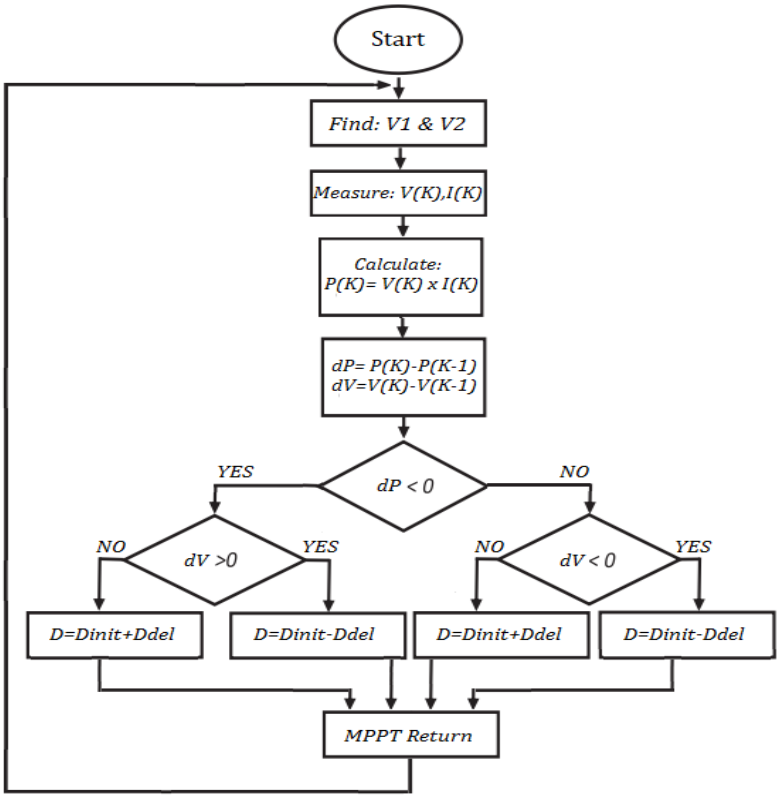

Figure 4. 10: Flowchart of P&O MPPT Algorithm for SWT with boost converter.

Although the wind speed varies greatly with time, the variation of power absorbed by the wind generator is relatively slowly, because of the slow dynamic response of the wind turbine. The converter duty ratio adjustment can be evaluated as (Miller et al., 1997):

$$\boldsymbol{D = D_{init} + C_1 \frac{\Delta P_{k-1}}{\Delta D_{init}}} \tag{4.37}$$

Where $\boldsymbol{D}$ and $\boldsymbol{D_{init}}$ are the duty ratios at iterations D and $\boldsymbol{D_{init}}$ respectively, $\frac{\Delta P_{k-1}}{\Delta D_{init}}$ is the SWT power gradient at step $\boldsymbol{D_{init}}$ and $\boldsymbol{C_1}$ is the step change.

With the wind speed variation, to ensure that the results converge towards the SWT MPP, the function must have a single extremum point, as depicted in Figure 4.3. It is obvious from Figure 4.3 that the MPP is reached when:

$$\frac{dp}{d\Omega} = \mathbf{0} \tag{4.38}$$

Where Ω is the wind rotor speed.

Using the chain rule, equation (4.38) can be written as:

$$\frac{dp}{d\Omega} = \frac{dp}{dD} \cdot \frac{dD}{dV_{SWT}} \cdot \frac{dV_{SWT}}{d\Omega_e} \cdot \frac{d\Omega_e}{d\Omega} = \mathbf{0} \tag{4.39}$$

Where V_{SWT} is the rectifier output voltage and Ω_e is the generator phase angular speed.

The power maximisation process is shown in Figure 4.13; because the duty ratio adjustment follows the $\frac{dP}{dD}$ direction, its value is increased in the high-speed zone of the SWT characteristic curve, resulting in a rotor speed decrease and power increase the MPP is reached. Similarly, in case the starting point is in the low-speed zone, following the direction of $\frac{dP}{dD}$, the duty ratio decreases and subsequently converges towards the MPP since the SWT rotor speed is gradually increased.

$$V_{SWT} = (1 - D)V_O, \frac{dV_{SWT}}{dD} = V_O \neq 0 \tag{4.40}$$

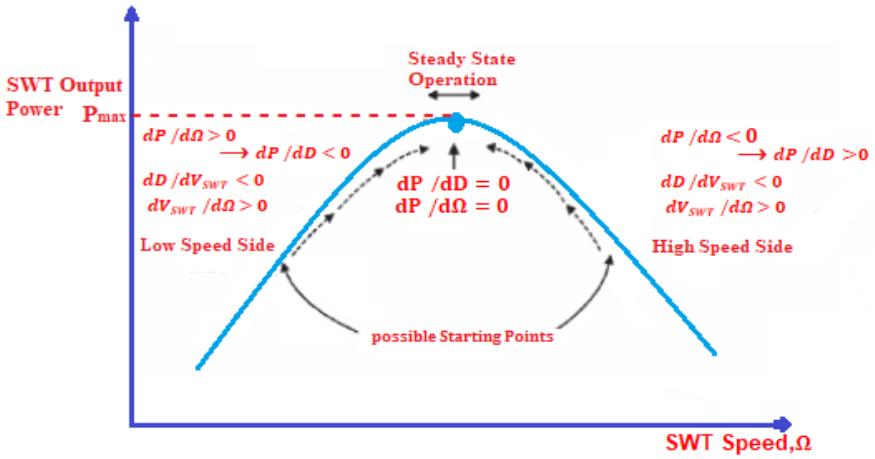

Figure 4. 11: MPPT Process diagram. (Padmanabhan & Kaliyappan, 2014)

As shown in Figure 4.11, the algorithm considers the voltage measurements V[k] and the current measurements I[k] at a predetermined time interval, referred to as the MPPT period. This time span governs how often the algorithm decides to vary the system operating point. Subsequently, the algorithm assesses the power P[k], the variation in power ΔP, and voltage ΔV. The ΔP and ΔV values are determined by using the measurements at the present instant V[k] and I[k] as well as the previous measurements V[k-1] and I[k-1]. Then, the algorithm uses basic logic to decide what to do. The ΔP and ΔV values are each compared against zero to determine if they have risen or dropped. Table 4.2 shows the summary of the P&O algorithm. Thus, in this way, the SWT curve is checked by small perturbations to find the MPP that raises the algorithm's response time. Conversely, if the perturbation size is enlarged, it generates steady-state oscillations about the MPP. Many researchers have proposed

modifications in the P&O algorithm to overcome the response time problem and steady-state oscillations (Kamran et al., 2018). According to the algorithm, the output resulting perturbation is used to drive either the duty ratio or the reference voltage. To summarize, if the power goes up after a certain perturbation, the next perturbation should remain unchanged; however, if the power goes down, the resulting perturbation should be in the opposite direction (Esram & Chapman, 2007).

Table 4. 2: P&O algorithm.

Perturbation	ΔP	Resulting
+Ve	-Ve	+Ve
+Ve	+Ve	-Ve
-Ve	-Ve	+Ve
-Ve	+Ve	-Ve

Any change in the duty ratio will have an inverse effect on the converter's input resistance and, hence, have an inverse effect on the operating voltage. The algorithm then observes the effect of that change in the duty cycle on the output power to determine the next cycle's appropriate command. The output power can increase or decrease depending on whether the current operating voltage level is before or after the power graph's knee point, as shown in Figure 4.13. If the operating level is beyond the knee point or the MPP, then an increase in the voltage will decrease the output power and vice versa. For instance, a decrease in the duty cycle causes an increase in input resistance or operating voltage and increases the output power. This means that the current operating level is before the MPP. By increasing the voltage, the output power will increase. Thus, in the next duty cycle, the algorithm will increase the voltage, which can be achieved by reducing the duty cycle.

4.6 Summary

This part focused on with the development of an SWT DC microgrid model. The first section was dedicated to the considered load profile presentation, while the next section focused on wind aerodynamics modelling. Thereafter, the microgrid components such as the permanent magnet synchronous generator, the full-bridge diode rectifier, and the DC-to-DC boost converter were modelled. The last section of this chapter covered the P&O MPPT controller's modelling to track the maximum power while also regulating the boost converter's output voltage.

CHAPTER FIVE
IMPLEMENTING THE P&O METHOD FOR A SMALL WIND TURBINE

5.1 Introduction

Figure 5.1 shows the layout of the small wind turbine DC microgrid considered in this thesis. It consists of an SWT based on PMSG, a three-phase diode rectifier, a P&O MPPT controller, a DC-to-DC boost converter, and a DC load. This research aims to develop a modified P&O MPPT controller to achieve a constant output voltage and power at the output of the boost converter. The parameters of the SWT DC microgrid are given in Tables 5.1 and 5.2. The system is considered to operate under variable wind speeds. Therefore, the variable voltage and current obtained from the wind turbine are used as inputs to the diode rectifier to converts the SWT variable output AC voltage to DC voltage. After rectification, a boost converter increases the voltage to a higher regulated DC voltage level suitable for the load. The voltage and current from the boost converter's input terminals are used as inputs to the P&O MPPT controller. The voltage and current are continuously used to evaluate the duty ratio, which is then fed to the boost converter. According to the duty ratio, the boost converter controls the voltage level to keep tracking the maximum power point at all times. Finally, the boost converter's output is then connected to a resistive load, which acts as a demand-side load of the DC microgrid.

Table 5. 1: Wind turbine and PMSG system parameters.

Description	Rating
Rated Power (P)	3 kW
Output Voltage (V_{out})	120 V
Air density (ρ)	1.225 kg/m^3
Impedance (R_a)	0.9585 Ω
Inductance (L_q and L_d)	5.25 mH
Blade length radius	1.76 m
Magnetizing flux (Øm)	0.16616 wb
Coefficient of friction (B)	0
Pair of Poles (P_p)	4
Torque/Current (T/A)	0.99696 Nm/A
Cut-in wind speed (V_d)	5 m/s
Rated wind speed (V_n)	12 m/s
Moment of inertia (J)	0.0006329 kg/m^2
viscous damping (F)	0.0003035 (N.m.s)
Pitch angle (β)	0 degree

Table 5. 2: Boost converter parameter specifications

Description	Ratings
Converter power	P= 3 kW
Input Voltage	V_{in} =120 V
Output Voltage	V_{out} = 240 V
Boost Inductor	L = 1.263x10-8H
DC Link Capacitors	C = 260.4 µF
Load Resistance	R = 19.2 Ω
Switching frequency	f_s = 10 kHz
peak-to-peak inductor current	0.4 A
Output capacitance ripple	0.01 %
Output Voltage ripple	0.04 %
Sample time	Ts=50x10^{-6} s
Capacitance ripple	0.01%

5.2 An overview system description of block diagram of the wind turbine system

Figure. 5.1 shows the layout of the DC microgrid considered in this research. The system consists of a small wind turbine generating 3 kW AC power at 120 V. This power is then rectified using a full-bridge three-phase diode rectifier. At the rectifier's output terminal, a DC link capacitor is connected to keep a stable voltage. The DC-link capacitor is connected to the boost converter's input terminals to boost the voltage from 120 V to 240 V. Then, the boost converter supplies power to a DC load connected to its output terminals.

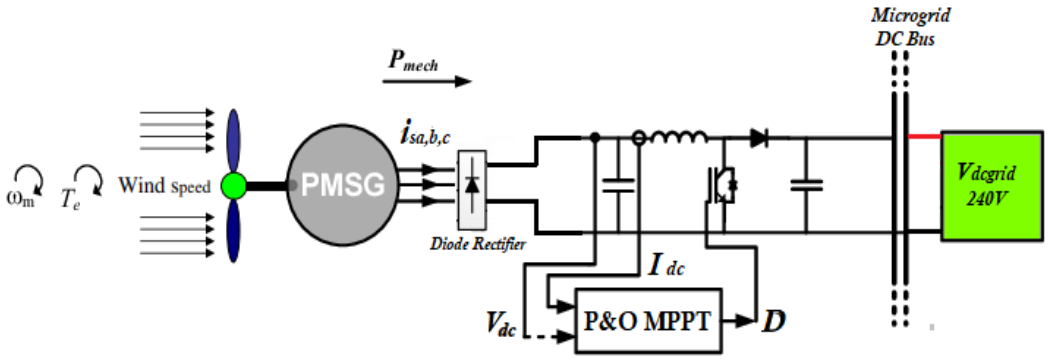

Figure 5. 1: SWT with PMSG and DC-to-DC converter model.

5.2.1 Small wind turbine model

The wind turbine was modelled using the mathematical equations was presented in chapter four. The quantity of power that a small wind turbine can extract from the wind is dependent on the turbine design. Factors such as the rotor diameter and the wind speed affect the power that a turbine can extract from the wind.

5.2.2 Electrical system model

The electrical system comprises the permanent magnet synchronous generator, an uncontrolled three-phase rectifier, and a DC-to-DC converter, as shown in Figures 4.7 and 4.8. The DC-to-DC boost converter and DC link capacitor's modelling parameters value are obtained using the converter equations given in chapter four. These parameters are based on the converter power rating, the SWT power capacity, and the converter voltage ripple requirements.

5.2.3 Control simulation model

The boost converter control uses the perturb and observe method to the converter control duty ratio and provide a constant voltage of 240 VDC at the rated power of 3 kW. The developed Matlab/Simulink model of the maximum power tracking shown in Figure 5.2 is based on the algorithm depicted in Figure 4.10.

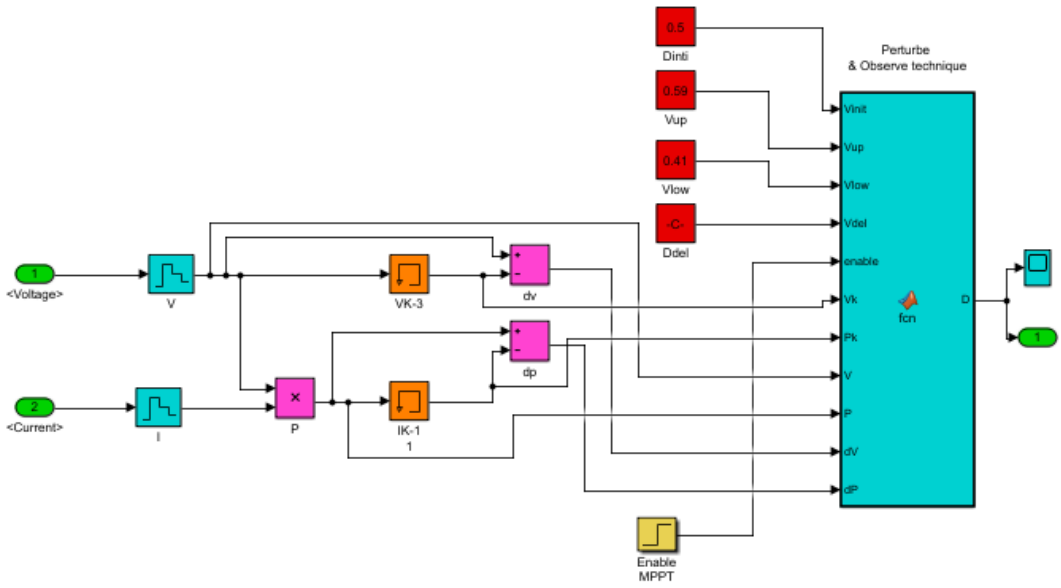

Figure 5. 2: Simulink Model control MPPT by P&O Method.

5.3 Results and discussion

The model in Figure 5.1 was simulated using MATLAB/Simulink environment and based on parameters in Tables 5.1 and 5.2 to evaluate the SWT DC microgrid performance, specifically the performance and the robustness of the proposed control algorithm. The simulation's overall results are presented using three indicators, namely wind turbine results analysis, electrical system results analysis, and control system analysis.

5.3.1 Wind turbine results

The system is simulated for different wind speeds. Simultaneously, the output voltage at the boost converter terminals is maintained constant and as close as possible to the maximum voltage based on the wind speed. This is done to evaluate the performance of the proposed MPPT control algorithm. Figure 5.3 shows the wind speed profile used as a function of time; four different wind speeds are considered in the simulation. The initial wind speed is 5 m/s, then after the speed is increased to 7 m/s, then after a short lapse of time, the speed goes up to 11 m/s and finally to 12 m/s.

For each wind speed, the turbine's rotor speed will drive the generator to yield maximum power. The system is expected to generate the rated power of 3 kW when the wind speed is equal to 12 m/s. Hence, for wind speeds lower than the rated value, the SWT DC microgrid generates power lower than the rated power of 3 kW. The turbine mechanical power will then follow the optimum power curve with a slight overshoot when wind speed varies, and the generator can extract maximum power under variable wind speeds. The simulation is carried out for a duration of 3 s. A step change of 0.05 s is introduced to vary the speed from 5 m/s to 12 m/s. Thereafter, the speed is kept constant.

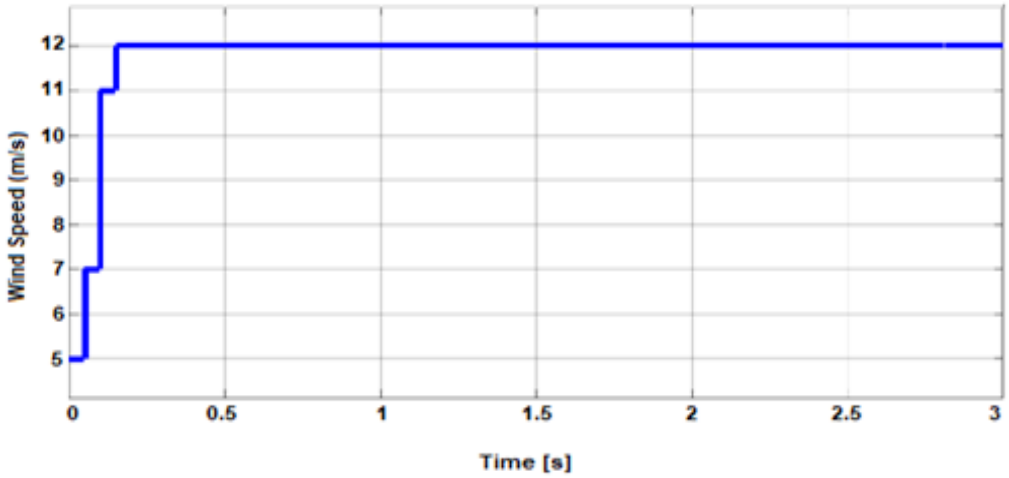

Figure 5. 3: Variable wind speed.

While the wind speed is increasing, it can also be observed an increase of power generated, resulting in an increase of the power at the boost converter's output terminal (voltage and current). When the wind speed is 5 m/s, the SWT's AC output power is around 860 W. This power is then rectified to obtain DC power. The boost converter interfaced between the rectifier and load increases the DC power voltage to a corresponding maximum voltage based on the MPPT algorithm. Once the wind speed reaches 7 m/s, the SWT's output power increases to 1.4 kW. At this power, the AC

output voltage of the SWT is around 80 V. After rectification, the boost converter increases the voltage of the DC power to obtain its corresponding maximum voltage based on the MPPT algorithm. Once the wind speed rises to 11 m/s, the output power of the SWT increases to 1.74 kW, and the voltage goes up to 99.5 V. This voltage is then rectified and boost to allow the connection of the DC load. At the rated wind speed of 12 m/s, the power reaches 3 kW at an AC voltage of 114 V AC, rectified to DC, then boosted to about 240 V.

Figure 5.4 shows the SWT pitch angle curve as a function of time. As indicated in Table 5.1, the pitch angle value was selected to be zero degrees as it is the case for most small wind turbines. In Figure 5.4, it can also be seen that the pitch angle remains constant and equal to zero degrees for all duration of the simulation.

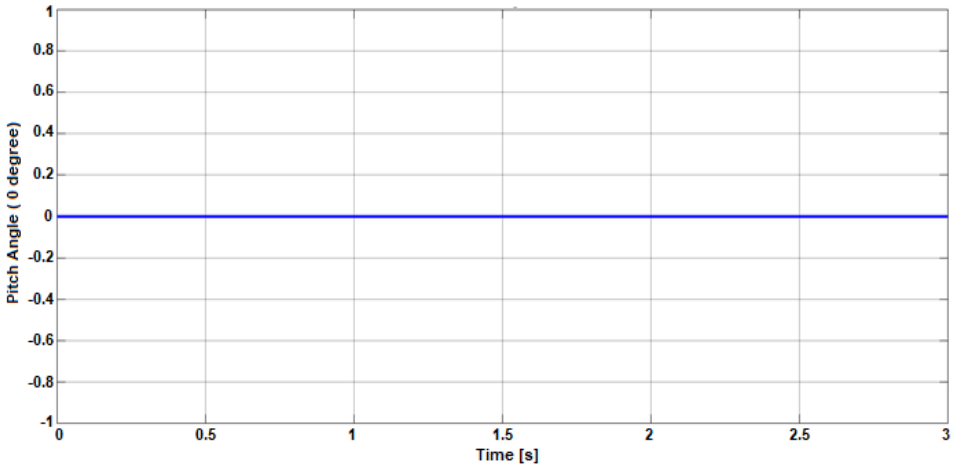

Figure 5. 4: Pitch angle.

5.3.2 SWT results

The output voltage at the terminals of the SWT is depicted in Figure 5.5; the signal exhibits an undershoot of 2 %, which represents the distortion of the voltage signal below its steady-state value and the overshoot which refers to the distortion of the voltage signal above its steady-state value is 0.456 %. At the same time, the rise time is 146.362 ms. From the initial state at t = 0 s to t= 0.039 s, the voltage rises to 40.5V, then, at time t = 0.053 s increases again to 56.55 V, and finally, the steady-state voltage of 114 V is reached at time t = 0.4 s.

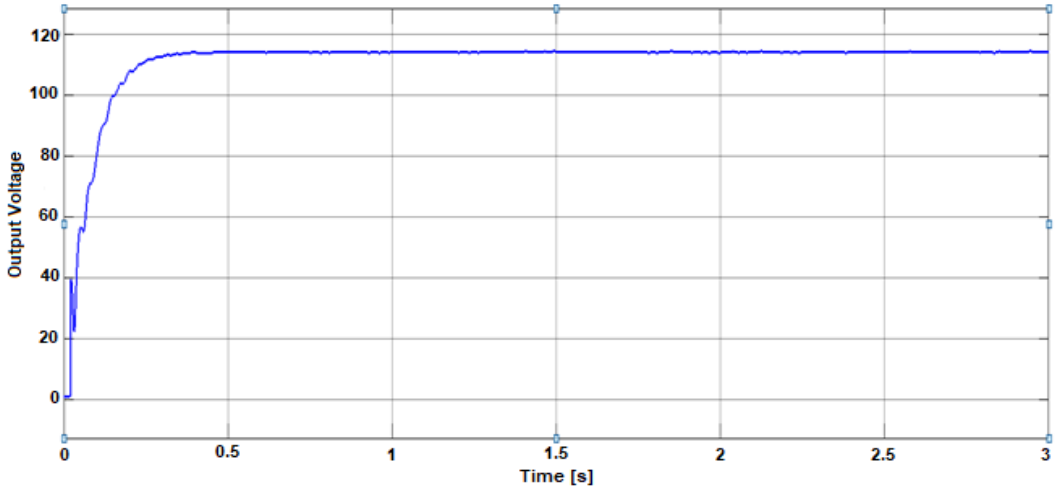

Figure 5. 5: SWT voltage.

Figure 5.6 shows the rotor rotational speed expressed in rad/s; the signal displays an overshoot and an undershoot of 1.581 % and 0.862 %, respectively, while the rise time is 99.98 m/s. The initial wind speed is 5 m/s, which occurs between t = 0 s and t= 0.05 s. At that wind speed, the rotational speed of the rotor is around 131.8 rad/s, between t = 0.05 s and t = 0.1 s, the wind speed goes up to 7 m/s, causing the rotor speed to rise to 185.6 rad/s, between t = 0.1 s and t = 0.15 s, the wind speed increases to 11 m/s and as a result, the rotor rotational speed reaches 293.2 rad/s and lastly, from t = 0.2 s. In contrast, the wind speed is 12 m/s, the rotor speed increases to 320 rad/s.

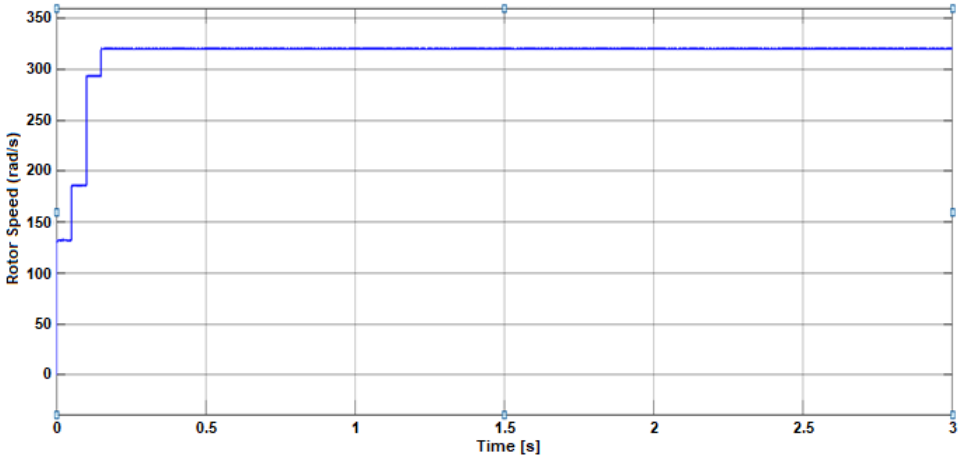

Figure 5. 6: SWT rotor rotational speed.

The line to line voltage at the output terminals of the SWT is shown in Figure 5.7; at steady, which occurs at time t = 0.25 s, the line voltage is around 120 Vac. This signal is used as an input for the rectifier.

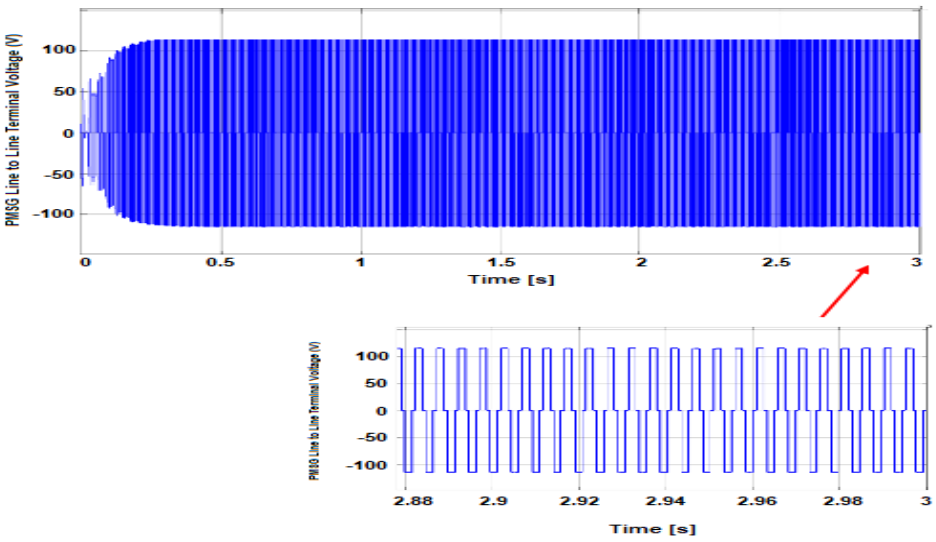

Figure 5. 7: SWT line to line voltage.

The PMSG stator current distortion occurs before the time t = 0.15 s. Thereafter, the stator current remains steady at around 25 A, after an overshoot of 0.995 %, as shown in Figure 5.8. The current varies with the variation of the wind speed. For the wind speed equal to 5 m/sec, the current is approximately 15 A, and for the wind speed equal to 11 m/sec, the current around 29.9 A.

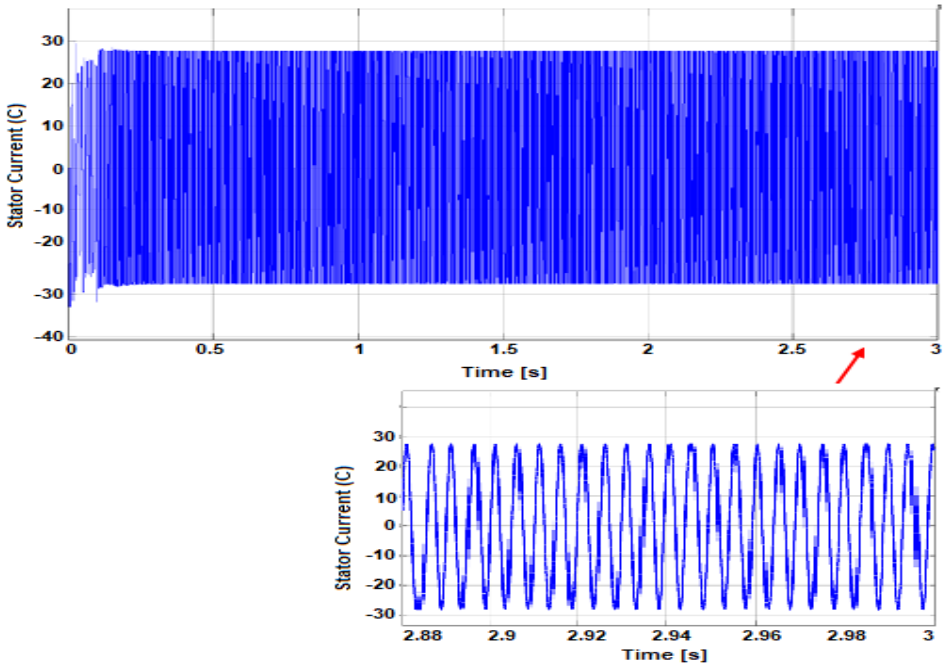

Figure 5. 8**: PMSG Stator Current.**

5.3.3 DC-to-DC boost converter results analysis

The boost converter input terminal receives 3 kW DC power from the full-bridge three-phase diode rectifier at 120 V. Figure 5.9 shows both the boost converter inductance

current and the ripple current. The inductance current (Figure 5.9a) exhibits high fluctuations from the simulation start until the wind speed reaches 7 m/s. The current reaches up to 35.29 A. Thereafter, the signal gets to the steady-state value of 25 A. On the other hand, the boost converter inductance ripple current (Figure 5.9b) shows slight ripple variations around 24 A to 27 A.

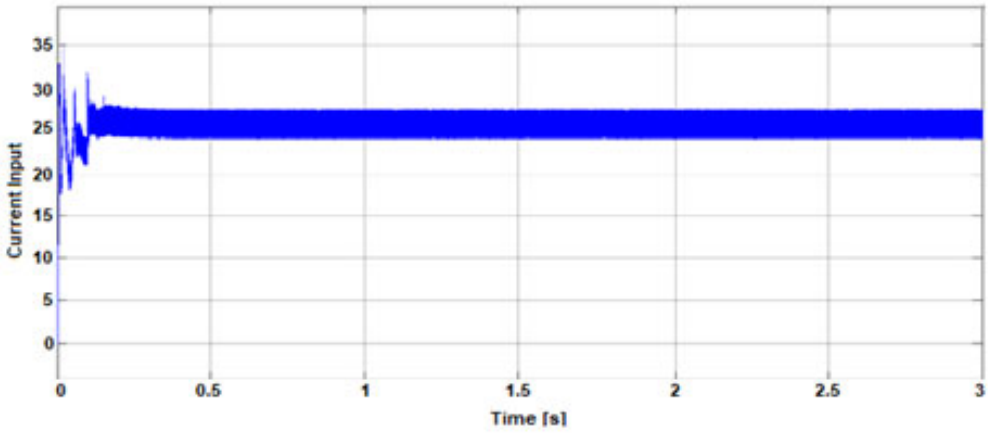

(a)

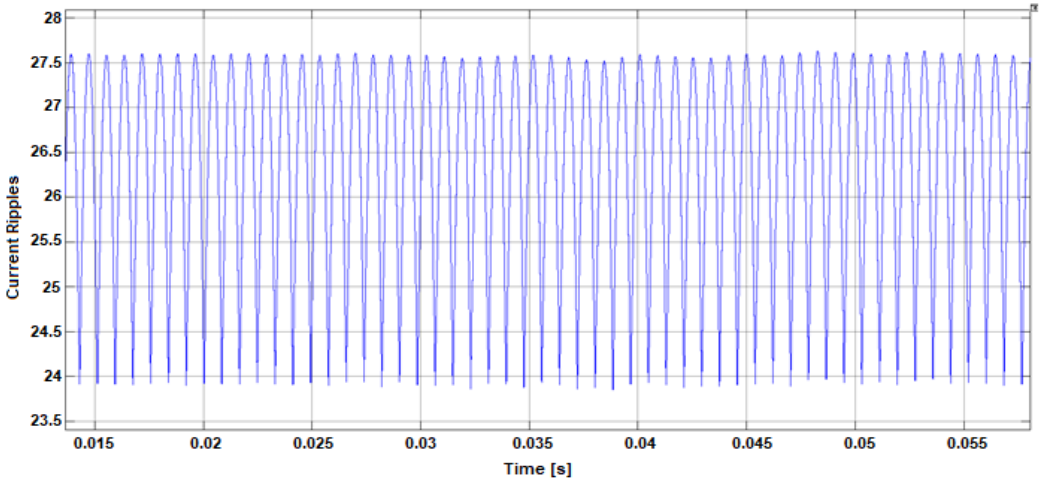

(b)

Figure 5. 9: (a) Boost converter inductance current and (b) ripple current.

The voltage at the full-bridge diode rectifier's output terminals is shown in Figure 5.10; its steady-state value is around 114 V; the signal exhibits overshoot and undershoot of 0.347 % and 2.633 %, respectively, before getting to its stable value. Before the steady-state, the signal significant fluctuations voltage between time t = 0 s and t = 0.4 s. to reach its steady-state value, the signal took about 0.6 s.

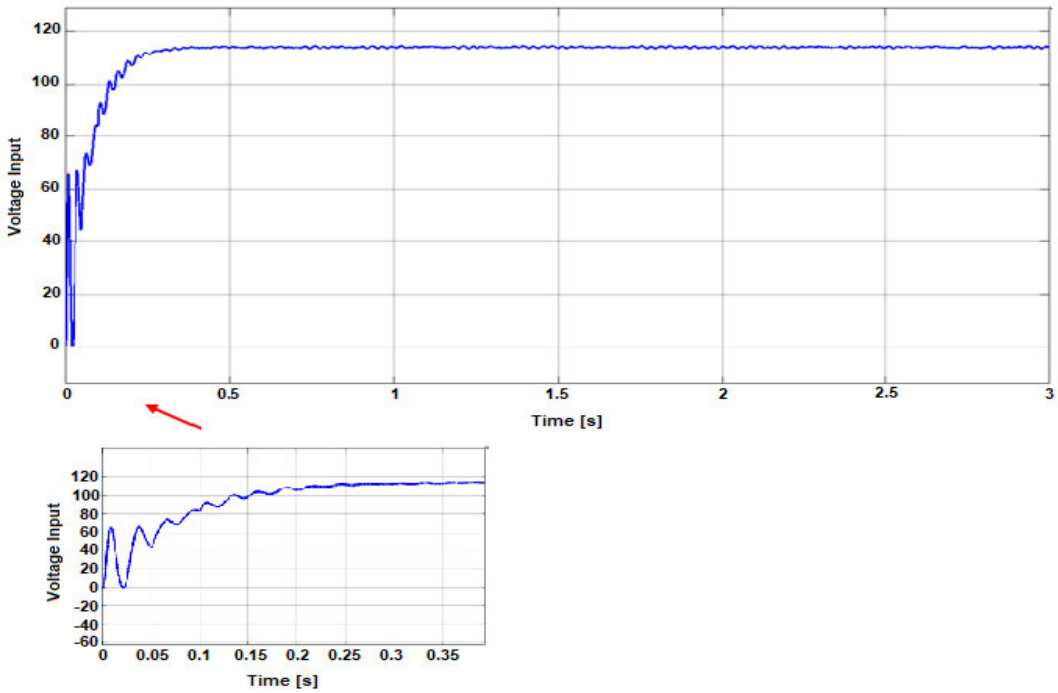

Figure 5. 10: Boost converter input voltage.

The duty ratio provided by the MPPT controller based on Perturb and Observe algorithm is depicted n figure 5.11; this duty ratio represents the on-state and off-state periods used to drive the boost converter switch to reach the MPP. It can be seen from the figure that depending on the operating conditions, and the MPPT controller provides a varying duty ratio between 0.4998 to 0.5002.

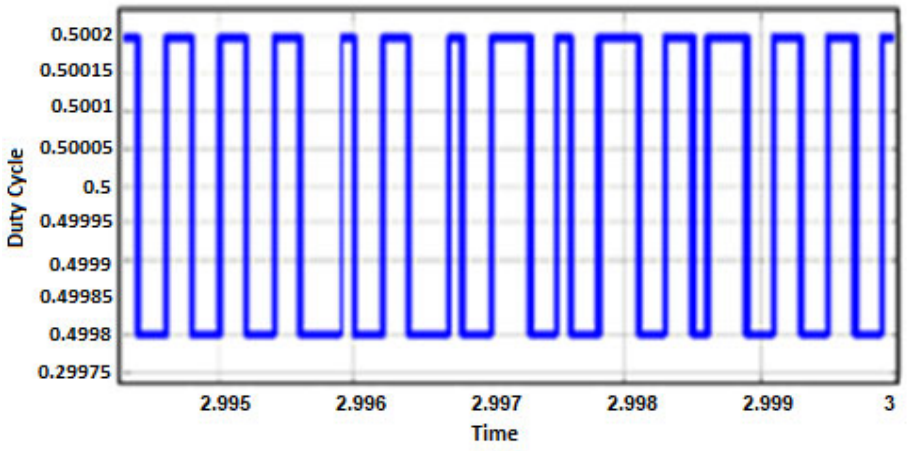

Figure 5. 11: Duty Cycle using the P&O MPPT algorithm.

The boost converter's output current is depicted in Figure 5.12; it is characterised by an overshoot of 0.774 % and an undershoot of 2.131 %, while the rise time is 126.918 ms. The steady-state value of the current (12.5 A) occurs at 0.4 s and corresponds to a wind speed of 12 m/s. Initially, this current is equal to 4.26 A when the wind speed is

5 m/s between t =0 s and t= 0.05 s, thereafter, with the variation of the wind speed to 7 m/s between t = 0.1 s and t = 0.15 s, the current increases to 8.88 A, afterward, the wind speed varies again to 11 m/s between time t = 0.15 s and t = 0.2 s, and the current increases to 11 A until it gets to its steady-state value of 12.5 A.

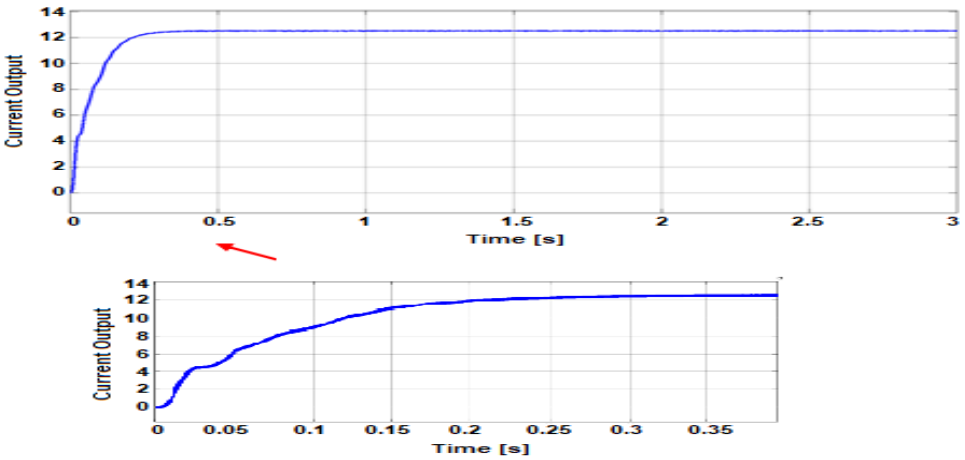

Figure 5. 12: Boost converter output Current.

The boost converter's output voltage is depicted in Figure 5.13; it is characterised by a rise time is 138.532 ms. The steady-state value of the voltage (240 V) occurs at 0.4 s when the duty ratio is 0.5 and corresponds to a wind speed of 12 m/s. Initially, this voltage is equal to 81.78 V when the wind speed is 5 m/s between t =0 s and t= 0.05 s, thereafter, with the variation of the wind speed to 7 m/s between t = 0.1 s and t = 0.15 s, the voltage increases to 117.5 V, afterward, the wind speed varies again to 11 m/s between time t = 0.15 s and t = 0.2 s, and the voltage increases to 211.5 V until it gets to its steady-state value of 240 V.

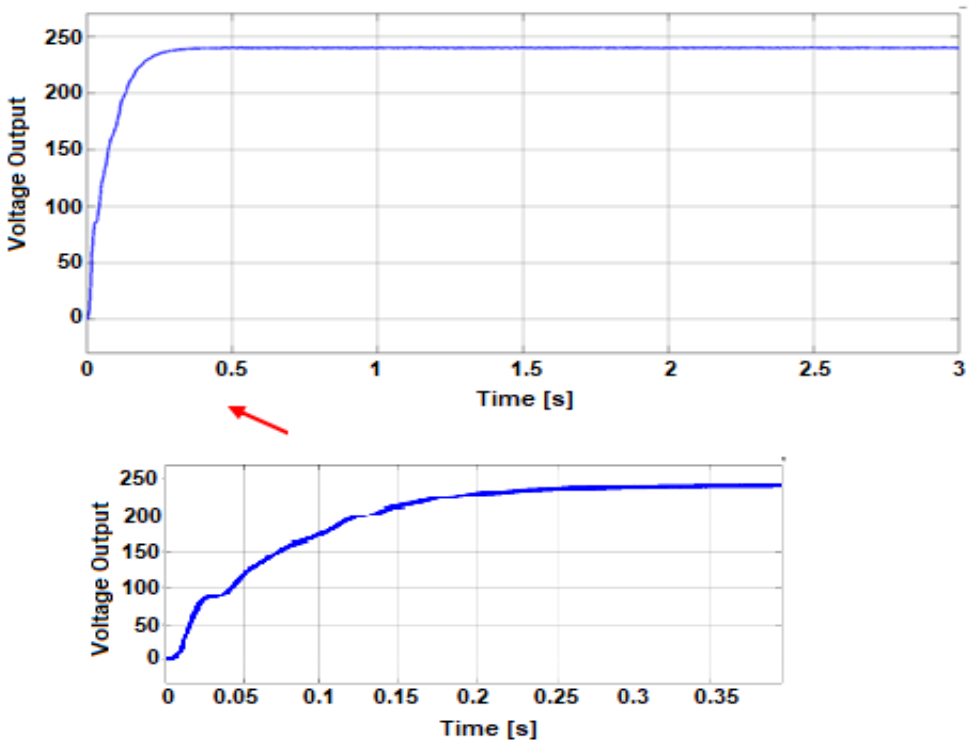

Figure 5. 13 : Boost converter output voltage.

The boost converter's output power is depicted in Figure 5.14; it is characterised by overshoot and undershoot of 0.433 % and 2.173 %, respectively, while the rise time is 174.712 ms. The rated power (3 kW) occurs at 0.4 s and corresponds to a wind speed of 12 m/s. Initially, this power is equal to 718.5 W when the wind speed is 5 m/s between t =0 s and t= 0.05 s, thereafter, with the variation of the wind speed to 7 m/s between t = 0.1 s and t = 0.15 s, the power increases to 1514 W, afterward, the wind speed varies again to 11 m/s between time t = 0.15 s and t = 0.2 s and the power increases to 2330 W until it gets to its rated value of 3 kW.

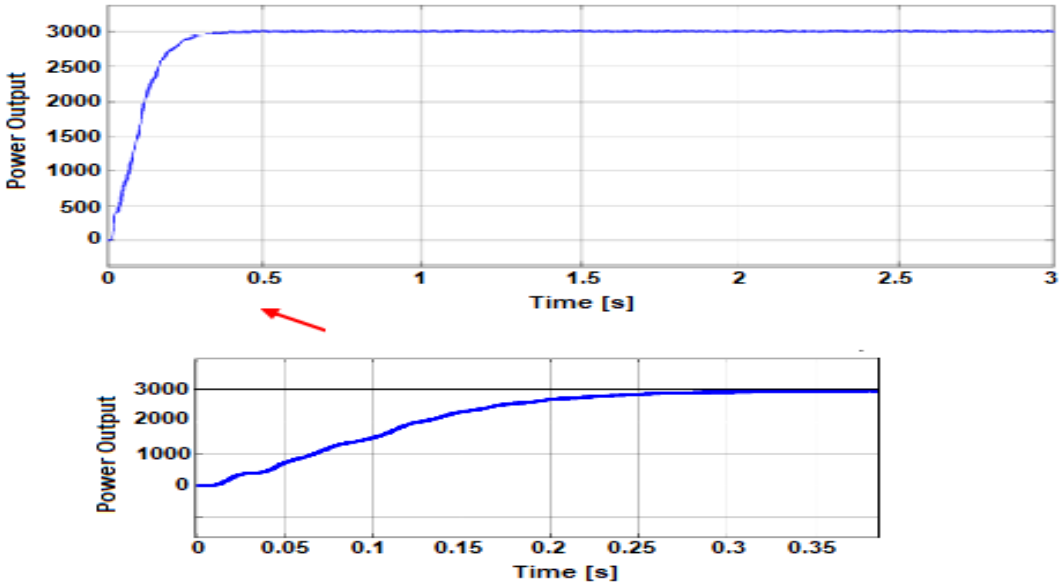

Figure 5. 14: Boost Converter Output Power Under Varying Conditions Using P&O MPPT.

5.4 Case Studies

Based on the control of the boost converter, two case studies are considered to evaluate the adopted control algorithm's effectiveness and robustness. In the first case, the system is simulated without an MPPT controller to drive the boost converter, and the second case SWT model under constant speed condition considers the control of the boost converter using an MPPT control based on the P&O algorithm.

5.4.1 Case study one: SWT model without using Perturb & Observe algorithm

This case study considered the SWT DC microgrid operation without an MPPT control for the boost converter. The system is simulated for different wind speeds; the initial wind speed is 5 m/s, then after the speed is increased to 7 m/s, then, after a short lapse of time, the speed goes up again to 11 m/s and finally to 12 m/s. The results obtained from this scenario are depicted in Figure 5.15. The current signal (Figure 5.15a) displays an overshoot of 9.894 % and an undershoot of 9.657 % between t = 0 s and t = 3 s. The current resulting from the simulation was about 13.38 A. However, this current varied between 13.33 and 14.16 A with a rise time of 5.48 m/s.

On the other hand, as shown in Figure 5.15b, the output voltage magnitude at the load end is around 256.9 V. The signal exhibits a rise time of 54.79 ms, while the fall time was 0 ms. Additionally, the overshoot and undershoot were 9.89 % and 9.65 %, respectively. The rated power of the SWT DC microgrid is 3 kW. However, this case study's simulation results show that the power received at the output terminals of the boost converter is about 3.411 kW. In contrast, it shows that the SWT DC microgrid's

rated power is around 3.848 kW (Figure 5.15c). The power signal displays a rise time of 73.522 ms, while the overshoot is 13.03 % and undershoot 9.39 %.

The rated output voltage at the load end is 240 V; however, the simulation results returned a voltage of 259.9 V, which is higher than the rated value. In the same vein, the rated current at the output terminal on the boost converter is 12.5 A; however, the results from the simulation of this case study show a current of 13.38 A. Consequently, the simulation results when the SWT DC microgrid operates without an MPPT controller are above the rated value of the voltage and the current, hence the power.

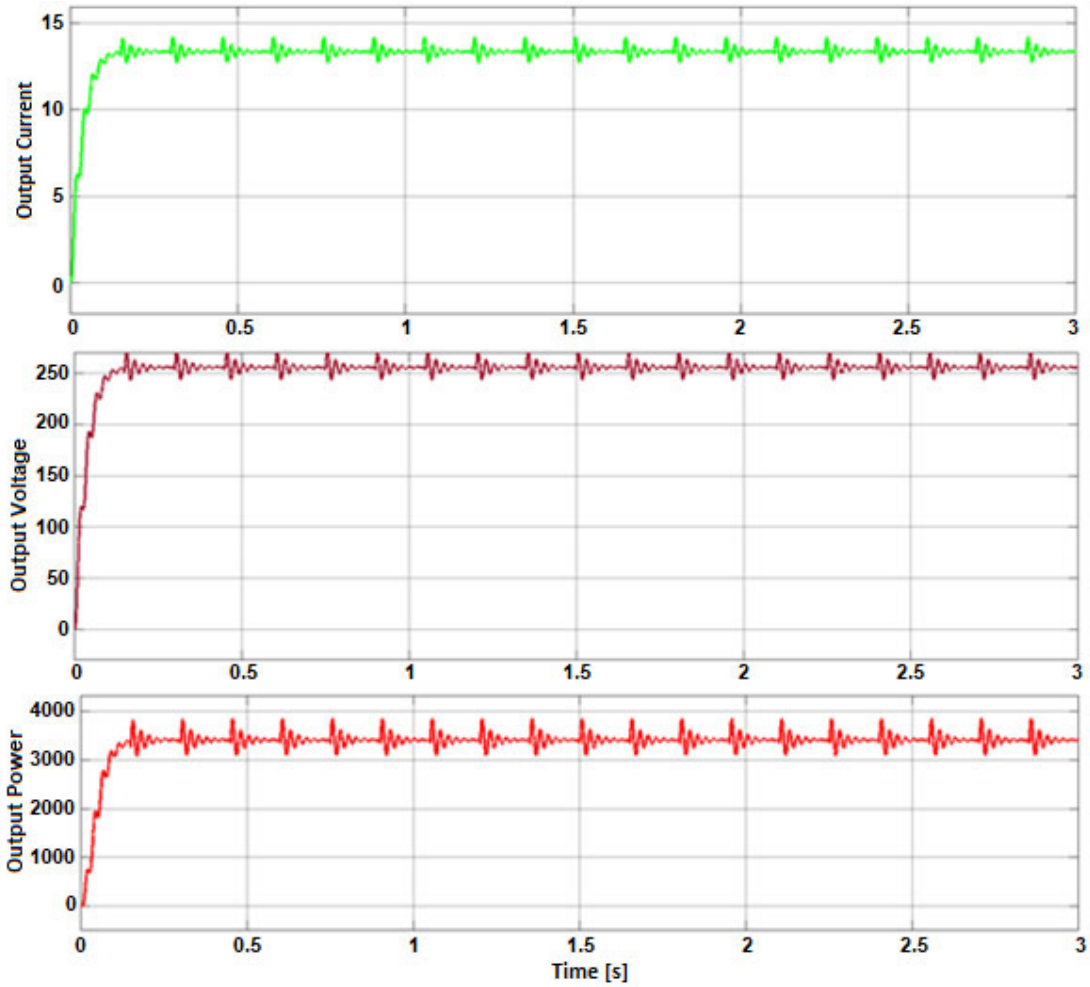

Figure 5. 15: (a) Current, (b) Voltage, and (c) power of boost converter.

5.4.2 Case study two: SWT model under constant speed condition

In this scenario, the SWT DC microgrid operates under a constant speed at 12 m/s, and the boost converter is controlled using a P&O MPPT controller. The results obtained from this scenario are depicted in Figure 5.16 and exhibits oscillations between t = 0 s and t = 0.4 s than when the system is operating under variable wind

speed. The current signal (Figure 5.16a) displays an overshoot of 9.894 % and an undershoot of 9.657 % between t = 0 s and t = 3 s. The current signal displays a rising time of about 97.7 ms between 0 s to 0.4 s. Whereas the overshoot and undershoot of the current are 0.803 % and 2.446 %, respectively. Similarly, the voltage at the boost converter's output terminals presents an overshoot, and an undershoot of 0.803 % and 2.446 %, respectively, between 0 and 0.4 s. The voltage obtained is 240 V (Figure 5.16b). Lastly, the power signal (Figure 5.16c) reaches its steady state of 3 kW at about 0.4 s. it shows a rising time of 142.294 ms, while the overshoot is 0.470% and the undershoot is 3.286 %.

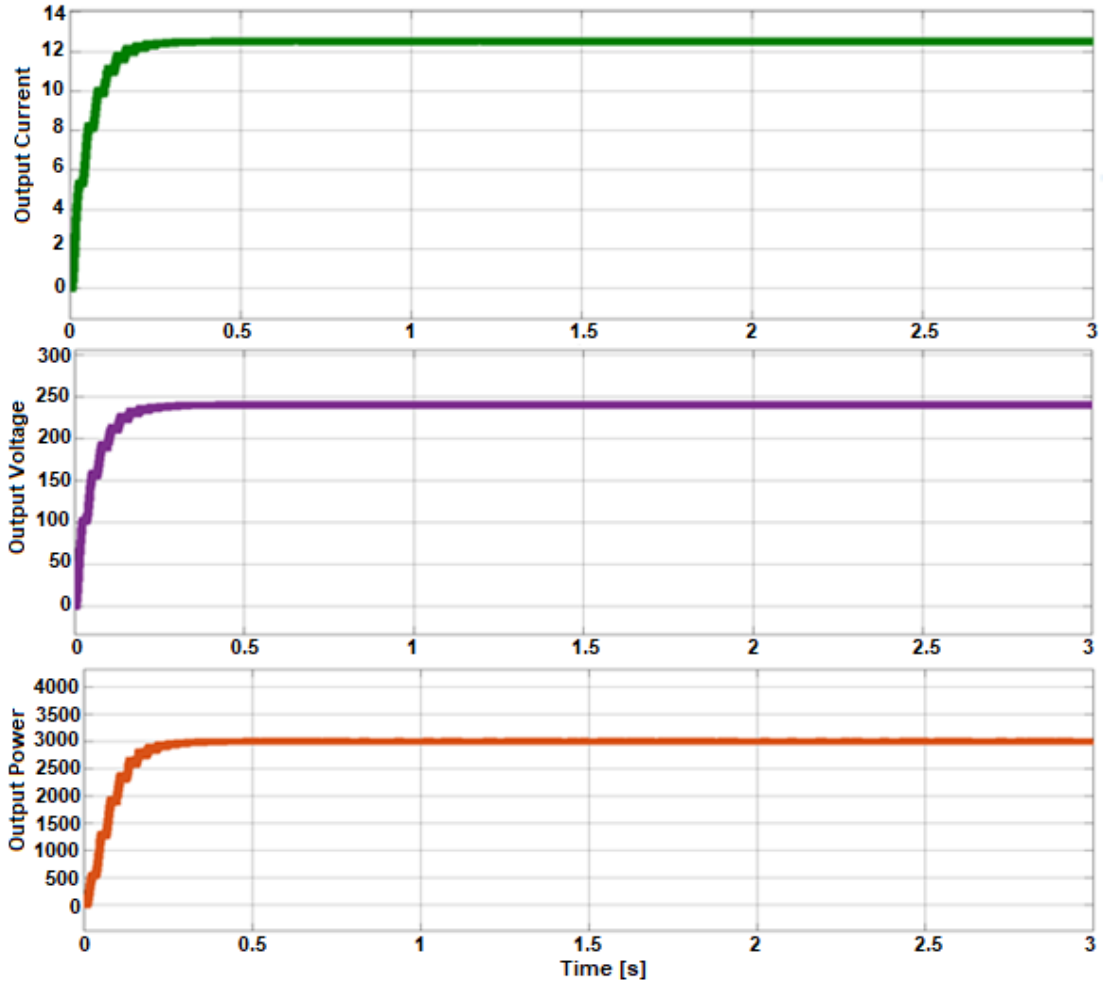

Figure 5. 16: (a) Current, (b) Voltage, and (c) Power of Boost Converter Load of SWT System Under Constant Speed Conditions Using P&O MPPT.

5.5 Summary

This chapter dealt with the presentation, analysis, and discussion of the results obtained from the simulation. These results were presented in three sections: wind turbine results, SWT results, and DC-to-DC boost converter results. The wind turbine results focused on the wind turbine's aerodynamics, including the wind speed and the

pitch angle. The SWT results comprised the simulation results of the voltage and the current of the 3 kW PMSG model used in this study. Lastly, the DC-to-DC boost converter results consisted of the converter's voltage, current, and power using the P&O MPPT controller. Additionally, case studies were considered to assess the performance of the system. The first case considered the SWT DC microgrid operation without an MPPT control for the boost converter, and the system was simulated for different wind speeds. And the second case considered the simulation of the SWT DC microgrid operating under a constant speed at 12 m/s, and the boost converter is controlled using a P&O MPPT controller.

CHAPTER SIX
CONCLUSION AND RECOMMENDATIONS

6.1 Conclusion

DC microgrids have appeared to be the sustainable solutions incorporating energy storage and distributed generation to provide power to various types of DC loads, including LED lights, Electric Vehicles, computers, laptops, TV sets, tablets, phones, and printers, etc. Furthermore, DC systems are becoming an attractive solution for industrial applications. Renewable generators such as photovoltaic and fuel cells can easily be integrated with DC systems as their output power is in DC form. In contrast, power sources such as wind turbines, wave power, and gas turbines can be more efficient by utilising only one converter instead of two back-to-back converters. This research dealt with the design and simulation of a small wind turbine DC microgrid to provide power to a residential load in the event of a power shortage or power cuts. The adopted system consisted of a small wind turbine generating 3 kW AC power at 120 V. This power was rectified using a full-bridge three-phase diode rectifier. At the rectifier's output terminal, a DC link capacitor was connected to keep a stable voltage. The DC-link capacitor was connected to the boost converter's input terminals to boost the voltage from 120 V to 240 V. The boost converter supplied power to a DC load connected to its output terminals. To extract the maximum power and control the boost converter's output voltage, an adjusted P&O MPPT algorithm was used to drive the switching element to accomplish fast MPP tracking and maintain the voltage constant irrespective of wind speed variation. To verify the designed system's effectiveness, a MATLAB Simulink model of the small wind turbine DC microgrid was developed. The overall results showed a good performance of the system. Furthermore, two case studies were considered to assess the adopted MPPT algorithm's robustness, and the results showed a better response to the adopted MPPT algorithm.

To achieve the aim of this research, the study was divided into six chapters. Apart from the introduction and the conclusion, the rest of the thesis can be summarised as follows:

Chapter two provided an overview of DC microgrids' islanded mode operation and small-scale wind turbines, including their components and current market. A section dedicated to wind energy conversion principle and operation was presented. Additionally, sections on power electronic converters for wind turbines and voltage flow stability and control compared with the other methods were also considered. Lastly, a

review of wind turbine power control approaches and maximum power point tracking algorithms were presented.

Chapter three dealt with the design considerations of a DC microgrid based on an SWT. The topics covered in this chapter included a brief investigation on a standalone small wind turbine in DC microgrids, including the site selection, the technologies, the power electronic converters topologies, and their maximum power point techniques.

Chapter four deals with the development of a small wind turbine DC microgrid model. The first section was dedicated to the considered load profile presentation, while the next section focused on wind aerodynamics modelling. Thereafter, the microgrid components such as the permanent magnet synchronous generator, the full-bridge diode rectifier, and the DC-to-DC boost converter were modelled. The last section of this chapter covered the P&O MPPT controller's modelling to track the maximum power while also regulating the boost converter's output voltage.

Chapter five dealt with the presentation, analysis, and discussion of the results obtained from the simulation. These results were presented in three sections: wind turbine results, SWT results, and DC-to-DC boost converter results. The wind turbine results focused on the wind turbine's aerodynamics, including the wind speed and the pitch angle. The SWT results comprised the simulation results of the voltage and the current of the 3 kW PMSG model used in this study. Lastly, the DC-to-DC boost converter results consisted of the converter's voltage, current, and power using the P&O MPPT controller. Additionally, case studies were considered to assess the performance of the system. The first case considered the SWT DC microgrid operation without an MPPT control for the boost converter, and the system was simulated for different wind speeds. And the second case considered the simulation of the SWT DC microgrid operating under a constant speed at 12 m/s, and the boost converter is driven using a P&O MPPT controller.

6.2 Recommendations for future research

Further research should focus on the following aspects:

- Development of an advanced energy management algorithm for on-grid and standalone operation of the small wind turbine DC microgrid considered,
- Real-time simulation and hardware implementation of the developed maximum power point tracking controller,

- Development of more advanced and efficient MPPT algorithms Development of a maximum power point tracking controller for a hybrid solar-wind power system.

- Development of an highly efficient MPPT technique for wind turbines dependent on variable step size and variable pitch angle.

REFERENCES

Abraham, J. & Plourde, B. 2014. *Small scale wind power.*

Acharya, P., Papadakis, A. & Shaikh, M.N. 2016. Modelling and Design of a 3 kW Permanent Magnet Synchronous Generator suitable for Variable Speed Small Wind Turbines. *MATEC Web of Conferences*, 55: 6–11.

Ahmed, A., Ran, L. & Bumby, J.R. 2010. Stalling region instability compensation for constant power soft stalling control. *IET Conference Publications*, 2010(563 CP).

Ahmed, G.E.-S., Ibrahim, E.-N.A. & Hassan Ali, H. 2016. Constant Power Operation Control of Variable Speed Wind Turbine DFIG using Genetic Algorithm. *International Journal of Engineering Trends and Technology*, 37(7): 384–393.

Ali M. Eltamaly, A.I.A. and H.M.F. 2012. Maximum Power Extraction from Utility-Interfaced Wind Turbines. *Intech*, i(tourism): 165–167. http://dx.doi.org/10.1039/C7RA00172J%0Ahttps://www.intechopen.com/books/advanced-biometric-technologies/liveness-detection-in-biometrics%0Ahttp://dx.doi.org/10.1016/j.colsurfa.2011.12.014.

Aubrée, R., Auger, F. & Dai, P. 2012. A new low-cost sensorless MPPT algorithm for small wind turbines. *2012 1st International Conference on Renewable Energies and Vehicular Technology, REVET 2012*, (March): 305–311.

Ayodele, T.R., Ogunjuyigbe, A.S.O. & Adetokun, B.B. 2017. Optimal capacitance selection for a wind-driven self-excited reluctance generator under varying wind speed and load conditions. *Applied Energy*, 190: 339–353.

Badreddine, L., Zouggar, S., Elhafyani, M.L. & Kadda, F.Z. 2014. Experimental Modeling and Control of a Small Wind PMSG Turbine. *IEEE*.

Baroudi, J.A., Dinavahi, V. & Knight, A.M. 2007. A review of power converter topologies for wind generators. *Renewable Energy*, 32(14): 2369–2385.

Barra, P.H.A., Coury, D. V. & Fernandes, R.A.S. 2020. A survey on adaptive protection of microgrids and distribution systems with distributed generators. *Renewable and Sustainable Energy Reviews*, 118(October 2019): 109524. https://doi.org/10.1016/j.rser.2019.109524.

Belakehal, S., Benalla, H. & Bentounsi, A. 2009. Power maximization control of small wind system using permanent magnet synchronous generator. *Revue des Energies Renouvelables*, 12: 2–307. http://www.cder.dz/download/Art12-2_13.pdf.

Blaabjerg, F., Chen, Z., Teodorescu, R. & Iov, F. 2007. Power electronics in wind turbine systems. *Conference Proceedings - IPEMC 2006: CES/IEEE 5th International Power*

Electronics and Motion Control Conference, 1: 46–56.

Bounechba, H., Bouzid, A., Snani, H. & Lashab, A. 2016. Real time simulation of MPPT algorithms for PV energy system. *International Journal of Electrical Power and Energy Systems*, 83: 67–78. http://dx.doi.org/10.1016/j.ijepes.2016.03.041.

Bratcu, I.M.• A.I. & Ceangχ, N.-A.C.• E. 2014. *Optimal Control of Wind Energy Systems*. Towards a. 2008 Springer-Verlag London Limited.

El Chaar, L., Lamont, L.A. & Elzein, N. 2011. Wind energy technology - Industrial update. *IEEE Power and Energy Society General Meeting*, (m): 1–5.

Chen, Y., Xiong, G., Li, W., Qian, J. & Hu, B. 2013. The design of boost circuit in small wind generation system. *Proceedings of 2013 IEEE International Conference on Service Operations and Logistics, and Informatics, SOLI 2013*, (2): 354–359.

Chen, Z., Guerrero, J.M. & Blaabjerg, F. 2009. A review of the state of the art of power electronics for wind turbines. *IEEE Transactions on Power Electronics*, 24(8): 1859–1875.

Chowdhury, M.M. 2014. Modelling and Control of Direct Drive Variable Speed Wind Turbine with Interior Permanent Magnet Synchronous Generator. , (June).

Daili, Y., Gaubert, J.P. & Rahmani, L. 2015. Implementation of a new maximum power point tracking control strategy for small wind energy conversion systems without mechanical sensors. *Energy Conversion and Management*, 97: 298–306. http://dx.doi.org/10.1016/j.enconman.2015.03.062.

Dalala, Z.M., Zahid, Z.U., Yu, W., Cho, Y. & Lai, J.S. 2013. Design and analysis of an MPPT technique for small-scale wind energy conversion systems. *IEEE Transactions on Energy Conversion*, 28(3): 756–767.

Díaz, S.A., Silva, C., Juliet, J. & Miranda, H.A. 2009. Indirect sensorless speed control of a PMSG for wind application. *IEEE International Electric Machines and Drives Conference, IEMDC '09*: 1844–1850.

Dragicevic, T., Vasquez, J., Guerrero, J. & Škrlec, D. 2014. Advanced LVDC Electrical Power Architectures and Microgrids. *IEEE Electrification Magazine*, 2(1): 54–65.

EARNEST, J. & RACHEL, S. 2019. *Wind Power Technology*. Third Edit. Delhi: Asoke K. Ghosh, PHI Learning Private Limited, Rimjhim House,.

Echchhibat, M.Y.E. 2017. An adapted method for a small wind turbine to extract the optimal power. , 16.

Esram, T. & Chapman, P.L. 2007. Comparison of photovoltaic array maximum power point tracking techniques. *IEEE Transactions on Energy Conversion*, 22(2): 439–449.

Estima, J.O. 2012. Development and Analysis of Permanent Magnet Synchronous Motor Drives with Fully Integrated Inverter Fault-Tolerant Capabilities.

Fan, S., Lim, T., Zhang, H. & Finney, S. 2011. Design and control of wind energy conversion system based on resonant DC/DC converter. *Generation (RPG 2011)*. http://ieeexplore.ieee.org/xpls/abs_all.jsp?arnumber=6136079.

Femia, N., Petrone, G., Spagnuolo, G. & Vitelli, M. 2004. Increasing the Efficiency of P&O MPPT by Converter Dynamic Matching. *Ieee*, (1): 1017–1021.

De Freitas, T.R.S., Menegáz, P.J.M. & Simonetti, D.S.L. 2016. Rectifier topologies for permanent magnet synchronous generator on wind energy conversion systems: A review. *Renewable and Sustainable Energy Reviews*, 54: 1334–1344. http://dx.doi.org/10.1016/j.rser.2015.10.112.

Gite, S.S. & Pawar, S.H. 2017. Modeling of wind energy system with MPPT control for DC microgrid. *Proceedings of the 2017 2nd IEEE International Conference on Electrical, Computer and Communication Technologies, ICECCT 2017*: 1–6.

Haque, M.E., Muttaqi, K.M. & Negnevitsky, M. 2009. A control strategy for output maximisation of a PMSG-based variable-speed wind turbine. *Australian Journal of Electrical and Electronics Engineering*, 5(2009): 263–270.

Hau, E. 2006. *Wind Turbines: Fundamentals, Technologies, Application, Economics*. 2nd editio. Berlin, German: Springer.

J.F. Manwell, J.G.M. and A.L.R. 2002. *Wind Energy Explained-Theory , Design an Application*. Chicheste: John Wiley & Sons.

Jahromi, M.J., Maswood, A.I., Tseng, K.J., Bhangu, B. & Tehrani, N.H. 2012. Maximum power extraction of tidal streams. *2012 IEEE PES Innovative Smart Grid Technologies, ISGT 2012*: 1–6.

Jain, A., Shankar, S. & Vanitha, V. 2018. Power generation using Permanent Magnet Synchronous Generator (PMSG) based variable speed wind energy conversion system (WECS): An overview. *Journal of Green Engineering*, 7(4): 477–504.

John, A.R. & Divya, N.A. 2016. Performance Comparison of Grid Integrated Micro Wind System with Diode Rectifier and Active Rectifier. : 2370–2375.

Kakigano, H., Miura, Y. & Ise, T. 2013. Distribution voltage control for DC microgrids using fuzzy control and gain-scheduling technique. *IEEE Transactions on Power Electronics*, 28(5): 2246–2258.

Kakigano, H., Miura, Y. & Ise, T. 2010. Low-Voltage Bipolar-Type DC Microgrid for Super High Quality Distribution. , 25(12): 3066–3075.

Kamran, M., Mudassar, M., Fazal, M.R., Asghar, M.U., Bilal, M. & Asghar, R. 2018. Implementation of improved Perturb & Observe MPPT technique with confined search space for standalone photovoltaic system. *Journal of King Saud University - Engineering Sciences*. https://doi.org/10.1016/j.jksues.2018.04.006.

Katiraei, F., Iravani, M.R. & Lehn, P. 2005. Micro-grid autonomous operation during and subsequent to islanding process. *IEEE Transaction on Power Delivery*, 20(1): 248–257.

Kesraoui, M., Korichi, N. & Belkadi, A. 2011. Maximum power point tracker of wind energy conversion system. *Renewable Energy*, 36(10): 2655–2662. http://dx.doi.org/10.1016/j.renene.2010.04.028.

Kesraoui, M., Korichi, N. & Belkadi, A. 2018. Power Management of a Hybrid Wind Gas Electrolyze Micro grid. *International Renewable Energy Congress*, (Irec).

Khadiri, K. El & Qjidaa, H. 2014. Inverting Buck-Boost Dcdc Converter Design Challenges. *International Journal of Embedded Systems and Applications (IJESA)*, 4(1): 1–12.

Kinnares, V. & Sawetsakulanond, B. 2013. Characteristic requirements of a small scale squirrel cage induction generator for effective electricity generation from wind energy. *Energy Procedia*, 34: 26–49.

Kumar, D., Zare, F. & Ghosh, A. 2017. DC Microgrid Technology: System Architectures, AC Grid Interfaces, Grounding Schemes, Power Quality, Communication Networks, Applications, and Standardizations Aspects. *IEEE Access*, 5: 12230–12256.

Kumar, J., Agarwal, A. & Agarwal, V. 2019. A review on overall control of DC microgrids. *Journal of Energy Storage*, 21: 113–138.

Kumar, K., Ramesh Babu, N. & Prabhu, K.R. 2017. Design and analysis of modified single P&O MPPT control algorithm for a standalone hybrid solar and wind energy conversion system. *Gazi University Journal of Science*, 30(4): 296–312.

Kumar Tiwari, S., Singh, B. & Goel, P.K. 2018. Design and Control of Microgrid Fed by Renewable Energy Generating Sources. *IEEE Transactions on Industry Applications*, 54(3): 2041–2050.

Lee, K.D., Leeb, S.B., Norford, L.K., Armstrong, P.R., Holloway, J. & Shaw, S.R. 2005. Estimation of variable-speed-drive power consumption from harmonic content. *IEEE Transactions on Energy Conversion*, 20(3): 566–574.

Mahesa, D., Rio, A. & Bahatmaka, A. 2020. Analytical Review of Material Criteria as Supporting Factors in Horizontal Axis Wind Turbines : Effect to Structural Responses. *Procedia Structural Integrity*, 27(2019): 155–162. https://doi.org/10.1016/j.prostr.2020.07.021.

Masood, B., Siddique, M.S., Asif, R.M. & Zia-Ul-Haq, M. 2015. Maximum power point tracking using hybrid perturb & observe and incremental conductance techniques. *International Conference on Engineering Technology and Technopreneuship, ICE2T 2014*, 2014-Augus(August): 354–359.

Matayoshi, H., Howlader, A.M., Datta, M. & Senjyu, T. 2018. Control strategy of PMSG based wind energy conversion system under strong wind conditions. *Energy for Sustainable Development*, 45: 211–218. https://doi.org/10.1016/j.esd.2018.07.001.

Miller, A., Muljadi, E. & Zinger, D.S. 1997. A variable speed wind turbine power control. *IEEE Transactions on Energy Conversion*, 12(2): 181–186.

Mohammadi, E., Fadaeinedjad, R. & Naji, H.R. 2018. Flicker emission, voltage fluctuations, and mechanical loads for small-scale stall- and yaw-controlled wind turbines. *Energy Conversion and Management*, 165: 567–577.

Muhammad, S., Kazmi, R., Goto, H. & Guo, H. 2011. A Novel Algorithm for Fast and Efficient Speed-Sensorless Maximum Power Point Tracking in Wind Energy Conversion Systems. *IEEE Transactions on Industrial Electronics*, 58(1): 29–36.

Muhssin, M.T. 2015. Small Microgrid Stability and Performance Analysis in Isolated Island. *IEEE*.

Nayak, S.K. & Vinod, H. 2017. Performance study of common DC link connected wind and PV hybrid system. *2016 IEEE 7th Power India International Conference, PIICON 2016*: 1–5.

Nayar, C. & Dehbonei, H. 2008. A Low Cost Power Electronic Interface for Small Scale Wind Generators in Single Phase Distributed Power Generation System. *AUPEC*: 1–7.

Ontiveros, L.J., Mercado, P.E. & Suvire, G.O. 2011. A new model of the double-feed induction generator wind turbine. *2010 IEEE/PES Transmission and Distribution Conference and Exposition: Latin America, T and D-LA 2010*, (June): 263–269.

Padmanabhan, S. & Kaliyappan, K. 2014. High performance MPPT based on variable speed generator driven by wind power generation in battery applications. *Journal of Electrical Engineering and Technology*, 9(1): 205–213.

Pathmanathan, M., Tang, C., Soong, W.L. & Ertugrul, N. 2008. Comparison of Power Converters for Small-Scale Wind Turbine Operation. *Australasian Universities Power Engineering Conference*, (January): 1–6.

Pitteloud, S.G. and J. 2016. *SMALL WIND WORLD REPORT*. Bonn. https://distributedwind.org/wp-content/uploads/2016/03/2016-Small-Wind-World-Report.pdf.

Pogaku, N., Prodanović, M. & Green, T.C. 2007. Modeling, analysis and testing of autonomous operation of an inverter-based microgrid. *IEEE Transactions on Power Electronics*, 22(2): 613–625.

Rahimi, M. 2017. Modeling, control and stability analysis of grid connected PMSG based wind turbine assisted with diode rectifier and boost converter. *International Journal of Electrical Power and Energy Systems*, 93: 84–96. http://dx.doi.org/10.1016/j.ijepes.2017.05.019.

Rashid, M.H. 2014. *Power Electronics Devices, Circuits & Applications*. Fourth Edi. Pensacola.

Reddy, K., N, S.A., Naga, N., Lakshmi, M., Reddy, A.V.K., Rajesh, B., Kumar, K. & Ali, S. 2015. A Brief Research , Study , Design and Analysis on Wind turbine. *Journal Of Modern Engineering Research (IJMER)*, 5(October 2015): 26.

Rosato, M.A. 2019. *Small Wind Turbines for Electricity and Irrigation, Design and Construction*. Latisana: Taylor & Francis Group, LLC.

Shaikh, P.H., Jan, T. & Baloch, A.A. 2017. Performance Analysis of Wind – Photovoltaic – Battery based DC Microgrid Setup for off – grid Applications. *IEEE*: 1–6.

Shehata, E.G. 2017. A comparative study of current control schemes for a direct-driven PMSG wind energy generation system. *Electric Power Systems Research*, 143: 197–205.

Subbiah, A.S. V & Neelaveni, R. 2017. Closed Loop Control of Permanent Magnet Synchronous Generator Wind Turbine for Standalone System along with MPPT Control. , 10(02): 275–284.

Sun, C., Zhang, J., Cai, X. & Shi, G. 2016. Voltage balancing control of isolated modular multilevel dc-dc converter for use in dc grids with zero voltage switching. *IET Power Electronics*, 9(2): 270–280.

Swapnil S. Sonekar. 2020. Modeling and Simulation of the Wind Energy Electric Conversion System using MATLAB/Simulink. *International Journal of Engineering Research and*, V8(12): 740–747.

Thongam, J.S., Bouchard, P., Ezzaidi, H. & Ouhrouche, M. 2009. Wind speed sensorless maximum power point tracking control of variable speed wind energy conversion systems. *2009 IEEE International Electric Machines and Drives Conference, IEMDC '09*: 1832–1837.

Urasaki, N., Senjyu, T. & Uezato, K. 2004. Relationship of parallel model and series model for permanent magnet synchronous motors taking iron loss into account. *IEEE Transactions on Energy Conversion*, 19(2): 265–270.

W. Hart Danial. 2011. *Power Electronics*. Indiana: McGraw-Hill.

Wang, C.P.B.S.R.L. 2018. Planning and optimization of autonomous DC microgrids for rural and urban applications in India. *Renewable and Sustainable Energy Reviews*, 82: 194–204.

Bin Wu, Yongqiang Lang, Navid Zargari, S.K. 2011. *Power conversion and control of wind energy systems*. I. Press, Ed., Toronto: John Wiley & Sons.

Yang, X., Patterson, D. & Hudgins, J. 2012. Permanent magnet generator design and control for large wind turbines. *PEMWA 2012 - 2012 IEEE Power Electronics and Machines in Wind Applications*.

Yaramasu, V., Wu, B., Sen, P.C., Kouro, S. & Narimani, M. 2015. High-power wind energy conversion systems: State-of-the-art and emerging technologies. *Proceedings of the IEEE*, 103(5): 740–788.

Yin Win, L. 2014. Simulation of Small-Scale Wind Power System. , 03(10): 1896–1899.

Yu, K.N. & Liao, C.K. 2015. Applying novel fractional order incremental conductance algorithm to design and study the maximum power tracking of small wind power systems. *Journal of Applied Research and Technology*, 13(2): 238–244.

Zammit, D., Spiteri Staines, C., Micallef, A. & Apap, M. 2018. MPPT with Current Control for a PMSG Small Wind Turbine in a Grid-Connected DC Microgrid. *2018 5th International Conference on Control, Decision and Information Technologies (CoDIT)*: 205–219. http://link.springer.com/10.1007/978-3-319-74944-0_14.

APPENDIX

P&O Matlab code

Matlab program software the gradually process to extract maximum power by using the proposed of P&O MPPT control algorithm from the small wind source is presented.

Step-1: Start the procedure

Step-2: Calculates change in power ΔP and change in voltage ΔV

For i=k (Maximum number of repetitions)

If change in power, ΔP is positive;

If change in voltage, ΔV is positive;

Decreases the V_{ref}, D =D_{init}, $-D_{del}$,

Else

if change in voltage, ΔV is negative;

Increase the V_{ref}, D =D_{init}, $+D_{del}$

End

Else

If change in voltage, ΔV < 0;

Increase the V_{ref}, D =D_{init}, $+D_{del}$

Else

If change in voltage, ΔV is negative;

Decreases the V_{ref}, D =D_{init}, $-D_{del}$

End

End

Step-3: else D= D_{init}

End

If D > V_{up} I D < = V_{low}

D = D_{init}

End

Step-4: Stop the process